AFOSR-TR- 83-0532

(12)

AD-A129579

DTIC FILE COPY

Approved for public release;
distribution unlimited.

83 06 20 041

UNCLASSIFIED

SECURITY CLASSIFICATION OF THIS PAGE (When Data Entered)

REPORT DOCUMENTATION PAGE	READ INSTRUCTIONS BEFORE COMPLETING FORM
1. REPORT NUMBER AFOSR-TR- 83-0532	2. GOVT ACCESSION NO. AD-A129579
	3. RECIPIENT'S CATALOG NUMBER
4. TIT STRUCTURAL AND KINETIC PROPERTIES OF GRAPHITE INTERCALATION COMPOUNDS	5. TYPE OF REPORT & PERIOD COVERED Final - March 1, 1978 - Feb. 30, 1983
	6. PERFORMING ORG. REPORT NUMBER
7. AUT D.D.L. Chung	8. CONTRACT OR GRANT NUMBER(s) AFOSR-78-3536
9. PERFORMING ORGANIZATION NAME AND ADDRESS Department of Metallurgical Engineering and Materials Science, Carnegie-Mellon University, Pittsburgh, PA 15213	10. PROGRAM ELEMENT, PROJECT, TASK AREA & WORK UNIT NUMBERS 2306-D2 61102F
11. CONTROLLING OFFICE NAME AND ADDRESS U. S. Air Force, Air Force Office of Scientific Research, Building 410, Bolling AFB, DC	12. REPORT DATE April 29, 1983
	13. NUMBER OF PAGES 185
14. MONITORING AGENCY NAME & ADDRESS(if different from Controlling Office) Not Applicable	15. SECURITY CLASS. (of this report) UNCLASSIFIED
	15a. DECLASSIFICATION/DOWNGRADING SCHEDULE

16. DISTRIBUTION STATEMENT (of this Report)

Approved for public release; distribution unlimited.

17. DISTRIBUTION STATEMENT (of the abstract entered in Block 20, if different from Report)

18. SUPPLEMENTARY NOTES

19. KEY WORDS (Continue on reverse side if necessary and identify by block number)

graphite, intercalation, graphite intercalation compounds, structure, kinetics

20. ABSTRACT (Continue on reverse side if necessary and identify by block number)

An extensive investigation was undertaken on the mechanism, kinetics and thermodynamics of intercalation of graphite. It was found that bromine intercalate transport in graphite at room temperature occurred by solid-state intercalate displacement. Upon exposure by stage-2 graphite-bromine to ICl, bromine was expelled by the incoming ICl, which dissolved the remaining bromine to form a solid solution with the ICl in-plane superlattice. During bromine intercalation, an intercalate front moved toward the center of the graphite. The first time-temperature-transformation (TTT) diagram describing the stage evolution during →

DD FORM 1 JAN 73 1473 EDITION OF 1 NOV 65 IS OBSOLETE

UNCLASSIFIED

SECURITY CLASSIFICATION OF THIS PAGE (When Data Entered)

intercalation was obtained. The TTT-curves for bromine intercalation were C-shaped for the growth of each stage, suggesting diffusion-controlled kinetics at low temperatures and interface-controlled kinetics at high temperatures. The pressure-temperature equilibrium diagram for stages 2-4 of graphite-bromine was determined. Based on the change in free energy from stage to stage and the intercalate diffusion rate, the kinetics of bromine intercalation of graphite was modeled. The activation energy for intercalate desorption from graphite-bromine was determined by thermogravimetric analysis to by 17 kcal/mol below the melting temperature (101°C) and 4 kcal/mol above this temperature. The amount of exfoliation increased with decreasing intercalate activity during intercalation. An intercalated single crystal retained its in-plane superlattice orientation throughout exfoliation and collapse. A 3-fold or 6-fold twinned monoclinic superlattice was observed in graphite-ICl single crystals and fibers.

STRUCTURAL AND KINETIC PROPERTIES OF GRAPHITE INTERCALATION COMPOUNDS

(AFOSR-78-3536)

FINAL SCIENTIFIC REPORT

TO THE

AIR FORCE OFFICE OF SCIENTIFIC RESEARCH

BY THE

DEPARTMENT OF METALLURGICAL ENGINEERING & MATERIALS SCIENCE

CARNEGIE-MELLON UNIVERSITY

PITTSBURGH, PENNSYLVANIA 15213

Grant Period: March 1, 1978 -- Feb. 28, 1983

Deborah Chung

Dr. D. D. L. Chung
Principal Investigator

April 29, 1983
Date

TABLE OF CONTENTS

RESEARCH OBJECTIVE

Accompanying the use of intercalated graphite as electrical conductors, catalysts, electrodes, etc. is the need for understanding the processes of intercalation, desorption and exfoliation. Understanding the process of intercalation is important for the fabrication of existing and new intercalation compounds, and for elucidating the mechanism of intercalation and the phenomenon of stage formation. Understanding the process of intercalate desorption from intercalated graphite is important for the use of intercalated graphite at various temperatures and environments. In spite of the low intercalate concentration of desorbed compounds, their stability makes them attractive for numerous applications. Understanding the process of exfoliation is important because exfoliated graphite is already being used commercially as a high temperature sealant, a thermal insulator for molten metals and metal fire extinction blankets. Moreover, exfoliated graphite is potentially useful as a battlefield obscurant and a laser armor.

The secondary objective is to characterize the structure of intercalated graphite fibers and exfoliated graphite. Of particular importance is the preparation of intercalated graphite fibers with a known stage and in-plane superlattice because of their potential applications as high temperature electrical conductors and conducting graphite-polymer composites.

STATUS OF THE RESEARCH EFFORT

1. Process of Intercalation

An extensive investigation was undertaken to study the mechanism, kinetics and thermodynamics of intercalation. A quantitative understanding of the kinetics of intercalation was achieved.

1.1 Mechanism

The mechanism of intercalate transport in graphite was studied by sequential intercalation of bromine and iodine monochloride, as described in Appendix 1. It was found that the transport involves intercalate displacement such that the first intercalate molecule to enter an interlayer space is the first to reach the center of the graphite sample. In spite of the fact that the intercalate is an ordered two-dimensional solid (with a well-defined in-plane superlattice) once it enters the graphite interlayer space, it remains mobile and diffuses toward the center of the graphite in the presence of a sufficient intercalate vapor pressure, which provides the chemical driving force. In the absence of the intercalate vapor pressure, the intercalate does not advance toward the center of the graphite, but rather desorbs. This mechanism is in contrast to that of oxide formation, in which oxygen diffusion through the immobile oxide is necessary for continued oxide formation.

An extended manifestation of intercalate displacement is intercalate exchange, which can provide an alternate route of forming a given intercalation compound. Upon exposure of stage-2 graphite-bromine to ICl, the in-plane superlattice diffraction pattern was observed to change from that of graphite-bromine to that of graphite-ICl, while the ICl intercalate distributed itself uniformly at a concentration level above that of the bromine intercalate. This is interpreted as the expulsion of bromine by the in-coming ICl, which dissolves the remaining bromine to form a solid solution with the ICl in-plane structure. This ternary compound is stage-1, with a c-axis repeat distance slightly larger

than that of stage-1 graphite-ICl.

1.2 Kinetics

X-ray absorption intercalate concentration profile measurement and surface profilometry in the plane perpendicular to the c-axis showed that the intercalation of bromine in graphite involves the movement of an intercalate front toward the center of the graphite. The front delineates a central region which is nearly pure graphite (except near the c-face surface) and an edge region which contains only a small amount of pure graphite. (See Appendix 2).

The first time-temperature-transformation (TTT) diagram describing the stage evolution during intercalation was obtained (Appendix 2). The TTT-curves for bromine intercalation are C-shaped for the growth of each stage, suggesting diffusion-controlled kinetics at low temperatures (the reaction rate increasing with increasing temperature) and interface-controlled kinetics at high temperatures (the reaction rate decreasing with increasing temperature). The stable stage varies with the temperature, such that, for intercalation in pure bromine, stage 2 is stable from room temperature up to $\sim 72^{\circ}C$, stage 3 is stable from $\sim 72^{\circ}C$ to $\sim 140^{\circ}C$, and stage 4 is stable above $\sim 140^{\circ}C$. Progressive stage decrease toward the stable stage occurs during intercalation. Also reported is a time-concentration-transformation (TCT) diagram which describes the dependence of the intercalation kinetics on the intercalate vapor pressure (i.e., the Br_2 concentration in the Br_2-CCl_4 solution containing the sample). The final stage decreases in discrete steps with increasing Br_2 concentration in Br_2-CCl_4, but the rate of intercalation increases linearly with increasing Br_2 concentration in Br_2-CCl_4.

1.3 Thermodynamics

The thermodynamics of intercalation of bromine in graphite was studied by determining the pressure-temperature equilibrium diagram for stages 2-4 (Appendix 3). The standard heat and entropy of reaction for the transformation from

stage n to stage n-1 (n = 5, 4, 3) were found to be roughly the same, though the enthalpy of reaction became slightly more negative as the stage number increased. The heat and entropy of formation from pure graphite were thus found to be -10.9 kcal mol^{-1} Br_2 and -30.4 cal mol^{-1} Br_2 K^{-1} respectively for stage 2, -11.3 kcal mol^{-1} Br_2 and -30.6 cal mol^{-1} Br_2 K^{-1} respectively for stage 3, and -11.5 kcal mol^{-1} Br_2 and -30.6 cal mol^{-1} Br_2 K^{-1} respectively for stage 4.

1.4 Model

The experimental kinetic and thermodynamic information was used to model the kinetics of intercalation, as described in Appendix 4. The model was based on the change in free energy from stage to stage and the diffusion rate of bromine, since the staging reaction and the intercalate transport within the graphite are the two possible rate-controlling steps in bromine intercalation. Largely on the basis of the high pressures needed for bromine intercalation, it was assumed that the transport of the intercalating species to the graphite surface and the adsorption on the surface are fast and hence not rate-controlling. Satisfactory agreement was found between the model and the experimental TTT-diagram. Furthermore, the model predicts that graphite-bromine is unstable at temperatures above ~250°C.

2. Process of Desorption

Thermogravimetric analysis was performed to study the kinetics of desorption, which was found to involve the out-diffusion of the intercalate. The activation energy for desorption was determined to be 17 kcal/mol below the melting temperature (101°C) and 4 kcal/mol above this temperature (Appendix 5).

3. Process of Exfoliation

By dilatometry, a single exfoliation event was found to consist of multiple expansion spurts, which occurred at ~150°C and ~240°C for first exfoliation, and

$\sim$100°C and $\sim$240°C for subsequent cycles. The amount of expansion was found to increase with decreasing intercalate activity during intercalation. With exfoliation cycles to higher temperatures or longer times, the amount of residual expansion after the collapse on cooling increased until no second exfoliation was observed on reheating. Due to intercalate desorption, the amount of expansion for concentrated samples increased with increasing sample width; desorbed samples showed little width dependence. Acoustic emission was observed before appreciable expansion during the first exfoliation cycle; it was not observed during the collapse or subsequent exfoliation cycles. A model of exfoliation involving intercalate islands is proposed (Appendix 6).

4. Structure

X-ray diffraction was used to characterize the structure of exfoliated graphite and intercalate graphite fibers.

4.1 Exfoliated graphite

By x-ray diffraction, exfoliated graphite-Br_2 was found to exhibit the same in-plane superlattice ordering as intercalated graphite prior to exfoliation. This ordering persisted even after heating for an hour at 1700°C. Furthermore, an intercalated single crystal flake retained its in-plane superlattice orientation throughout exfoliation and collapse (Appendix 7).

4.2 Intercalated graphite fibers

By using x-ray diffraction, a 3-fold or 6-fold twinned monoclinic $\sqrt{301}$ x 2 (-3.3°, 0°) superlattice (a=4.92 Å, b=42.68 Å, c=7.0 Å, γ=93.3°) was observed in stage-1 graphite-ICl single crystals intercalated in ICl vapor. This in-plane superlattice was also observed in stage-1 and stage-2 graphite-ICl, which were based on Thronel P-100 graphite fibers and prepared by the two-bulb method, in which ICl was at 25°C while the graphite was at 100°C for stage 1 and 130°C for stage 2. This work provides the first observation of in-plane intercalate ordering in intercalated graphite fibers and the first x-ray diffraction evidence

of ICl intercalation in graphite fibers. A different in-plane superlattice was observed in stage-1 graphite-ICl single crystals intercalated in ICl liquid (See Appendix 8).

PERSONNEL

Principal Investigator:	D. D. L. Chung
Graduate Students:	K. K. Bardhan (4/78-9/78 partial, 7/79-8/80, 10/80) S. H. Anderson (6/78-1/83) J. S. Culik (6/78-9/78) Yao-nan Chang (6/78-6/79) Hsein-Hua Lee (10/80-2/81, 6/81-7/81) Pong-Fei Lu (2/81, 5/81) Robit K. Gangwar (6/81-1/82, 3/82)
Undergraduate work-study students (hourly):	Terrance O'Donovan (11/79-1/80, 6/80-8/80, 10/80-1/81) Kimberly Egler (11/79-12/79, 2/80-5-80) Lorena Miller (9/81)
Technicians:	D. Ghosh (3/82-2/83, partial) C. Novak (7/81, 9/81, 11/81-6/82, partial) R. Miller (4/78, 6/78-9/82, partial) S. Pavlina (10/82, partial)
Administrators:	Judy Guy (4/78, 6/78-1/81, partial) Lynne Hyatt (1/82, 4/82, 5/82, 8/82, partial) Anne Sigerstad (10/82, partial)
Secretaries:	Cathy Hill (3/78, partial) Maxine Patterson (5/78-9/79, partial) Dorothy Rue (9/81, 11/81, partial) Linda Brzeczko (1/82-2/83, partial)

PUBLICATIONS

Papers in Journals

1. D.D.L. Chung, "Nomenclature of Graphite Intercalation Compounds," Mater. Sci. Eng. 39, 283 (1979).

2. D.D.L. Chung, "Graphite-Halogens As Temperature Calibration Standards for Transmission Electron Microscopy," Rev. Sci. Instrum. 51, 932 (1980).

3. J.S. Culik and D.D.L. Chung, "Thermal Gravimetric Analysis of Graphite-Bromine," Mater. Sci. Eng. 44, 129 (1980).

4. K.K. Bardhan and D.D.L. Chung, "A Kinetic Model of the First Intercalation of Graphite," Carbon 18, 303 (1980).

5. K.K. Bardhan and D.D.L. Chung, "Surface Profilometric Study of the Kinetics of the Intercalation of Graphite," Carbon 18, 313 (1980).

6. K.K. Bardhan, J.C. Wu, J.S. Culik, S.H. Anderson and D.D.L. Chung, "Kinetics of Intercalation and Desorption in Graphite," Synth. Met. 2. 57 (1980).

7. S.H. Anderson and D.D.L. Chung, "Exfoliation of Intercalated Graphite," Carbon, submitted.

8. D. Ghosh, R. Gangwar and D.D.L. Chung, "Superlattice Ordering in Graphite-ICl Single Crystals and Fibers," Carbon, submitted.

9. S.H. Anderson and D.D.L. Chung, "Intercalate Displacement and Exchange in Graphite," Synth. Met., to be submitted.

10. S.H. Anderson and D.D.L. Chung, "Kinetics of Intercalation of Bromine in Graphite," to be submitted.

Papers in Conference Proceedings

1. D.D.L. Chung, "Exfoliation of Graphite," Thermal Expansion 7, Edited by D.C. Larsen, Plenum, 1982, p. 37-44.

2. D.D.L. Chung, "Thermal Analysis of Graphite Intercalated with Bromine," Proceedings of 7th International Conference on Thermal Analysis, Ed. B. Miller, Wiley, 1982, Vol. I, p. 418-428.

3. S.H. Anderson and D.D.L. Chung, "Thermodynamics of Intercalation of Bromine in Graphite," Proceedings of Symposium on Intercalated Graphite Materials Research Society, Boston, 1982., Ed. M.S. Dresselhaus, Elsevier.

Extended Abstracts

1. S.H. Anderson, J.S. Culik and D.D.L. Chung, "Dilatometric Study of the Exfoliation of Graphite-Br_2," Ext. Abstr. Program - Bienn. Conf. Carbon 14, 262-3 (1979).

Extended Abstracts (continued)

2. K.K. Bardhan and D.D.L. Chung, "Mechanism of Intercalation of Graphite," Ext. Abstr. Program - Bienn. Conf. Carbon 14, 282-3 (1979).

3. J.S. Culik, S.H. Anderson and D.D.L. Chung, "Temperature Dependence of the Rate of Intercalate Desorption," Ext. Abstr. Program - Bienn. Conf. Carbon 14, 280-1 (1979).

4. S.H. Anderson and D.D.L. Chung, "Stage Evolution during Intercalation," Ext. Abstr. Program - Bienn. Conf. Carbon 15, 361-2 (1981).

5. S.H. Anderson, H.H. Lee and D.D.L. Chung, "Stage Dependence of the Exfoliation of Intercalated Graphite," Ext. Abstr. Program - Bienn. Conf. Carbon 15, 357-8 (1981).

6. S.H. Anderson and D.D.L. Chung, "Exfoliation of Single Crystal Graphite-Bromine," Ext. Abstr. Program - Bienn. Conf. Carbon 16 (1983).

7. S.H. Anderson and D.D.L. Chung, "Model of Intercalation of Bromine in Graphite," Ext. Abstr. Program - Bienn. Conf. Carbon 16 (1983).

INTERACTIONS

Spoken Papers

American Physical Society, General Meeting, March 1979, Chicago, IL:

D. D. L. Chung and Yao-nan Chang, "Scanning Electron Microscope Study of Graphite-Br_2."

Symposium on Properties of Low Dimensional Solids, Honolulu, Hawaii, April 1979:

K. K. Bardhan and D. D. L. Chung, "Kinetics of the Intercalation of Graphite."

14th Biennial Conference on Carbon, June 1979, University Park, PA:

S. H. Anderson, J. S. Culik and D. D. L. Chung, "Dilatometric Study of the Exfoliation of Graphite-Br_2."
J. S. Culik, S. H. Anderson and D. D. L. Chung, "Temperature Dependence of the Rate of Intercalate Desorption."
K. K. Bardhan and D. D. L. Chung, "Mechanism of Intercalation of Graphite."

American Physical Society, General Meeting, March 1980, New York, NY:

D. D. L. Chung, S. H. Anderson and J. C. Wu "Graphite-Aluminum Halides: Preparation, Intralayer Crystal Structure and Order-Disorder Transformation."
J. C. Wu and D. D. L. Chung, "Surface Profilmetric Study of the Kinetics of Intercalate Sorption and Desorption in Graphite."
S. H. Anderson and D. D. L. Chung, "Pressure and Temperature Dependence of the Kinetics of the Intercalation of Graphite."

2nd International Conference on the Intercalation Compounds of Graphite, May 1980, Provincetown, MA:

J. C. Wu, J. S. Culik and D. D. L. Chung, "Kinetics of Intercalate Desorption."

TMS-AIME Fall Meeting, October 1980, Pittsburgh, PA:

K. K. Bardhan, J. C. Wu, S. H. Anderson and D. D. L. Chung, "Kinetics of Intercalation and Desorption: A Model."
J. C. Wu, K. K. Bardhan, S. H. Anderson and D. D. L. Chung, "Kinetics of Intercalation: A Surface Profilometric Study of Graphite-Halogens."

12th Central Regional Meeting of the American Chemical Society, November 1980, Pittsburgh, PA:

C. G. Woychik, D. D. L. Chung and A. W. Thompson, "Mechanical Properties of Graphite-Bromine."

15th Biennial Conference on Carbon, Philadelphia, PA, June 22-26, 1981

S. H. Anderson, H. H. Lee and D. D. L. Chung, "Stage Dependence of the Exfoliation of Intercalated Graphite."
S. H. Anderson and D. D. L. Chung, "Stage Evolution During Intercalation"

TMS-AIME Fall Meeting, Louisville, KY, October 11-15, 1981

S. H. Anderson and D. D. L. Chung, "Exfoliation of Intercalated Graphite"

Spoken Papers (continued)

11th Annual Conference of the North American Thermal Analysis Society, New Orleans, LA, October 19-21, 1981

S. H. Anderson and D. D. L. Chung, "Thermogravimetric Analysis of the Kinetics of Intercalate Desorption from Graphite Intercalation Compounds."
S. H. Anderson, H. H. Lee and D. D. L. Chung, "Thermal Acoustic Emission: Study of the Exfoliation of Graphite."

Annual Meeting of AIME, Dallas, TX, February 15-18, 1982

S. H. Anderson and D. D. L. Chung, "X-ray Studies of the Kinetics of the Intercalation of Graphite."

General Meeting of the American Physical Society, Dallas, TX, March 8-11, 1982

D. D. L. Chung and S. H. Anderson, "Time-Temperature-Transformation Diagram for Stage Formation During Intercalation of Graphite with Br_2."
S. H. Anderson and D. D. L. Chung, "Exfoliation of Bromine-Graphite Intercalation Compounds."

Annual Meeting of Materials Research Society, Symposium on Intercalated Graphite, Boston, MA, November 1-4, 1982

S. H. Anderson and D. D. L. Chung, "Thermodynamics of Intercalation of Bromine in Graphite."

General Meeting of the American Physical Society, Los Angeles, CA, March 21-25, 1983

R. Gangwar, D. Ghosh and D. D. L. Chung, "In-plane Superlattice in Graphite-ICl Fibers."

Poster Paper

110th AIME Annual Meeting, February, 1981, Chicago, IL:

S. H. Anderson and D. D. L. Chung, "Electrointercalation and Exfoliation of Graphite."

APPENDIX 1

Synth, Met., to be submitted

INTERCALATE DISPLACEMENT AND EXCHANGE IN GRAPHITE*

S.H.Anderson and D.D.L.Chung
Department of Metallurgical Engineering
and Materials Science
Carnegie-Mellon University
Pittsburgh, PA 15213

Abstract

The mechanism of intercalate transport in graphite was studied by sequential intercalation of bromine and iodine monochloride. It was found that the transport involved solid-state intercalate displacement such that the first intercalate molecule to enter an interlayer space is the first to reach the center of the graphite sample. Upon exposure of stage-2 graphite-bromine to ICl, the in-plane superlattice diffraction pattern was observed to change from that of graphite-bromine to that of graphite-ICl, while the ICl intercalate distributed itself uniformly at a concentration level above that of the bromine intercalate. This is interpreted as the expulsion of bromine by the in-coming ICl, which dissolved the remaining bromine to form a solid solution with the ICl in-plane structure.

* Research sponsored by the Air Force Office of Scientific Research, Air Force Systems Command, USAF, under Grant No. AFOSR-78-3536. The United States Government is authorized to reproduce and distribute reprints for governmental purposes notwithstanding any copyright notation hereon.

1 Introduction

The question of intercalate transport is important from a technological viewpoint. In batteries, for example, intercalate transport would have a direct bearing on the cell current. Intercalate transport also must be considered in replacement or exchange reactions where the first intercalation compound to be formed is an intermediate to the final compound. Examples of replacement reactions include the formation of transition metal intercalation compounds from alkali metal intercalation compounds [1], and the reaction of aluminum bromide with residue graphite–bromine compounds [2].

The keynote of work pertaining to the mechanism of intercalate transport is Hooley's [3, 4] observation that intercalation begins at the basal edges adjacent to basal surfaces, and that the intercalating species migrate between the basal planes. Studies of reaction kinetics can suggest transport mechanisms; it was the observation of the kinetics of the oxidation of intercalated potassium which led Daumas and Herold [5] to explain staging with the concept of intercalate islands. This concept carries the notion of intercalate displacement by the movement of the intercalate islands. However, most studies of intercalation kinetics have involved vapor phase transport of the intercalate to the sample and the rate–controlling step in the overall intercalation reaction appears to be at the sample surface. For example, condensation and adsorption appear to be rate–controlling in the intercalation of alkali metals [6] and metal halides [7, 8], while charge transfer and reaction at the surface appear rate–controlling for the intercalation of nitric acid [9] and in general in the intercalation of metal dichalcogenide hosts [10]. As a consequence of reaction control at the surface, little information is available pertaining to transport within the graphite. The kinetics of bromine intercalation, on the other hand, appears to be controlled by the diffusion of bromine within the graphite under conditions of both vapor phase and liquid phase intercalation. Furthermore, the diffusion coefficient of bromine as determined during intercalation and desorption [11, 12] is very similar to that observed by Aronson for the self–

diffusion of bromine in intercalated graphite [13]. Two diffusion mechanisms are possible; first, the already present intercalation compound can be considered as the reference frame through which fresh intercalate molecules diffuse, as in the case of many oxide films. Second, the intercalate molecules may be considered as diffusing within the graphite, allowing the first molecules to be injected at the crystal edges to be the first molecules to reach the center of the crystal. Measurements of diffusion coefficients generally have implicitly assumed that the second case was correct. By observing the displacement of intercalated bromine by iodine monochloride, we have obtained explicit evidence of this transport mechanism for bromine in graphite.

2 Experimental Techniques

We have tried to clarify the intercalation mechanism by sequentially intercalating graphite with bromine and iodine monochloride. Both highly oriented pyrolytic graphite (HOPG, 4 mm x 4 mm) and large single crystal flakes (~4 mm diameter) were used. Samples were intercalated in a variety of methods, all of which were carried out at room temperature.

Method 1: a control sample was prepared by partially intercalating HOPG in liquid Br_2, then allowing it to desorb in liquid CCl_4.

Method 2: an HOPG sample and a single crystal flake were partially intercalated in liquid Br_2, and then intercalated in a 2 mol% solution of ICl and CCl_4.

Method 3: an HOPG sample and a single crystal flake were intercalated to completion in liquid Br_2, and then immersed in liquid ICl.

Method 4: an HOPG sample was intercalated to completion in a solution of 50 mol% Br_2 and 2 mol% ICl in CCl_4.

Method 5: an HOPG sample and a single crystal flake were intercalated to completion in a sclution of 50 mol% Br_2 and 50 mol% ICl.

Staging in the compounds was determined with a diffractometer using Cu Kα radiation and a monochromator. The in-plane structure was observed by the transmission Laue method using Mo Kα radiation. The intercalate concentration distribution perpendicular to the c-axis was determined by measuring the x-ray

absorption of monochromatic Cu Kα and Mo Kα radiation as an intercalated sample was transported through an x-ray beam. Table 1 lists the absorption coefficients and intercalate layer densities for Br_2, ICl and C. The difference in the absorption coefficients at the two wavelengths allowed the mapping of the bromine and iodine monochloride distributions within the graphite. The density used to convert the mass absorption coefficient to a linear mass absorption coefficient was the density calculated for a single intercalate layer. The stoichiometries indicated in Table 1 were used to calculate the density. The stoichiometries were obtained from the work of Ghosh et al. [14, 15]

It was assumed that the ICl remained a molecular species with little tendency to decompose. With a known initial graphite thickness, the pointwise bromine and ICl concentrations could be determined by the following two equations with two unknowns:

$$\left(\frac{I}{I_o}\right)^{Cu} = \exp-[\mu_C^{Cu} x_C + \mu_{Br_2}^{Cu} x_{Br_2} + \mu_{ICl}^{Cu} x_{ICl}]$$

$$\left(\frac{I}{I_o}\right)^{Mo} = \exp-[\mu_C^{Mo} x_C + \mu_{Br_2}^{Mo} x_{Br_2} + \mu_{ICl}^{Mo} x_{ICl}],$$

where I_o is the unabsorbed beam intensity, I is the transmitted beam intensity, μ_a^λ is the absorption coefficient for component a at wavelength λ, and x_a is the thickness of component a. In the succeeding graphs the concentration of a is determined by the ratio of x_a and the product of the initial graphite thickness and the nominal expansion of a first stage compound. In a single-component and single-stage compound, the indicated concentration is the reciprocal of the stage number. The use of Cu Kα and Mo Kα radiation is particularly appropriate as the bromine absorption coefficient is smaller than that of ICl with Cu Kα but larger than ICl with Mo Kα radiation. As a consequence, a difference in the distributions of Br and ICl is very clearly evident even in the raw data. The relative amounts of bromine and ICl can be very accurately determined, but the absolute concentrations cannot. The primary reason for this arises in the measurement of the initial graphite thickness and difficulties in ensuring that the sample is actually perpendicular to the beam.

For these experiments the graphite thickness was measured by x-ray absorption prior to intercalation, and the sample was within 5° of the perpendicular. A further error is possible from the counting statistics, especially in the case of first stage graphite-ICl with Cu radiation. Thus, the absolute concentration values have an uncertainty of ~10%.

3 Experimental Results

The first curve in Fig. 1 illustrates the distribution of bromine within a sample after a 10 min exposure to Br_2 (Methods 1 and 2). The distribution is consistent with the "window-pane" morphology commonly observed in bromine intercalation. The second and third curves indicate the bromine concentration after the subsequent 36 and 74 hours in CCl_4 respectively (Method 1). It can be seen that there was virtually no further transport of the bromine into the sample: only desorption of bromine into the CCl_4 occurred.

The behavior on desorption can be contrasted with that occurring when a partially bromine intercalated sample is then exposed for 36 hr to 2 mol% ICl (Method 2, Fig. 2). The concentration profile (Fig. 2) indicates that the bromine had migrated toward the center of the sample while the edge region contained predominantly ICl. The 00/ diffraction pattern indicated the presence of both stage 1 and stage 2 compounds. The in-plane superlattice was very similar to that observed for stage 1 graphite-ICl (See Fig. 1 of Ref. 15). As discussed below, the same in-plane superlattice was observed when a sample saturated with bromine was exposed to liquid ICl (Method 3) and when a sample was intercalated in a mixture of 50 mol% Br_2 - 50 mol% ICl (Method 5).

The concentration profile in Fig. 2 suggested that at short ICl intercalation times both a graphite-bromine phase and a graphite-ICl phase should coexist. To confirm this, a flake of graphite was immersed in liquid Br_2 for 5 min, and then immersed in liquid ICl for 11 min. Fig. 3 shows the transmission Laue patterns obtained from near the edge and near the center of the flake. Fig. 3(a), the pattern

obtained near the edge, indicates that both the graphite-bromine and the graphite-ICl structures were present. Near the center of the flake, however, the graphite-bromine structure was still the dominant phase (Fig. 3(b)).

Fig. 4 shows the results obtained when a stage 2 graphite-bromine compound was immersed in liquid ICl (Method 3). Fig. 4(a) indicates that, despite the initial saturation of the sample with bromine, much of the bromine was displaced by the in-coming ICl. This is supported by the diffraction results; the in-plane structure was similar to graphite-ICl and the 00/ diffraction pattern (Fig. 4(b)) indicates that stage 1 predominated. The apparent expulsion of bromine from the sample in Method 3 can be explained by preferential intercalation by ICl due to a larger reaction energy.

Samples intercalated in a mixture of Br_2 and 2 mol% ICl (Method 4) showed a uniform distribution of bromine and ICl (Fig. 5(a)), and the 00/ diffraction pattern (Fig. 5(b)) was quite similar to that of a fourth stage graphite-bromine compound, with the exception of a peak where the first stage ICl (001) line may be expected.

With 50 mol% of ICl in the ICl-Br_2 solution (Method 5), the bromine distribution was relatively uniform (Fig. 6(a)). The 00/ diffraction pattern (Fig. 6(b)) shows a predominantly first stage pattern, with a small amount of stages 2 and 3. The repeat distance, 7.12 Å, for this first stage compound is the same as that observed after sequential intercalation of ICl into stage 2 graphite-bromine (Method 3). This value is somewhat larger than the repeat distance of 7.06 Å, which was observed in a first stage graphite-ICl compound made by immersion in ICl liquid.

4 Discussion

The evidence in Fig. 3, where both bromine and ICl superlattices are present within the same sample, indicates that initially bromine is displaced by the in-coming ICl toward the central unintercalated region of the sample. This indicates that the presence of an alternate species, ICl, is sufficient to cause bromine to intercalate,

even though only desorption occurs if no other intercalate is available. Calculations made by Enriquez et.al. [16] suggest that the loss of intercalate molecules into the regions between the islands is not energetically favorable. This in turn suggests that diffusion may predominantly be due to the migration of islands rather than the movement of molecules through or between islands. Observations of island boundaries by transmission electron microscopy also suggests that island mobility may be quite high [17]. On the other hand, it is evident that interdiffusion of bromine and ICl between islands occurs, as is shown by the similar repeat distance and in-plane structure observed after sequential intercalation (Method 3), and after intercalation from a Br_2-ICl solution (Method 5). Furthermore, since the in-plane structure appears similar to that observed for graphite-ICl, we suggest that bromine is dissolving into the ICl structure, forming an ICl-rich solid solution. Since graphite-bromine and graphite-ICl have different in-plane structures, at least two solid solutions are expected - one ICl-rich, with an ICl in-plane structure, and one bromine-rich, with a bromine in-plane structure. The preference observed in this work for the ICl-rich structure is probably due to the high ICl reactivity in the environments used.

5 Acknowledgements

We wish to thank Dr. W. W. Mullins and Dr. D. H. Ghosh for helpful discussions, and we are grateful to Dr. A. W. Moore and Dr. M. B. Dowell for providing HOPG and graphite flakes. The x-ray diffraction equipment grant from the Division of Materials Research of the National Science Foundation under Grant No. DMR-800538 is acknowledged. Support from the Materials Research Laboratory Section, Division of Materials Research, National Science Foundation under Grant No. DMR 76-81561 A01 is also acknowledged.

9

References

1. M.E.Vol'pin, Y.N.Novikov, N.D.Lapkina, V.I.Kasatochkin, Y.T.Struchkov, M.E.Kazakov, R.A.Stukan, V.A.Povitskij,Yu.S.Karimov, and A.V.Zvarikina, "Lamellar Compounds of Graphite with Transition Metals. Graphite as a Ligand," *Journal of the American Chemical Society*, Vol. 97, 1975, pp. 3366-3373.

2. T.Sasa, Y.Takahashi, T.Mukaibo, "Lamellar reactions of graphite with Aluminum Halides," *Bulletin of the Chemical Society of Japan*, Vol. 45, 1972, pp. 937-938.

3. J.G.Hooley and J.L.Smee, "The Mechanism of the Bromination of Graphite," *Carbon*, Vol. 2, 1964, pp. 135-138.

4. J.G.Hooley, "Physical Chemistry and Mechanism of Intercalation in Graphite," *Materials Science and Engineering*, Vol. 31, 1977, pp. 17-24.

5. N.Daumas and A.Herold, "Sur les entre la notion de stade at les mechanismes reactionnels dans les compose's d'insertion du graphite," *Comt. Rend. Acad. Sci.(Paris)*, Vol. Serie C,268, 1969, pp. 373.

6. A.Hamwi, P.Touzain, L.Bonnetain, A.Boeuf, A.Freund and C.Riekel, "A real time gamma ray diffraction study of potassium intercalation into graphite," *Materials Science and Engineering*, Vol. 57, 1983, pp. 161-169.

7. S.Flandrois, J.M.Masson, J.C.Rouillon, J.Gaultier and C.Hauw, "Intercalation compounds of graphite with nickel chloride: Synthesis, structure, and mechanism of intercalation," *Synth. Met.*, Vol. 3, 1981, pp. 1-13.

8. F. Baron, S. Flandrois, C. Hauw and J. Gaultier, "Charge transfer and islands in metal halides-graphite intercalation compounds: New evidence from x-ray diffraction of intercalated MnCl2," *Solid State Communications*, Vol. 42, 1982, pp. 759-762.

9. W.C. Forsman, F.L. Vogel, D.E. Carl and J. Hoffman, "Chemistry of graphite intercalation by nitric acid," *Carbon*, Vol. 16, 1978, pp. 269-271.

10. J.V.Acrivos, "On the intercalation reaction," in *Physics and Chemistry of Materials with Layered Structures*, D. Reidel Publishing Co., Dordrecht, Holland, 1979, pp. 33-98.

11. K.K.Bardhan, J.C.Wu, J.S.Culik, S.H.Anderson, and D.D.L.Chung, "Kinetics of intercalation and desorption in graphite," *Synthetic Metals*, 1980, pp. 57-84.

12. M.B.Dowell and D.S.Badorek, "Diffusion coefficients of Br_2, HNO_3, and $PdCl_2$ in graphite," *Carbon*, Vol. 16, 1978, pp 241-249.

13. S.Aronson, "Bromine exchange in graphite-bromine lamellar compounds," *Journal of Inorganic and Nuclear Chemistry*, Vol. 25, 1963, pp. 907-918.

14. D. Ghosh and D.D.L. Chung, "Two-dimensional structure of bromine intercalated graphite", submitted for publication

15. D.Ghosh, R.Gangwar and D.D.L.Chung, "Superlattice ordering in graphite-ICl single crystals and fibers", submitted for publication

16. F.Enriquez, M.A.G.Quintas, and E.Santos, "Calculation of the expansion in a graphite crystal by C_n interstitials," *Carbon*, Vol. 13, 1975, pp. 225-231.

17. M.Heerschap, P.Delavignette and S.Amelinckx, "Electron microscope study of interlamellar compounds of graphite with bromins,iodine monochloride and ferric chloride," *Carbon*, Vol. 1, 1964, pp. 235-243.

Table 1: X-ray mass absorption coefficients of Br, ICl and C

μ/ρ (cm^2/g)	Br_2	ICl	C
Cu Kα	92.6	268	4.22
Mo Kα	82.2	33.2	0.535
Layer density (g/cm^3)	3.93	3.13	2.27
Stoichiometry	$C_{14}Br_2$	C_9ICl	-

Fig. 1. Distribution of bromine in an HOPG sample after desorption for 0 hrs (▲), 36 hrs (●) and 74 hrs(○).

Fig. 2. Distribution of bromine (○) and ICl (●) within graphite flake after partial intercalation in Br_2, then intercalation in 2 mol% ICl–CCl_4 (Method 2).

Fig. 3. Transmission Laue photographs taken from (a) the edge, and (b) the center of graphite flake immersed in liquid bromine 5 min, then immersed in liquid ICl for 11 min.

Fig. 4. (a) The distribution of bromine (○) and ICl (●), and (b) the 00/ diffraction pattern obtained from an initially stage 2 graphite–bromine compound after immersion in liquid ICl (Method 3).

Fig. 5. (a) The distribution of bromine (○) and ICl (●), and (b) the 00/ diffraction pattern obtained from HOPG intercalated in a solution of 50 mol% Br_2 and 2 mol% ICl in CCl_4 (Method 4).

Fig. 6. (a) The distribution of bromine (○) and ICl (●), and (b) the 00/ diffraction pattern obtained from HOPG intercalated in a solution of 50 mol% Br_2 and 50 mol% ICl (Method 5).

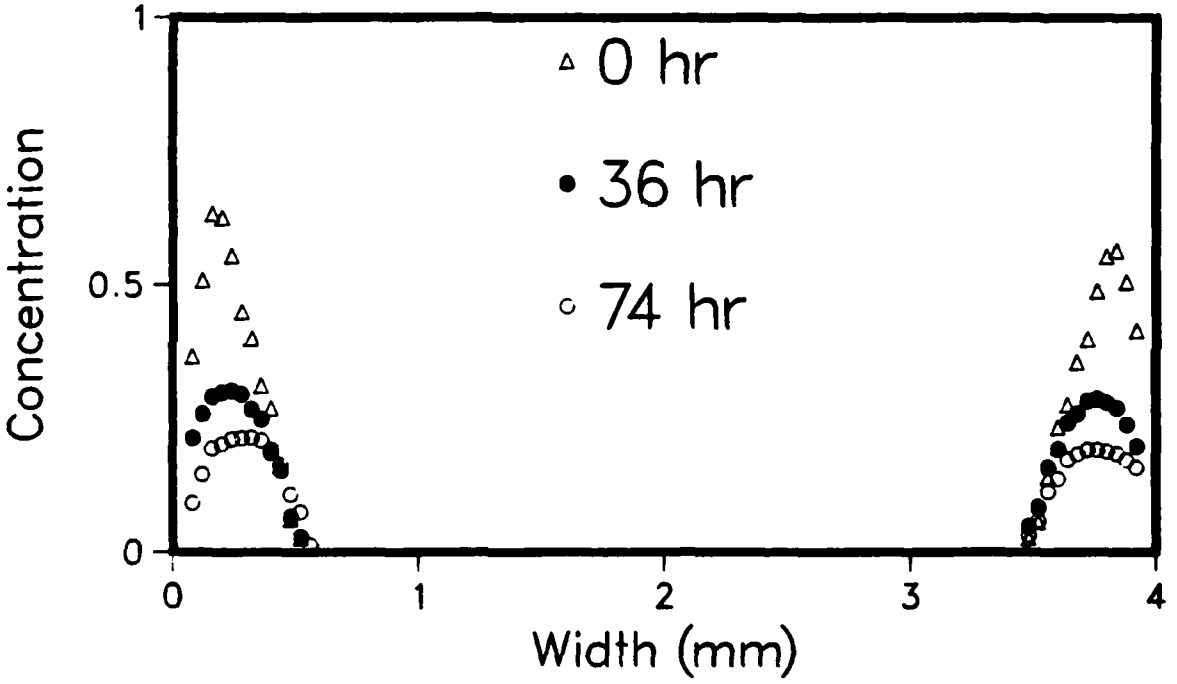

Fig. 1

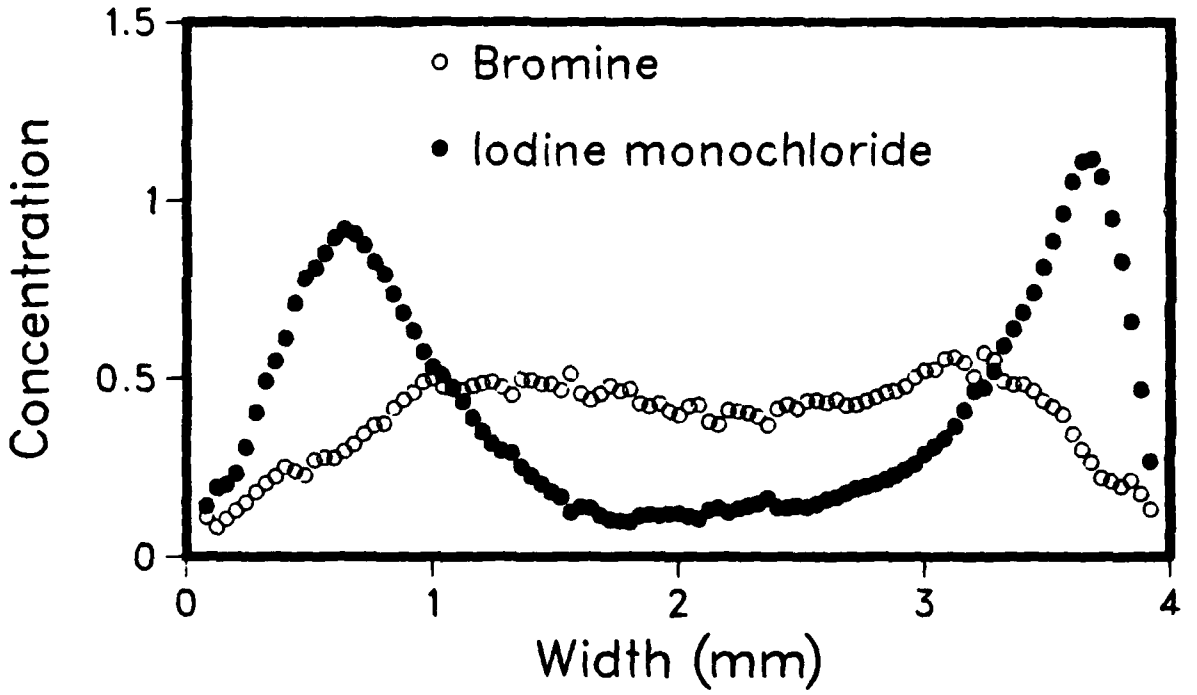
1.5
1
0.5
0
Concentration
Bromine
Iodine monochloride
0
1
2
3
4
Width (mm)

Fig. 2

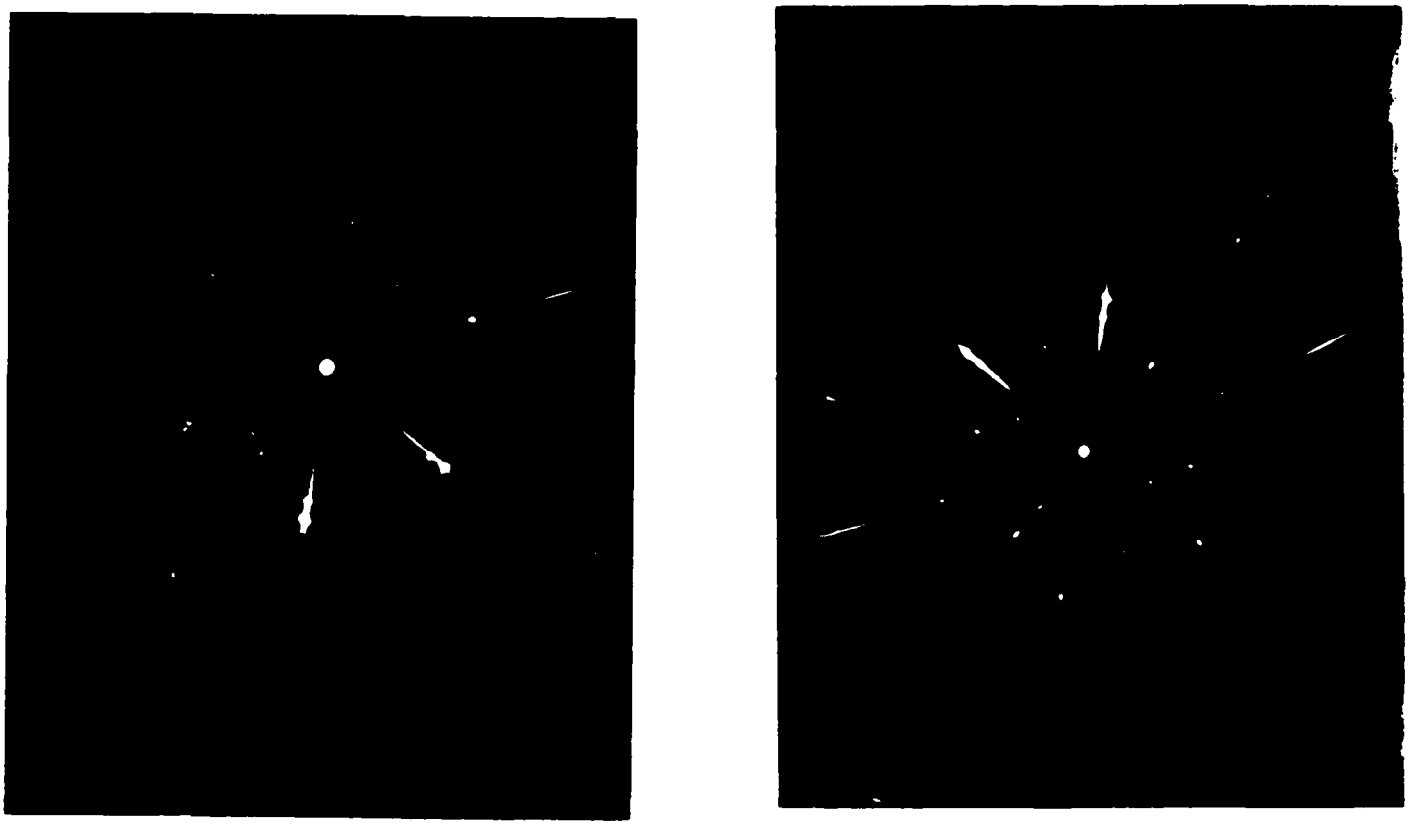

a

b

Fig 3

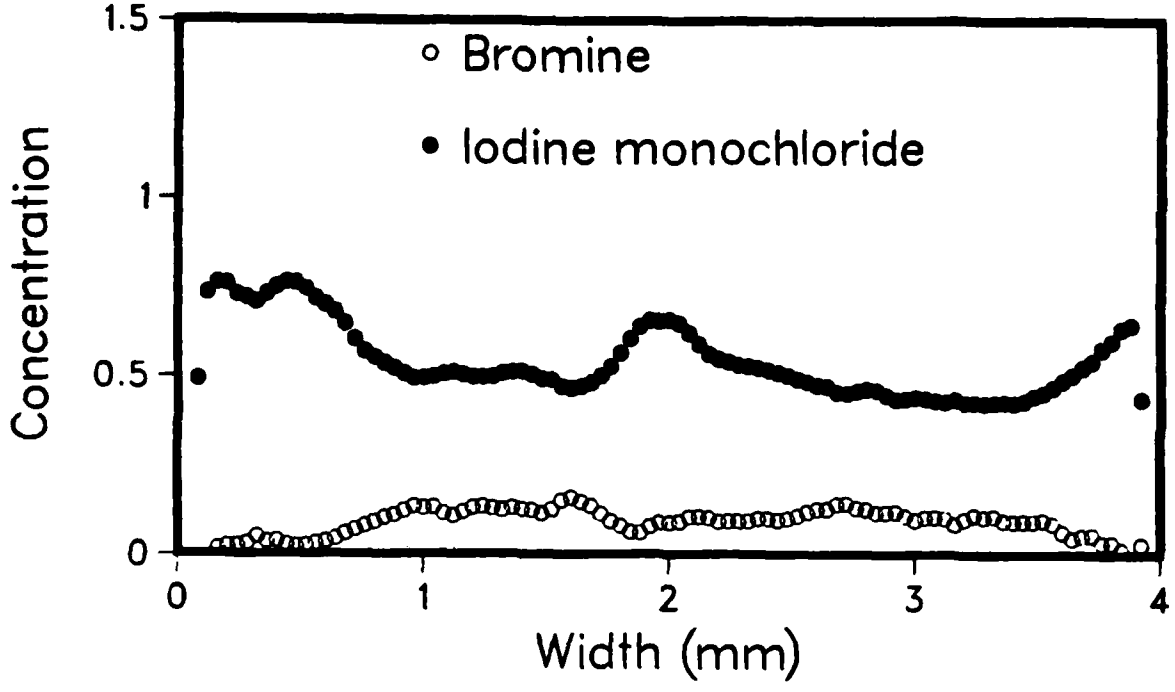
1.5
1
0.5
0
Concentration
Bromine
Iodine monochloride
0
1
2
3
4
Width (mm)

a

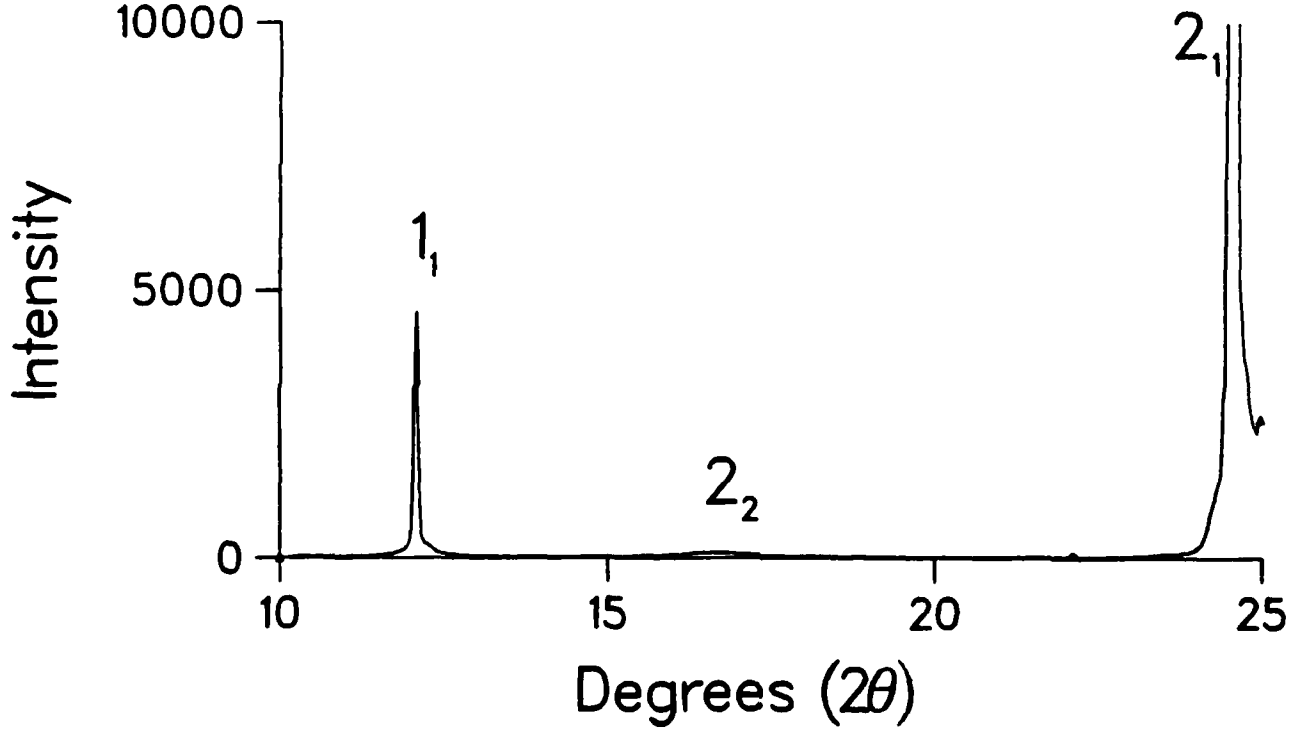
10000
5000
0
Intensity
1₁
2₁
2₂
10
15
20
25
Degrees (2θ)

b

Fig. 4

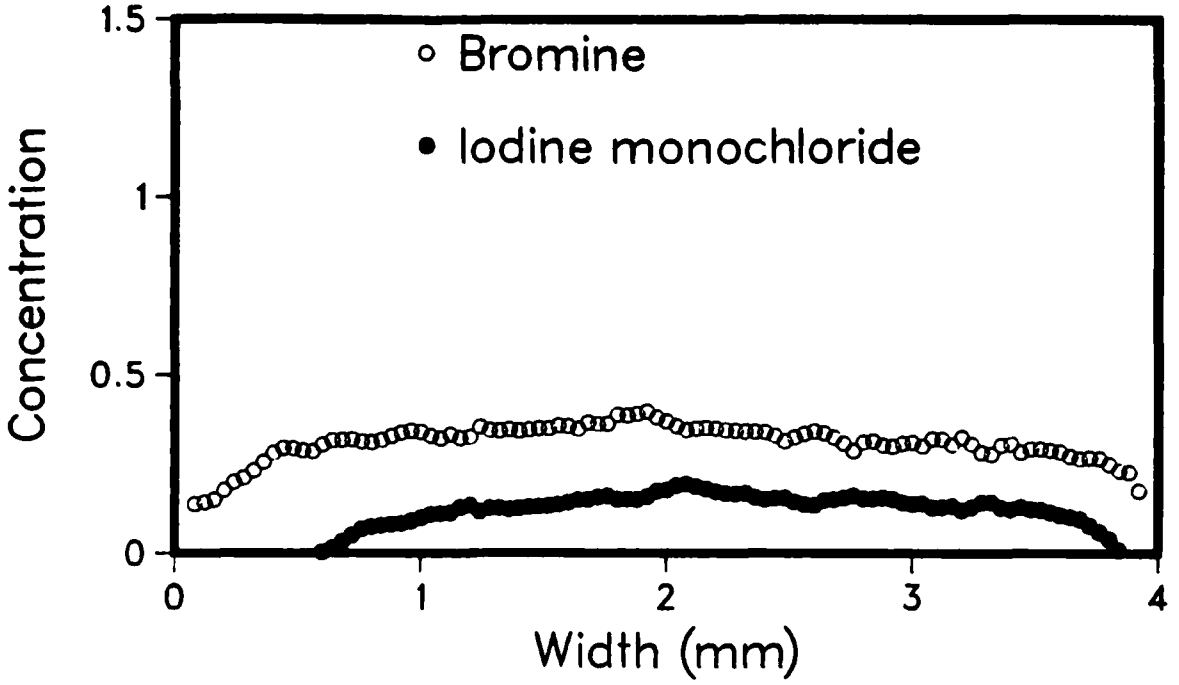
1.5
1
0.5
0
Concentration
Bromine
Iodine monochloride
0
1
2
3
4
Width (mm)

a

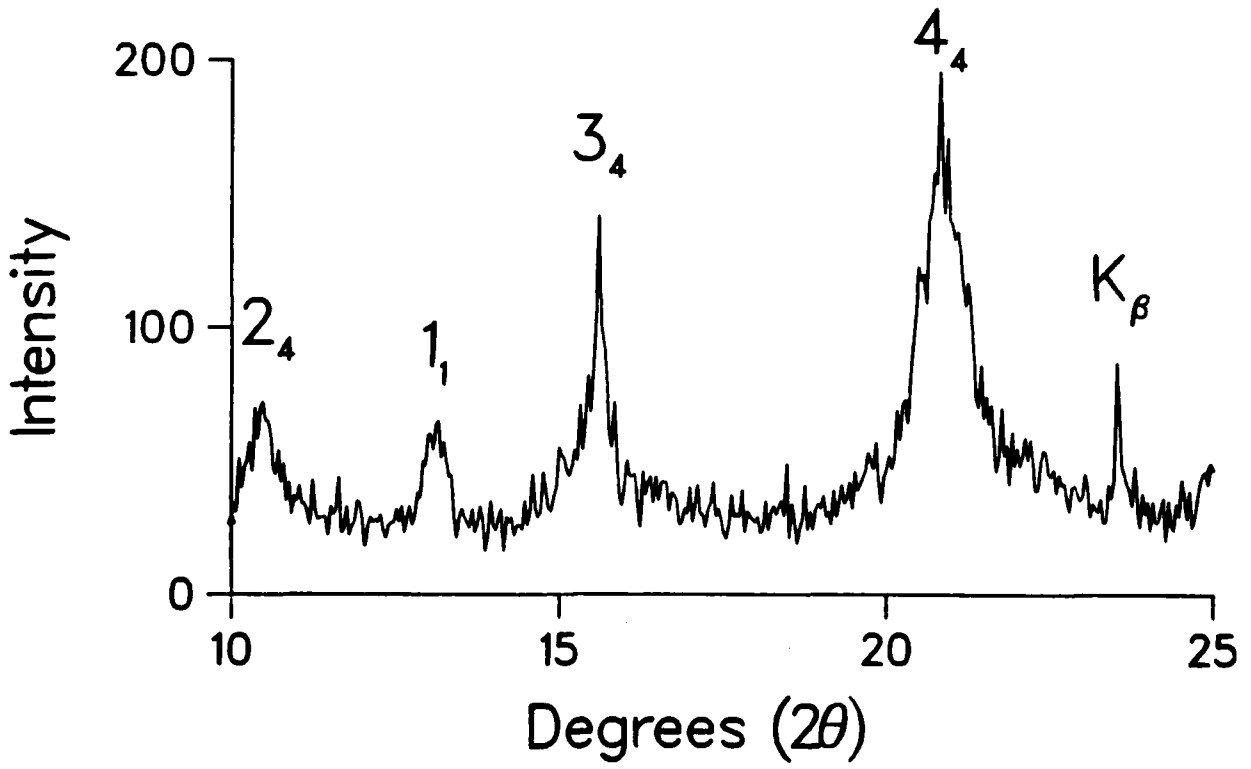
200
100
0
Intensity
2_4
1_1
3_4
4_4
K_β
10
15
20
25
Degrees (2θ)

b

Fig. 5

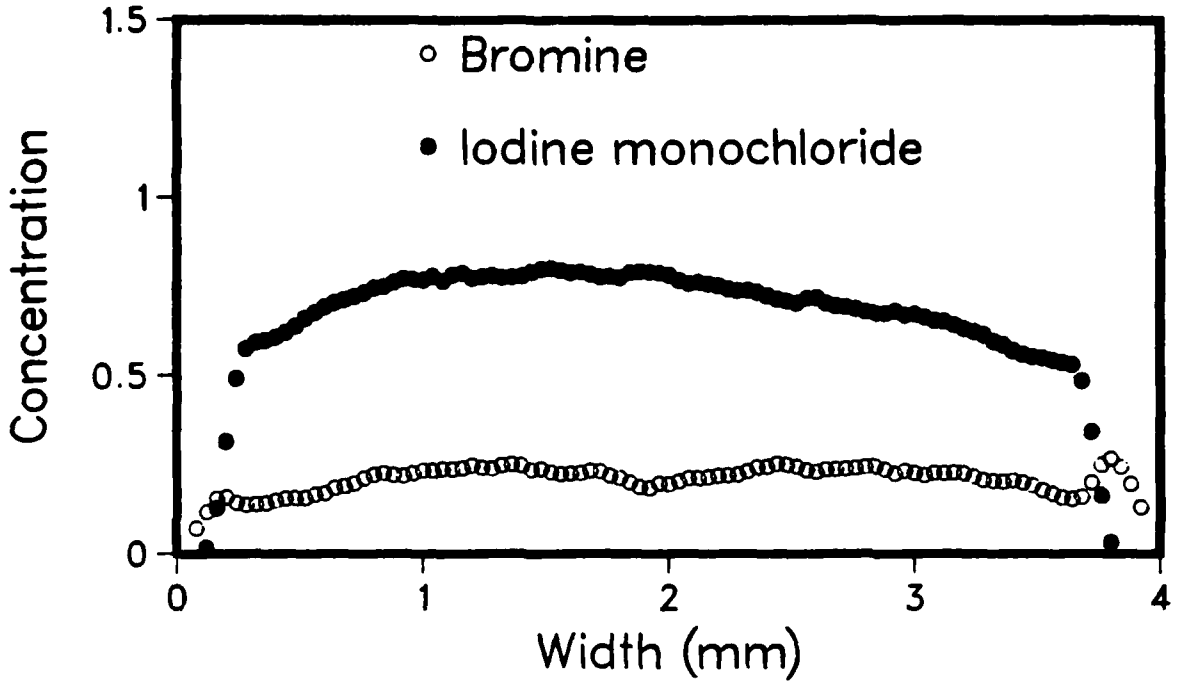
1.5
1
0.5
0
Concentration
Bromine
Iodine monochloride
0
1
2
3
4
Width (mm)

a

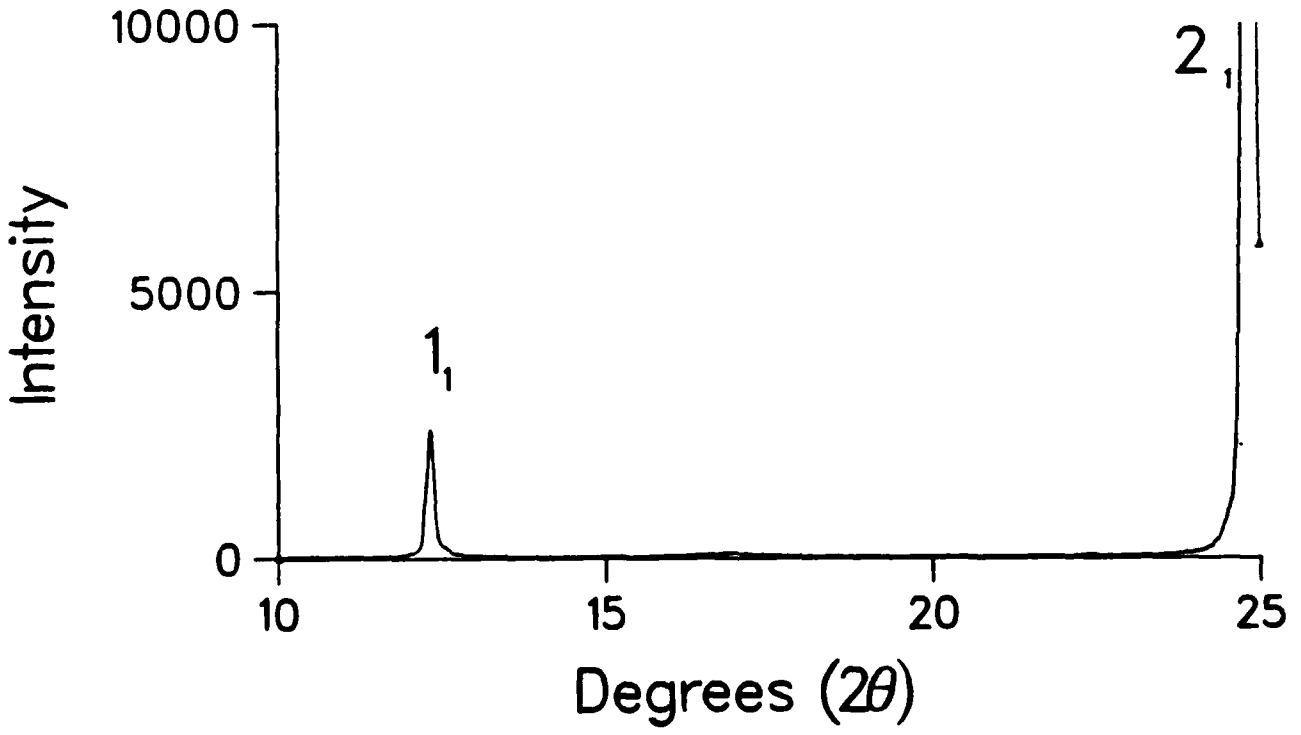
10000
5000
0
Intensity
1_1
2_1
10
15
20
25
Degrees (2θ)

b

Fig. 6

APPENDIX 2

To be submitted

KINETICS OF INTERCALATION OF BROMINE IN GRAPHITE*

S. H. Anderson and D. D. L. Chung

Department of Metallurgical Engineering and Materials Science

Carnegie-Mellon University

Pittsburgh, PA 15213

* Research sponsored by the Air Force Office of Scientific Research, Air Force Systems Command, USAF, under Grant No. AFOSR-78-3536. The United States Government is authorized to reproduce and distribute reprints for governmental purposes notwithstanding any copyright notation here.

ABSTRACT

X-ray diffraction, x-ray absorption, optical microscopy (in situ) and weight measurement were used to follow the process of intercalation of bromine in highly oriented pyrolytic-graphite. X-ray diffraction gave the stage distribution; x-ray absorption gave the intercalate concentration distribution, optical microscopy gave the location of the intercalate fronts; weight measurement gave the overall intercalate concentration. Multiple intercalate fronts were observed; the first front delineated a central region which was nearly pure graphite (except near the c-face surface) and an edge region which contained a very small amount of pure graphite, as previously suggested by results of surface profilometry. Bromine intercalation by immersion in pure bromine at room temperature appeared to involve direct formation of the final stage of 2 but the actual progressive stage decrease toward the final stage was clearly observed by changing the relative intercalation rates of different stages by either raising the temperature or by lowering the Br_2 concentration in the Br_2-CCl_4 solution containing the sample. For intercalation in pure bromine, the final stage was 2 from room temperature up to $\sim$72°C, 3 from $\sim$72°C to $\sim$140°C, and 4 above $\sim$140°C. The final stage decreased in discrete steps with increasing Br_2 concentration in the Br_2-CCl_4 solution containing the sample, but the rate of intercalation increased linearly with increasing Br_2 concentration in the solution. The first time-temperature-transformation (TTT) diagram describing the stage evolution during intercalation was obtained. The TTT-curves were C-shaped for the growth of each stage, suggesting diffusion-controlled kinetics at low temperatures and interface-controlled kinetics at high temperatures within the temperature regime for the particular stage to form.

1. INTRODUCTION

Accompanying the use of intercalated graphite as electrical conductors, catalysts, electrodes, etc. is the need for understanding the kinetics of intercalation of graphite. This understanding is also important for elucidating the mechanism of intercalation and the process of stage formation. This paper is concerned with the kinetics of intercalation of bromine in graphite. Bromine was the intercalate species chosen for this study because it is one of the most well-known intercalate species and the kinetics of bromine intercalation had been studied[1-14] more extensively than any of the other intercalate species.

The intercalation of graphite involves the transformation of graphite to a lamellar compound which exhibits a superlattice having a periodicity or stage number controlled by the intercalation condition. For example, a change in stage can result from a change in the vapor pressure of the intercalate in the case of vapor-phase intercalation. How does the superlattice form? Does the formation of a given final stage involve prior formation of a higher stage (e.g., stage 3 → stage 2 for a final stage of 2), or does the final stage develop at the onset of intercalation without prior formation of higher stages?

Before addressing this question of superlattice formation, it is necessary to note the difference between two intercalation procedures -- stepwise intercalation and one-step intercalation. Stepwise intercalation involves stepwise increase of the intercalate vapor pressure, such that equilibrium or quasi-equilibrium is achieved at a given vapor pressure before the vapor pressure is increased by a small step. Step-wise intercalation is usually used to obtain intercalation isotherms[15] and isobars[16, 17]. One step intercalation, also known as rapid intercalation[15], involves exposure of graphite directly to the intercalate

vapor at a chosen vapor pressure, which remains constant during the entire intercalation process. In order to investigate the step-wise intercalation process, it is necessary to investigate first the process within a single step. Therefore, one-step intercalation is more fundamental to the study of the kinetics of intercalation and this procedure is used in the present work.

Stepwise intercalation necessarily involves a decrease in the stage number as the vapor pressure is increased. However, does one-step intercalation also involve a decrease in the stage number before the final stage is completely formed? A progressive decrease in the stage number was observed by x-ray diffraction during one-step intercalation of HNO_3 at room temperature[18] and during one-step intercalation of K with the two-bulb method[19]; direct formation of the final stage without a progressive change in stage number was observed by x-ray diffraction during one-step intercalation of Br_2 at room temperature[15] and was also suggested by the variation of the magnetic anisotropy with temperature[7]. By performing x-ray diffraction after various times of one-step intercalation in liquid bromine at intercalation temperatures from 25°C to 50°C, Anderson and Chung[14] observed that direct formation of the final stage of 2 occurs in liquid bromine at low intercalation temperatures (25°C), whereas a progressive decrease in stage occurs at high intercalation temperatures (50°C). In this work, the dependence of the intercalation kinetics on temperature was studied systematically for temperatures ranging from 20°C to 140°C. The resulting time-temperature-transformation (TTT) diagram suggests that the reaction rate can be described by a solid-state reaction rate equation, which implies that the reaction rate is limited by diffusion at low temperatures and limited at high temperatures by a reaction free energy change ΔG, with a maximum rate at intermediate temperatures. The TTT-diagram suggests that intercalation in pure bromine to 2nd stage is diffusion-controlled to about $\sim$58°C and interface-controlled from $\sim$58° to $\sim$72°C, whereas 3rd stage growth is diffusion-controlled

to ∿110°C and interface-controlled from ∿110°C to ∿140°C.

By surface profilometry on the c-face during bromine intercalation of highly oriented pyrolytic graphite (HOPG) at room temperature, Bardhan and Chung[12] found that intercalation in saturated bromine vapor involves the movement of a sharp intercalate front, which results in a bucket-shaped surface profile that changes to a V-shaped profile when the fronts meet at the center of the sample. By using x-ray absorption to measure the intercalate concentration distribution and by using x-ray diffraction to measure the stage distribution during bromine intercalation of HOPG at room temperature, Anderson and Chung[14] found that the intercalate front indeed delineates the interface between a region of intercalate concentration close to that of the pure final stage and a region of very low intercalate concentration. In this work, the shape deformation observed ex situ by surface profilometry[12] was investigated in situ at room temperature by optical microscopy. The in situ observation was further made as a function of the mole fraction of Br_2 in the Br_2-CCl_4 solution above which the sample was located during vapor-phase intercalation. In addition, x-ray absorption and x-ray diffraction were used to follow the intercalate concentration distribution and the stage distribution during intercalation for various mole fractions of Br_2 in the Br_2-CCl_4 solution containing the sample. This systematic study of the dependence of the intercalation kinetics on the external intercalate concentration resulted in a "time-concentration-transformation" ("TCT") diagram for the stage formation process. This diagram shows that the intercalation rate increases with increasing external intercalation concentration. As a result, intercalation appeared to involve the direct formation of the final stage of 2 at high external intercalate concentrations, but a progressive stage decrease was clearly observed for low external intercalate concentrations.

2. EXPERIMENTAL TECHNIQUES

2.1 Materials

All samples were highly oriented pyrolytic graphite (HOPG) kindly provided by Union Carbide Corp. Intercalation was carried out in the presence of air by immersion in liquid bromine or a Br_2-CCl_4 solution of a controlled concentration (i.e., liquid-phase intercalation), or by exposure to the vapor above liquid bromine or a Br_2-CCl_4 solution (i.e., vapor-phase intercalation). Due to the volatility of bromine, the bromine concentration in a Br_2-CCl_4 solution was kept constant by renewing it periodically, at approximately 100-hour intervals. Room temperature vapor-phase intercalation was used during the in situ optical microscopic observation of the intercalate front. Liquid-phase intercalation was used during the ex situ x-ray absorption and x-ray diffraction measurements. The liquid-phase intercalation was carried out at various constant temperatures ranging from room temperatures to 140°C. Intercalation at temperatures above room temperature was performed by sealing the sample with liquid bromine in a Monel ampoule and placing the ampoule in a water bath at a controlled temperature. Thus, the sample and the liquid bromine were at the same temperature. Each ex situ x-ray run was performed after the sample had been removed from the solution and weighed. In the case of room temperature intercalation, the sample was returned to the solution for continued intercalation after each x-ray run. The time from the removal from the solution to the return to the solution was typically $\sim$40 min. In the case of intercalation at temperatures above room temperature, the sample was not allowed to be further intercalated after the ex situ x-ray analysis.

The samples used for optical microscopy were of size 2mm x 6mm in the basal plane. This rectangular shape was chosen in order to obtain nearly parallel intercalate fronts over most of the periphery of the sample surface perpendicular to the c-axis. The samples used for x-ray studies were typically of size 4mm x 12mm in the basal plane, with a typical thickness of ~0.3mm in the c-direction.

2.2 Optical Microscopy

Optical microscopy was performed in situ during vapor-phase intercalation at room temperature. The sample was positioned in a glass bottle containing a Br_2-CCl_4 solution such that the c-face was perpendicular to the incident light beam. The bottle was sealed and placed under an optical microscope. The sample surface was photographed in situ at different times of intercalation. As intercalation progressed, the part of the surface which had been deformed reflected light away from the sample normal, resulting in the appearance of dark bands on the surface where the intercalate front had reached.

2.3 X-ray Absorption

The x-ray absorption technique gives more information than the optical microscopic observation of the intercalate front. This is because the amount of x-ray absorbed is related to the bromine concentration. Due to the large difference in atomic mass between carbon and bromine, x-ray absorption gives a rather accurate determination of the bromine concentration. The absorption measurement was performed in the transmission geometry. Hence, the whole sample thickness was analyzed at any one time, irrespective of the surface topography.

The x-ray radiation used was CuKα. The x-ray beam was collimated by a slit of size 0.01mm x 2mm. The sample was mounted so that the middle

of its long edge intersected the beam. It was translated through the beam on a motor driven micrometer stage, such that the direction of translation was along the long edge of the sample. The transmitted beam intensity was measured as the total number of counts detected within a counting interval. Counting started before the beam impinged upon the sample and continued after the sample left the beam in order to determine the incident beam intensity. A 0.1mm receiving slit was located behind the sample. A graphite monochromator tuned to CuKα was located behind this slit.

2.4 X-ray Diffraction

X-ray diffraction was performed by using a θ-2θ x-ray powder diffractometer. The ooℓ diffraction pattern was obtained from the basal plane, with the rectangular cross-section of the x-ray beam perpendicular to the long edge of the sample. The CuKα radiation was used. For diffraction at selected areas of a sample, lead or tantalum foil was used to mask the area at which diffraction was not desired. For a typical sample of width 4mm, the diffraction pattern of the central 2-mm wide portion of the sample was obtained by masking the remaining regions near the two long edges of the sample. Similarly, the diffraction pattern of the two edge regions (each edge region being 1mm wide) was obtained by masking the central 2-mm wide portion of the sample. Diffraction patterns were typically taken for a 2θ range of 15 to 25°C. This range allowed the diffraction run to be obtained in a reasonable length of time while showing the strongest superlattice lines not coincident with the graphite lines. Though a monochromator was used, the graphite (002) line due to the Kβ radiation was quite pronounced. No attempt was made to measure the graphite (002) K_{α_1} line because its intensity was so high that it overloaded the detector.

To indicate the relative depths from the basal surface of different stages present within a sample during intercalation, diffraction patterns were obtained with both CuKα and MoKα radiations on a 12mm x 12mm x 0.15mm HOPG sample, which was intercalated in pure bromine at room temperature and removed for analysis intermittantly. The MoKα radiation, having a higher energy than CuKα, yields a greater penetration distance. Hence phases farther from the surface can contribute more to the diffraction pattern obtained with MoKα than is the case with CuKα. Selected area x-ray diffraction was also done on this sample; masking was such as to allow observation of either 4mm of the center region or 4mm of the two edge regions combined (i.e., 2mm of each edge region).

3. EXPERIMENTAL RESULTS

3.1 Shape Deformation

An indication of the progress of intercalation is the deformation of the sample shape or surface profile during intercalation. The shape deformation known as the "ash tray effect" accompanies the intercalation of graphite for most intercalates. This effect involves the sharp bending of the graphite layers at the intercalate front due to the large thickness increase in the region behind the intercalate front[12].

As the deformation of the basal surface does represent the presence of intercalation[14], we have used this deformation to observe in situ the growth of the intercalation compound by using an optical microscope. Due to the specular surface of HOPG, under perpendicular lighting, undeformed regions reflect the light back upon itself while deformed regions scatter the light out of the field of view. In short, flat regions are bright and bent regions are dark. Figure 1 shows optical micrographs of a sample after different times of intercalation at room temperature , together with the schematic surface profiles. Intercalation was performed at room temperature by exposure of the sample to the vapor above a 15 mole % solution of Br_2 in CCl_4, which produced a final stage of 4. By this optical method, the deformed region was quite sharply delineated and could be seen to propagate toward the center of the sample. Figure 2 is a plot of the width of the deformed (edge) region behind the intercalate front as a function of time during intercalation. It can be seen from Fig. 2 that the deformed region grew quickly initially, followed by a region where growth was of apparently constant velocity, in agreement with the results of ex situ surface profilometry[12]. The constant velocity suggests interface-controlled growth[11,12]. On the other hand, these data can be plotted as a function of the square root of time, as shown in Fig. 3. That this plot is quite linear suggests the intercalate

growth to be diffusion-controlled. Comparison of Fig. 2 and Fig. 3 indicates that the overall linear fit is better in Fig. 3, so that the diffusion-controlled mechanism is probably the case for this intercalation condition. However, based on these figures alone, the interface-controlled mechanism cannot be ruled out. To better elucidate the mechanism, a study of the temperature dependence of the intercalation rate was performed, as described in Section 3.4, where the TTT-diagram was found to support the diffusion-controlled mechanism for intercalation at room temperature.

The dependence of the growth rate on the intercalate concentration in the Br_2-CCl_4 solution was investigated systematically by in situ optical microscopy. The results are given in Section 3.3.

3.2 Intercalate Concentration Distribution and Stage Distribution

Shown in Fig. 4(a) is the intercalate concentration profile across the c-face obtained after 297 hr of room temperature intercalation in liquid bromine. This intercalation condition yields a final stage of 2. The sample was of size 12mm x 12mm x 0.15mm and weighed 50 mg before intercalation. The intercalation was interrupted intermittantly for x-ray analysis. The average weight loss due to intercalate desorption was 2 mg during each interruption, which typically lasted $\sim$1.5 hr. The vertical axis in Fig. 4(a) describes the intercalate concentration in terms of the stage number. For example, the intercalate concentration corresponding to that of pure stage 2 is labeled "2" in the vertical axis; similarly the intercalate concentration corresponding to that of pure stage 3 is labeled "3" in that axis. Figure 4 (a) shows that the concentration changed from

a region of nearly pure stage 2 to a region of negligible intercalate concentration over a narrow spatial region. This front moved inward as intercalation proceeded. This is consistent with the surface deformation of the sample during intercalation. X-ray diffraction patterns obtained from the "center" and "edge" regions are shown in Fig. 4(b) and (c) for CuKα and MoKα radiations, respectively. The widths of the center and edge regions are indicated in Fig. 4(a). Each diffraction peak in Fig. 4(b) and (c) is labeled by the ℓ index of the (00ℓ) Miller indices, with the subscript indicating the stage (G indicating graphite) and the superscript, if present, indicating the $K\alpha_1$, $K\alpha_2$ or $K\beta$ component. The difference between Fig. 4(b) and (c) illustrates the depth dependence of the stage distribution. Figure 4(b) and (c) show that the edge region is predominantly stage 2, whereas the center region is predominantly graphite, except that the center region near the surface has a considerable amount of stage 2. In other words, there is a significant depth dependence of the stage distribution in the center region.

3.3 Dependence on External Intercalate Concentration

The dependence of the intercalation kinetics on the Br_2 concentration in the Br_2-CCl_4 solution was systematically investigated by (i) weight uptake measurement of the overall intercalate concentration, (ii) optical microscopic observation of the intercalate front position, (iii) x-ray absorption observation of the front position , and (iv) x-ray diffraction observation of the stage formation.

Shown in Fig. 5 is the plot of weight uptake against the square root of time during room temperature intercalation by immersion of the samples in Br_2-CCl_4 solutions of various concentrations ranging from 5 mol % Br_2 to 50 mol % Br_2. The weight measurement was carried out ex situ by using

a Perkin-Elmer AD-2Z Autobalance. X-ray analysis was performed on the samples immediately after each weight measurement. The curves in Fig. 5 are quite linear for the first half of the time axis and they deviate from linearity at long intercalation times. This deviation from linearity is attributed to be due to the meeting of the intercalate fronts at the center of the sample. When the fronts met, the intercalation rate changed. The meeting of the fronts was indeed observed by x-ray absorption at roughly the times when the weight curves deviate from linearity.

Shown in Fig. 6 are representative intercalate concentration profiles (obtained by x-ray absorption) and x-ray diffraction patterns of the edge and center regions at different times during intercalation by immersion in a 50 mol % Br_2 Br_2-CCl_4 solution at room temperature. After 34 hr of intercalation, there was not much evidence for appreciable intercalation in the center region, which was ahead of the intercalate front, although some weak stage 3 and stage 4 superlattice (00ℓ) lines were observed. On the other hand, the edge region was mainly stage 2, which coexisted with smaller quantities of stage 3, stage 4 and graphite. After 210 hr of intercalation, the fronts had met, the stage 4 and graphite components in the edge region had disappeared, the stage 4 and stage 3 components in the center region had grown, a stage 2 component had appeared in the center region, and the graphite component had greatly diminished in the center region. After 1187 hr of intercalation, the concentration profile was flat, indicating that intercalation was essentially complete. Furthermore, both the edge and center regions were almost pure stage 2, which was the final stage for this intercalation condition. In addition to the major intercalate front (also referred to as "the first front") ahead of which was mainly pure graphite, a second front was observed behind the first front as shown in Fig. 6. Both the

first and second fronts moved toward the center during intercalation, but they progressed at different rates. Of interest is that the shoulder in the concentration profile between the first and second fronts occurred at a concentration roughly corresponding to that of pure stage 3. Also note that the maximum in each concentration profile approximately corresponds to the concentration of pure stage 2. It is probable that the shoulder was due to the completion of intercalating the whole sample thickness to stage 3, so that the region between the maximum and the shoulder consisted of a mixture of stages 2 and 3. However, x-ray diffraction at this small area was not carried out to confirm this hypothesis. In some cases, a third front was also observed, though it was not as clear as the first and second fronts.

Representative concentration profiles and diffraction patterns obtained after 600 hr of intercalation in various concentrations of Br_2-CCl_4 solutions at room temperature are shown in Fig. 7. After 600 hr of intercalation in a 15 mol % Br_2 solution, stage 4 was the main phase present. Because the first fronts had not met, pure graphite was also present in the center region. After 600 hr of intercalation in a 25 mol % Br_2 solution, stage 3 was dominant in the edge region and stage 4 was dominant in the center region. Because the fronts had met, pure graphite was absent. After 600 hr of intercalation in a 30 mol % Br_2 solution, stage 3 was dominant in both the center and the edge regions. Note the presence of the second front in Fig. 7. The second front was clearest for external intercalate concentrations near the limits for giving a certain final stage, such as 40 mol % Br_2 (final stage = 2) and 15 mol % Br_2 (final stage = 3). The latter is one of the concentrations shown in Fig. 7. Refer to Table 2 for these limits.

The stage evolution during intercalation is illustrated in Table 1 for two representative external intercalate concentrations (50 and 20 mol % Br_2). The table lists the stages present in the edge and center regions

at various intercalation times, together with the percentage weight gain at each time. The symbol denoting the main phase (indicated by the stage number or G for graphite) was underlined. Note that the center region was always taken as the central 2-mm wide region, irrespective of the front position. For the case of the 50 mol % Br_2 solution, stage 2 was the final stage, which was attained as a pure stage after 663-1182 hr of intercalation. Before this, stages 3 and 4 and pure graphite were also observed. Stage 2 was the dominant stage at all times in the edge region, whereas stages 4, 3 and 2 were successively dominant in the center region. The pure graphite phase was dominant in the edge region for the first 15-24 hr of intercalation, whereas it was dominant in the center region for the first 140-210 hr of intercalation. For the case of the 20 mol % Br_2 solution, stage 3 was the final stage, which was attained as a pure stage after 667-1812 hr of intercalation. Before this, stages 4 and 5 and pure graphite were also observed. Pure graphite, stage 4 and stage 3 were successively the dominant stage in both the edge and center regions. However, the pure graphite phase was dominant in the edge region for the first 63-66 hr of intercalation, whereas it was dominant in the center region for the first 355-667 hr of intercalation.

Table 2 compares the stages obtained after 468-689 hr of intercalation for various external intercalate concentrations. Also indicated in Table 2 are the final stages for the various concentrations. For a final stage of 2, concentrations above ~40 mol % Br_2 is required; for a final stage of 3, concentrations from 15 to 30 mol % Br_2 are appropriate.

Both Table 1 and Fig. 6 show that the intercalation involved a progressive decrease in the stage number rather than the direct formation of the final stage. However, the higher the external intercalate concentration, the more it appears to be direct final stage formation, as can be seen in Tables 1 and 2 and the TCT-diagram shown in Fig. 8.

The dependence of the intercalation rate on the external intercalate concentration is summarized in the TCT-diagram in Fig. 8. The curves there give the times for a certain stage to start forming and to finish forming, so that the curves separate regions in the diagram corresponding to the co-existence of different combinations of phases, which are indicated by the stage number or G for the pure graphite phase. To see how the phasesevolve during intercalation at a particular external intercalate concentration, the TCT-diagram should be read horizontally from left to right. The normalized time in the horizontal scale in Fig. 8 is the time divided by the square of the width behind the first front, so that its unit is s/cm^2. For example, at a mole fraction of 0.2 for the Br_2 concentration in the Br_2-CCl_4 solution, stage 4 began forming after $\sim 7 \times 10^4$ s/cm^2, stage 3 began forming after $\sim 2 \times 10^5$ s/cm^2, stage 4 finished forming after $\sim 4 \times 10^7$ s/cm^2 and stage 3 finished forming after $\sim 3 \times 10^8$ s/cm^2. As a result, pure graphite was the only phase observed before $\sim 7 \times 10^4$ s/cm^2, stage 4 and graphite coexisted from $\sim 7 \times 10^4$ s/cm^2 to $\sim 2 \times 10^5$ s/cm^2, stage 3, stage 4 and graphite coexisted from $\sim 2 \times 10^5$ s/cm^2 to $\sim 4 \times 10^7$ s/cm^2, stages 3 and 4 coexisted (without graphite) from $\sim 4 \times 10^7$ s/cm^2 to $\sim 3 \times 10^8$ s/cm^2, and stage 3 (the final stage) was present alone after $\sim 3 \times 10^8$ s/cm^2, which was when intercalation was complete. The horizontal bands in Fig. 8 separate the different ranges of mole fraction which give different final stages. These ranges are also given in Table 3. Because of the significant error involved in measuring the time when a certain stage higher than the final stage just began to form, the error bars for such data points probably extend to the left more than indicated, as implied by the arrows pointing to the left for such error bars in Fig. 8. The other curves are more accurate; each error bar covers the data points obtained from the results of x-ray diffraction, x-ray absorption and optical microscopy.

The x-ray absorption observation of the intercalate fronts was made for various external intercalate concentrations from 0.05 to 1.00 in Br_2 mole fractions. Figure 9 shows the plot of the square of the width of the region behind the first front as a function of time during intercalation for various external intercalate concentrations. This plot yielded quite good linear fits to each set of data points, whereas a plot of the width (not squared) versus time did not give good linear fits. This is consistent with the optical microscopy results shown in Fig. 2 and 3. Hence, a parabolic growth rate seems to apply to the progress of the first front, indicating a diffusion-controlled growth. On the other hand, the second front does not follow a parabolic rate law, but rather shows a better fit to a linear rate. Because of the large scatter of the data for the second front compared to the first front, the rate of movement of the second front did not allow quantitative analysis. The slope of the plot in Fig. 9 gives the growth rate, which is the same as 4 times the diffusion coefficient D. This rate is plotted against the external intercalate concentration in Fig. 10. Included in Fig. 10 are growth rates determined by x-ray absorption and optical microscopy. As mentioned at the end of Section 3.1 optical microscopy observation of the front position was made at various external intercalate concentrations. Figure 10 shows that the dependence of the growth rate on the concentration is approximately linear. This dependence suggests that the intercalation reaction may be best understood as a reaction involving a single intercalate layer, while staging is more or less imposed by other constraints in the system, such as elastic or electrostatic stresses.

Based on the diffusion-controlled mechanism for the intercalation process for all the external intercalate concentrations at room temperature (23°C), we calculated the diffusion coefficients D from results of optical microscopy, x-ray absorption and weight measurement. The D values are

listed in Table 3 for various external intercalate concentrations. The D values obtained from the three experimental techniques are in good agreement with one another. Moreover, the D value of 2.36×10^{-8} cm^2/s which we obtained for pure bromine liquid at 23°C is in close agreement with the D value of 2.45×10^{-8} cm^2/s reported by Dowell and Badorrek[9] for near-saturated bromine vapor at 30°C. Table 3 shows that D increases with increasing external intercalate concentration.

3.4 Dependence on Temperature

X-ray diffraction and x-ray absorption were also used ex situ to follow the intercalate concentration profiles and stage evolution during intercalation at various constant temperatures from room temperature to 140°C. Intercalation was performed by immersion of the sample in pure bromine sealed in a Monel ampoule, such that the sample and bromine were at the same temperature, which was controlled by a water bath.

Shown in Fig. 11 are a series of x-ray diffraction patterns obtained after 2 hr of Br_2 intercalation at various temperatures toward a final stage of 2. Samples were intercalated in liquid bromine. They were 4 mm x 14 mm x 0.5 mm and mounted so that the full 4 mm width was in the x-ray beam. Due to the deformation caused by intercalation, quantitative intensity measurements could not be made. Nonetheless, the dependence on temperature can be clearly seen in Fig. 11. At 25°C, essentially only stage 2 was observed after 2 hr; above 30°C, increasing amounts of stage 3 were observed, till at 50°C, no stage 2 peak was evident after 2 hr. However, the final stage was pure stage 2 for all the temperatures from 25°C to 50°C, as shown by x-ray diffraction after a week of intercalation. This dependence on temperature is further illustrated in Fig. 12, where the relative integrated intensities of the stage 2 (003) peak and the stage 3 (004) peak after 2 hr of intercalation are shown as a function of the temperature. Therefore,

the higher the intercalation temperature, the faster the kinetics of stage 3 formation compared to that of stage 2 formation, even though the final stage is 2 for all these temperatures.

We have also allowed samples (4.5 x 12 mm; thickness: 0.1 - 0.25 mm) to be intercalated in liquid bromine for 2 hr at 72°C, 81°C, 90°C and 100°C. Note that the intercalation conditions are the same as those used in Fig. 11 except that these temperatures are higher. After 2 hr of intercalation at 72°C, a weight increase of 24 %(1.9 mole % Br_2) was observed; after 2 hr of intercalation at 81°C, a weight incrased of 34 % (2.6 mole % Br_2) was observed; after 2 hr of intercalation at 90°C, a weight increase of 43 % (3.3 mole % Br_2) was observed; after 2 hr of intercalation at 100°C, a weight increase of 54 % (4.1 mole % Br_2) was observed. Shown in Fig. 13 are superlattice x-ray diffraction peaks obtained at the region behind the intercalate front (the edge region) by masking the center region with a 3 mm wide lead foil for the 72°C sample and with a 2 mm wide lead foil for the 81°C and 90°C samples. No mask was used for the 100°C sample. Corresponding intercalate concentration profiles across the whole sample width obtained by x-ray absorption are shown in Fig. 14, which indicates that the intercalation rate increased with increasing temperature and that intercalation was close to completion after 2 hr of intercalation at 100°C. Formation of stage 4 in addition to the final stage of 3 was observed after 2 hr of intercalation at 72, 81 and 90°C. Figure 13 shows that the higher was the temperature, the smaller was the proportion of the stage 4 component. This trend is a consequence of the fact that the stage 3 was the final stage and that the intercalation rate increased with increasing temperature, so that, after 2 hr of intercalation, intercalation was far from complete at 72°C but was relatively close to completion at 100°C, as shown by the concentration profiles in Fig. 14. The final stage was pure stage 3 for all the temperatures from 72°C to 100°C, as shown by x-ray

diffraction after about 2 weeks of intercalation.

The relative integrated intensities of the stage 3 (003) peak, the stage 4 (004) peak and the graphite (002) Kβ peak after 1 hr of intercalation are shown in Fig. 15. These particular superlattice lines were chosen for these stages because they were strong and well-resolved from one another. It should be emphasized that these intensity data only give qualitative trends of the phase quantities as a function of the temperature. Separately indicated in Fig. 15 are the relative intensities obtained in the center region and the edge region; the center region was the central 2-mm wide region whereas the edge region was the remaining areas of the 4-mm wide sample. The final stage was 3 at all these temperatures. It was attained as a pure stage for both the center and edge regions after 1 hr of intercalation at 100°C. The intermediate phase of stage 4 was observed to be strongest at an intermediate time not too close to the beginning nor the completion of intercalation. As a result, it was strongest after 1 hr of intercalation at 80°C compared to the other temperatures shown in Fig. 15. The graphite phase decreased while stage 3 increased with increasing temperature because the intercalation rate increased with increasing temperature.

Similar measurements were made after various intercalation times at various temperatures. The results are summarized in the form of a TTT-diagram in Fig. 16. The diagram shows the phase evolution as a function of time during intercalation at various constant temperatures. The horizontal bands mark the temperature limits for obtaining particular final stages. For a final stage of 2, the temperature should be below ∿72°C; for a final stage of 3, the temperature should be between ∿72°C and ∿120°C; for a final stage of 4, the temperature should be above ∿120°C. Note that intercalation was by immersion in pure bromine at all temperatures. That the final stage increased by increasing the temperature was predicted by the reaction enthalpies and entropies measured by Aaronson and Salzano[20] for graphite-alkali metals

and by Sasa[21] for graphite-bromine, and was experimentally shown by Bach et al.[22] for the graphite-bromine by weight measurement.

Fig. 16 shows that the rate of stage 2 growth increases with increasing temperature from ∿20°C to ∿58°C, suggesting diffusion-controlled kinetics for this temperature range whereas it decreases with increasing temperature from ∿58°C to ∿72°C (∿72°C is the upper temperature limit for stage 2 stability), suggesting interface-controlled kinetics for this temperature range. A similar C-shaped TTT-curve was obtained for the time for the completion of growth of stage 3, indicating diffusion-controlled kinetics at ∿72 - ∿110°C and interface-controlled kinetics at ∿110 - ∿120°C. Of interest is that the C-shaped curves for stage 2 and stage 3 completion are roughly parallel to each other for both temperature regimes.

4. DISCUSSION

Experimentally there has not been much work done in determining the rate controlling parameters involved in intercalation. Hooley et al[1-3], Dowell[8] and Ubbelohde et al[4-6] have investigated the effects of pressure and graphite structure on the reaction rate of bromine intercalation, but until rather recently little other work has been done other than to establish conditions whereby a given intercalation compound can be formed, which other invesigators then use with apparently small concern for optimizing the reaction conditions. Nonetheless, some work has been done in investigating intercalation kinetics and in a related vein, thermodynamics involved with intercalation. Aronson et al[20] have determined a phase diagram for the alkali metals based on electrochemically determined enthalpies and entropies of reaction. Sasa[15] has investigated the graphite-Br_2 system and determined entropy and enthalpy for the reaction forming second stage graphite bromine from third stage. Metz and Seimsgluss[23], in the case of $FeCl_3$, and Dowell[9], for Br_2, HNO_3 and $PdCl_2$, have investigated rates of intercation to determine diffusion coefficients. Bardhan et al[11,12] have investigated the kinetics of bromine intercalation and interpreted their findings in terms of an interface-controlled reaction. Flandrois et al[24] have carefully investigated the kinetics of intercalation in the $NiCl_2$ system. Hamwi[19] et al have elegantly followed the course of intercalation of a graphite-potassium compound.

The overall results from these experiments can allow one to draw some interesting conclusions. Diffusion appears to be quite rapid, based on measurement in the case of Br_2, HNO_3 and $PdCl_2$[9], and suggested in the metal halide compounds by the observation that a uniform intercalate concentration is established in quite a short time in terms of the amount of intercalate which has been absorbed[9,23,24]. In several cases, i.e., HNO_3[18], $FeCl_3$[23], and K[19], it is observed that several stages are formed before the final lowest stage. In fact, in the study of K, Hamwi et al[19] were unable to positively identify the highest initial stage which formed. $NiCl_2$[24] and Br_2[15] have been reported to directly form the lowest stage, 2, upon intercalation. Recently however, reports have been made that in the case of Br_2, some higher stages are formed prior to the formation of second stage compound.[14] In this work we have found that x-ray diffraction of the inner, apparently unintercalated region does indicate the presence of higher stages though x-ray absorption suggests that the amount present is very small. In the studies made on K[19], $FeCl_3$[23] and $NiCl_2$[24], all the investigators came to the conclusion that the reaction was being controlled by processes outside the graphite, probably condensation and adsorption of intercalate onto the graphite surface. The kinetics of bromine intercalation appears to be limited by either diffusion or reaction within the graphite. While the difference in rate controlling step is most likely the result of the low partial pressures involved in the intercalation of the alkali metals and metal halides, it may be a

consequence of the difference between an electron acceptor and an electron donor. However, we have compared the relative reaction rates of graphite in liquid nitric acid and nitric acid vapor and have found that the reaction rate increased by about a factor of 10 in the liquid. Furthermore, 001 diffraction patterns obtained from the sample intercalated in liquid nitric acid were similar to graphite-bromine diffraction patterns in that the final stage was evident at early stages of the reaction. In the sample intercalated in nitric acid vapor this was not the case; higher than final stages predominated over a much greater fraction of the total intercalation time. These observations suggest that, in general, the rate-controlling step can be diffusion or reaction within the sample, provided the intercalate concentration at the surface of the graphite is large enough.

While several stages are present in the case of Br_2 intercalation, a contrast should be made with the sort of progressive staging observed in K. In K, the staging is a rather deliberate situation, even to the extent of having plateaus in the intercalate uptake versus time curves, which indicate that the one stage has nearly saturated the sample before the next stage appreciably has begun. Such is not the case for Br_2 where a well-defined intercalate front exists. Rather, weight versus time curves are smooth, and the concentration profiles indicate shoulders in the opposite sense, i.e., growth of the next lower stage is evident well before intercalation of the previous stage is complete. Furthermore the instance where a difference in stages is pronounced are those at high temperatures and low concentrations, instances where the reaction rate of the lowest stage may be expected to decrease for thermodynamic reasons. This is less clear in the case of low concentrations since the diffusion rate is also decreasing as a function of concentration. At high temperatures, however, the increase in the diffusion rate is quite dramatic while the decrease in reaction rate for a low stage is equally apparent. It may be pointed out that the shape of the C-curves, i.e., the sharpness of them, indicates that, for most temperatures, the reaction rate at the internal interface is considerably faster than the diffusion step.

5. CONCLUSION

This paper gives the first TTT-diagram for the intercalation of graphite. The TTT-curves were C-shaped. Within the temperature range where a given stage was stable, the reaction rate increased with increasing temperature at low temperatures (suggesting a diffusion-controlled mechanism) and decreased with increasing temperature at high termperatures (suggesting an interface-controlled mechanism). Also reported is a TCT-diagram describing the dependence of the intercalation kinetics on the external intercalate concentration (i.e., Br_2 concentration in the Br_2-CCl_4 solution containing the sample). The final stage decreased in discrete steps with increasing Br_2 concentration in the Br_2-CCl_4 solution containing the sample, but the

rate of intercalation increased linearly with increasing Br_2 concentration in the solution. Although bromine intercalation by immersion in pure bromine at room temperature appeared to involve direct formation of the final stage of 2, the actual progressive stage decrease toward the final stage was clearly observed by altering the relative intercalation rates of differentstages by either raising the temperature or by lowering the Br_2 concentration in the Br_2-CCl_4 solution containing the sample. The intercalate front first observed by surface profilometry[13] was found by x-ray diffraction and x-ray absorption to delineate a central region which was nearly pure graphite (except near the c-face surface) and an edge region which contained a very small amount of pure graphite.

REFERENCES

1. J. G. Hooley, W. P. Garby and J. Valentin, Carbon 3, 7 (1965).

2. J. G. Hooley, and J. L. Smee, Carbon 2, 135 (1964).

3. J. G. Hooley, Carbon 10, 155 (1972).

4. G. A. Saunders, A. R. Ubbelohde and D. A. Young, Proc. R. Soc. London, Ser. A, 271, 499 (1963)

5. G. A. Saunders, A. R. Ubbelohde and D. A. Young, Proc. R. Soc. London, Ser. A, 271, 512 (1963).

6. A. R. Ubbelohde, Carbon 10, 201 (1972).

7. A. Marchand, J. C. Rouillon and M. H. De Macuzo, Proc. 25th Int. Meeting of Societé de Chimie Physique, DIJON, July 1974, Elsevier, p. 242 (1975).

8. M. B. Dowell, Mater. Sci. Eng. 31, 129 (1977).

9. M. B. Dowell and D. S. Badorrek, Carbon 16, 241 (1978).

10. J. G. Hooley, Carbon 18, 83 (1980).

11. K. K. Bardhan and D. D. L. Chung, Carbon 18, 303 (1980).

12. K. K. Bardhan and D. D. L. Chung, Carbon 18, 313 (1980).

13. K. K. Bardhan, J. C. Wu, J. S. Culik, S. H. Anderson and D. D. L. Chung, Synth. Met. 2, 57 (1980).

14. S. H. Anderson and D. D. L. Chung, Ext. Abst. Program -- Bienn. Conf. Carbon 15, 361 (1981).

15. T. Sasa, Y. Takahashi, and T. Mukaibo, Carbon 9, 407 (1971).

16. A. Hérold, Bull. Soc. Chim. 999 (1955).

17. D. E. Nixon and G. S. Parry, J. Phys. D 1, 291 (1968).

18. D. E. Nixon, G. S. Parry, and A. R. Ubbelohde, Proc. R. Soc. (London) A291, 324 (1966).

19. A. Hamwi, P. Touzain, L. Bonnetain, A. Boeuf, A. Freund, and C. Riekel, Proceedings of the 3rd International Carbon Conference, Baden-Baden, Germany, July 1980; Mater. Sci. Eng. 57, 161 (1983).

20. S. Aronson, F. J. Salzano, and D. Bellafiore, J. Chem. Phys. 49, 434 (1968).

21. T Sasa, Carbon 11, 497 (1973).

22. B. Bach, M. Bagouin, F. Bloc and A. Herold, Compte Rend., Acad. Sci. (Series C) 257, 681 (1963).

23. W. Metz and L. Siemsgluss, Mat. Sci. Eng.,31,119 (1977).

24. S. Flandrois, J. M. Masson, J. C. Rouillon, J. Gaultier and C. Hauw Synth. Met., 3, 1, (1981).

Table 1 Stage evolution during intercalation for two representative external intercalate concentrations

Mole Fraction Br_2 in Br_2 - CCl_4	Time (hr)	Stages Present		Percent Weight Gain $(\frac{\Delta w}{w_i})$
		Edge	Center	
0.5	15	3 4 G	3 4 G	20
	24	2 3 4 G	2 3 4 G	23
	34	2 3 4 G	2 3 4 G	27
	64	2 3 4	2 3 4 G	34
	114	2 3 4	2 3 4 G	42
	140	2 3 4	2 3 4 G	46
	210	2 3	2 3 4 G	55
	308	2 3	2 3	63
	356	2 3	2 3 4	66
	663	2	2 3	77
	1182	2	2	81
0.2	40	4 G	4 G	16
	46	4 G	4 5 G	17
	63	4 G	4 5 G	18
	66	3 4 G	4 5 G	19
	119	3 4 5	4 5 G	24
	163	3 4	3 4 5 G	27
	311	3 4	3 4 5 G	34
	355	3 4	3 4 5 G	35
	667	3 4	3 4	43
	1812	3	3	53

Table 2 Stages present after 468-689 hr of intercalation for various external intercalate concentrations at 23°C.

Mole fraction Br_2 in Br_2-CCl_4	Final Stage	Stages Present		Percent Weight gain ($\Delta w/w_i$)	Time
		Edge	Center		
0.05	/	6 G	6 G	5	468
0.10	4	4 5	4 6 G	26	491
0.15	3	3 4	3 4 5 G	/	689
0.20	3	3 4	3 4	43	667
0.25	3	3 4	3 4	45	666
0.30	3	3	3 4	50	663
0.40	2	2 3	2 3	63	662
0.50	2	2	2 3	77	663

Table 3 Diffusion coefficients for liquid-phase bromine intercalation at 23°C

Mole Fraction Br_2 in Br_2-CCl_4	Diffusion Coefficient ($10^{-9}cm^2/s$)		
	Optical Microscopy	X-ray Absorption	Weight Increase
1.00	23.6		
0.80	26.4		
0.65	17.2		
0.50		10.83	13.14
0.40		9.18	8.24
0.30		6.75	7.59
0.25	6.35	4.28	5.06
0.20		5.00	4.44
0.15	2.78	3.25	
0.10		1.67	2.68
0.05		0.213	0.250

FIGURE CAPTIONS

Fig. 1 In situ optical micrographs and schematic surface profiles of a sample after different times of intercalation at room temperature.

Fig. 2 Width of the deformed region behind the intercalate front versus time during intercalation.

Fig. 3 Width of the deformed region behind the intercalate front versus the square root of time during intercalation.

Fig. 4 X-ray absorption profile and x-ray diffraction patterns of the edge and center regions obtained with CuKα and MoKα radiations after 297 hr of room temperature intercalation in liquid bromine. Each diffraction peak is labeled by the ℓ index of the (00ℓ) Miller indices, with the subscript indicating the stage (G indicating graphite) and the superscript, if present, indicating the $K\alpha_1$,$K\alpha_2$ or Kβ component.

Fig. 5 Percentage weight increases versus the square root of time during room temperature intercalation in Br_2-CCl_4 solutions of various Br_2 concentrations.

Fig. 6 X-ray absorption profiles and x-ray diffraction patterns of the edge and center regions at different times during intercalation by immersion in a 50 mol % Br_2 Br_2-CCl_4 solution at room temperature.

Fig. 7 X-ray absorption profiles and x-ray diffraction patterns of the edge and center regions obtained after 600 hr of intercalation in various constant concentrations of Br_2-CCl_4 solutions at room temperature.

Fig. 8 Time-concentration-transformation (TCT) diagram, showing the times for a given stage to start forming and to finish forming for various external intercalate concentrations. The phases present are indicated by the stage numbers and the symbol G for graphite. The horizontal scale indicates the time divided by the square of the width of the region behind the first front.

Fig. 9 The square of the width of the region behind the first front versus time during intercalation for various external intercalate concentrations.

Fig. 10 The growth rate (slope of Fig. 9) versus the external intercalate concentration.

Fig. 11 X-ray diffraction patterns obtained after 2 hr of intercalation in liquid bromine at various temperatures. The final stage was 2.

Fig. 12 Relative integrated intensities of the stage 2 (003) peak and the stage 3 (004) peak after 2 hr of intercalation as a function of temperature. The final stage was 2.

Fig. 13 Superlattice x-ray diffraction peaks obtained at the region behind the intercalate front after 2 hr of intercalation at various temperatures. A: 72°C, B: 81°C, C: 90°C, D: 100°C. The final stage was 3.

Fig. 14 X-ray absorption profiles obtained after 2 hr of intercalation at various temperatures. A: 72°C, B: 81°C, C: 90°C, D: 100°C. The final stage was 3.

Fig. 15 Relative integrated intensities of the stage 3 (003), stage 4 (004) and graphite (002) Kβ peak after 1 hr of intercalation as a function of temperature. Stage 3, stage 4 and graphite are indicated by 3, 4 and G, respectively.The contribution due to the edge region is shown by the solid bars; that due to the center region is shown by the empty bars.

Fog. 16 Time-temperature-transformation (TTT) diagram showing the times for a given stage to start forming and to finish forming for various isothermal temperatures. The phases present are indicated by the stage numbers and the symbol G for graphite. The horizontal scale indicates the time divided by the square of the width of the region behind the first front.

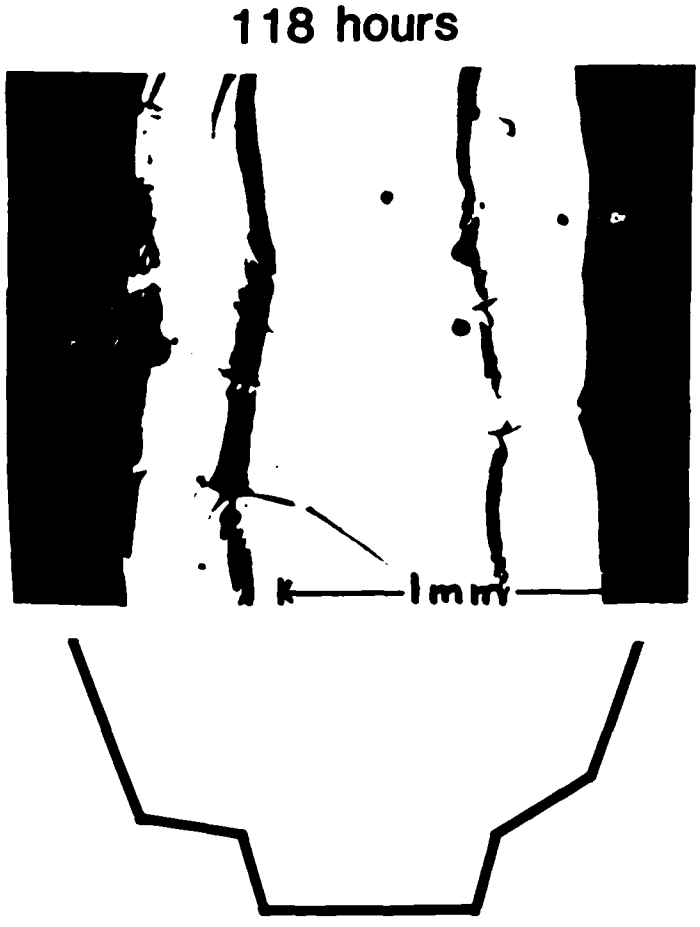

Fig. 1

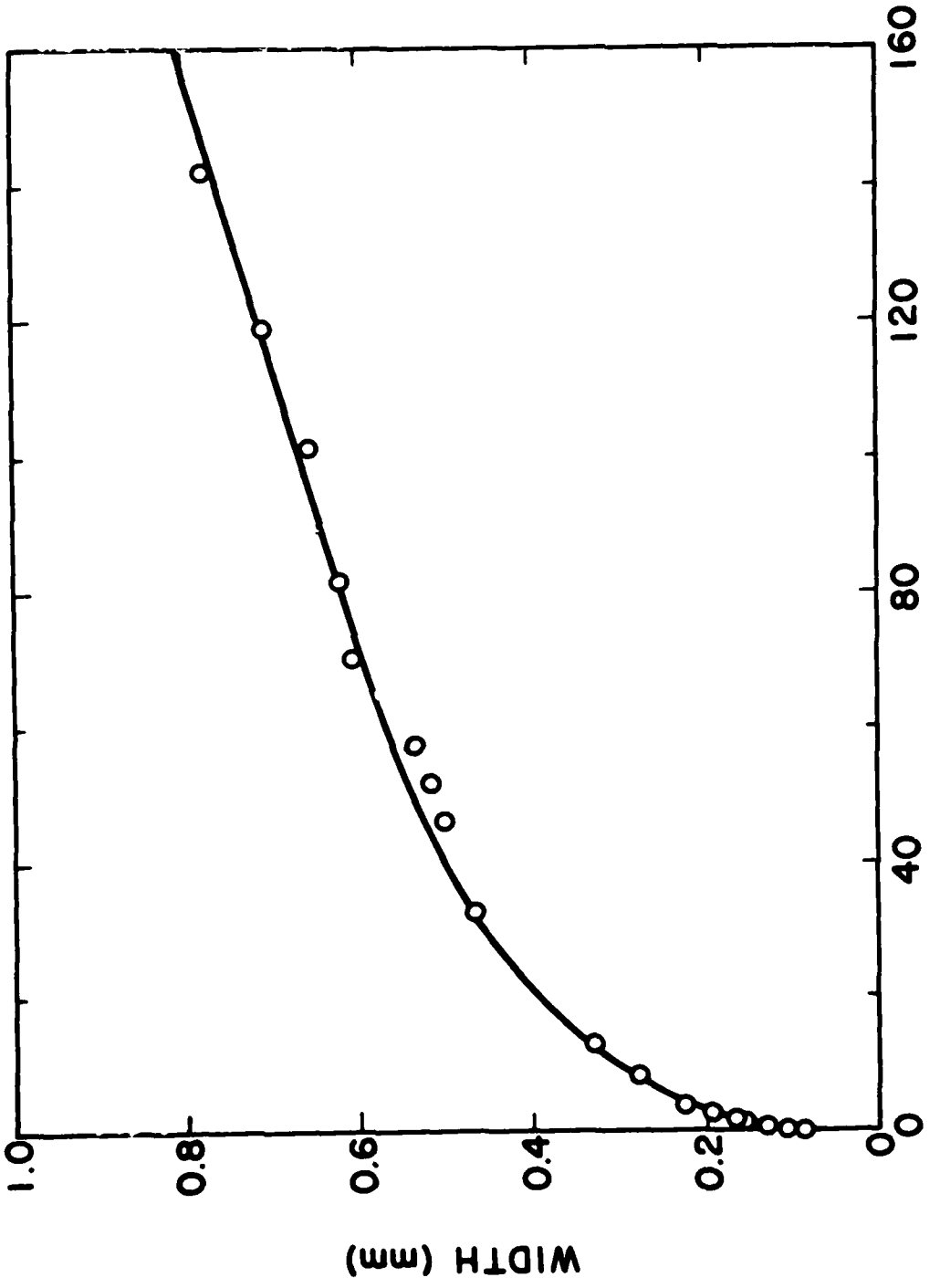

Fig. 2

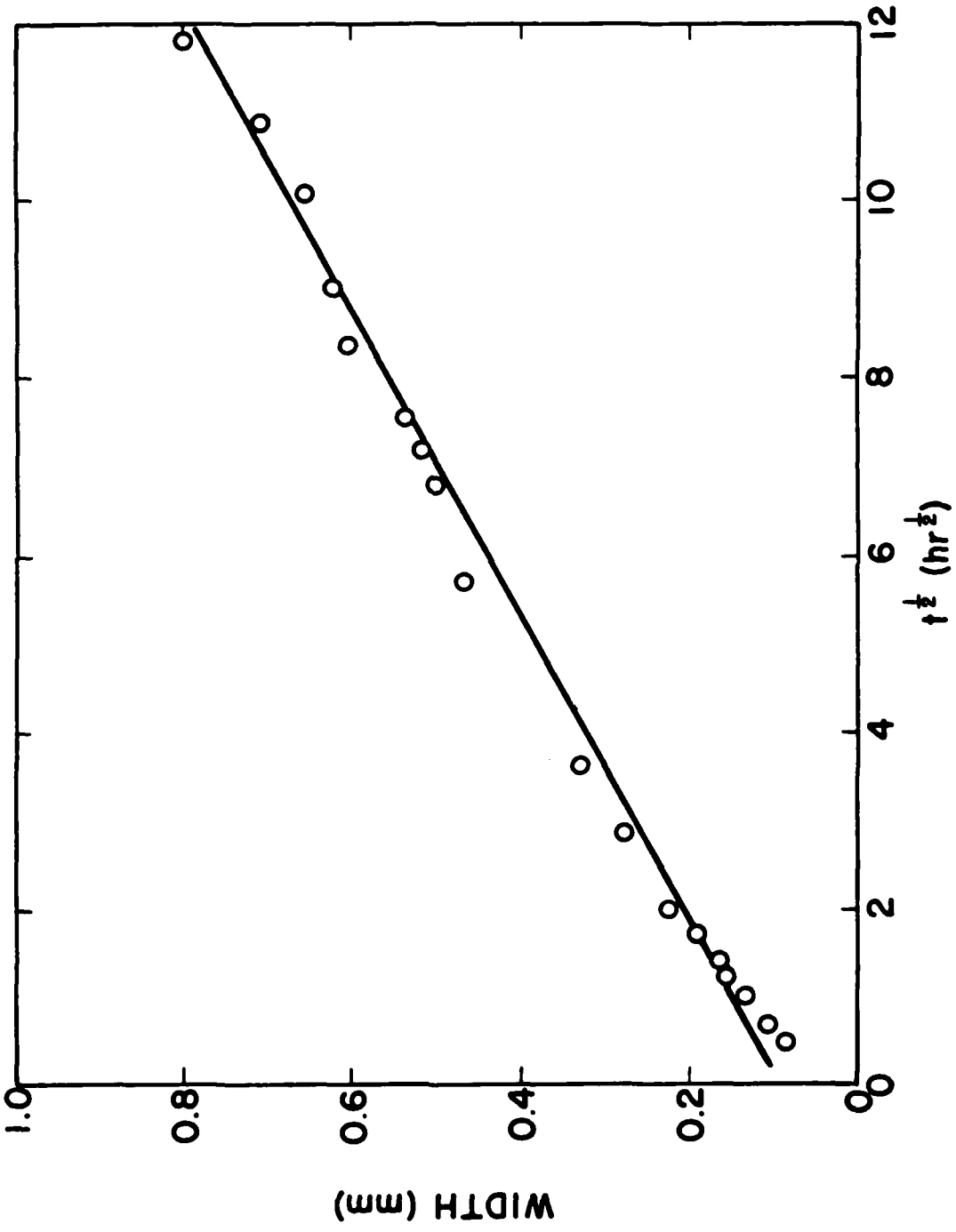

Fig. 3

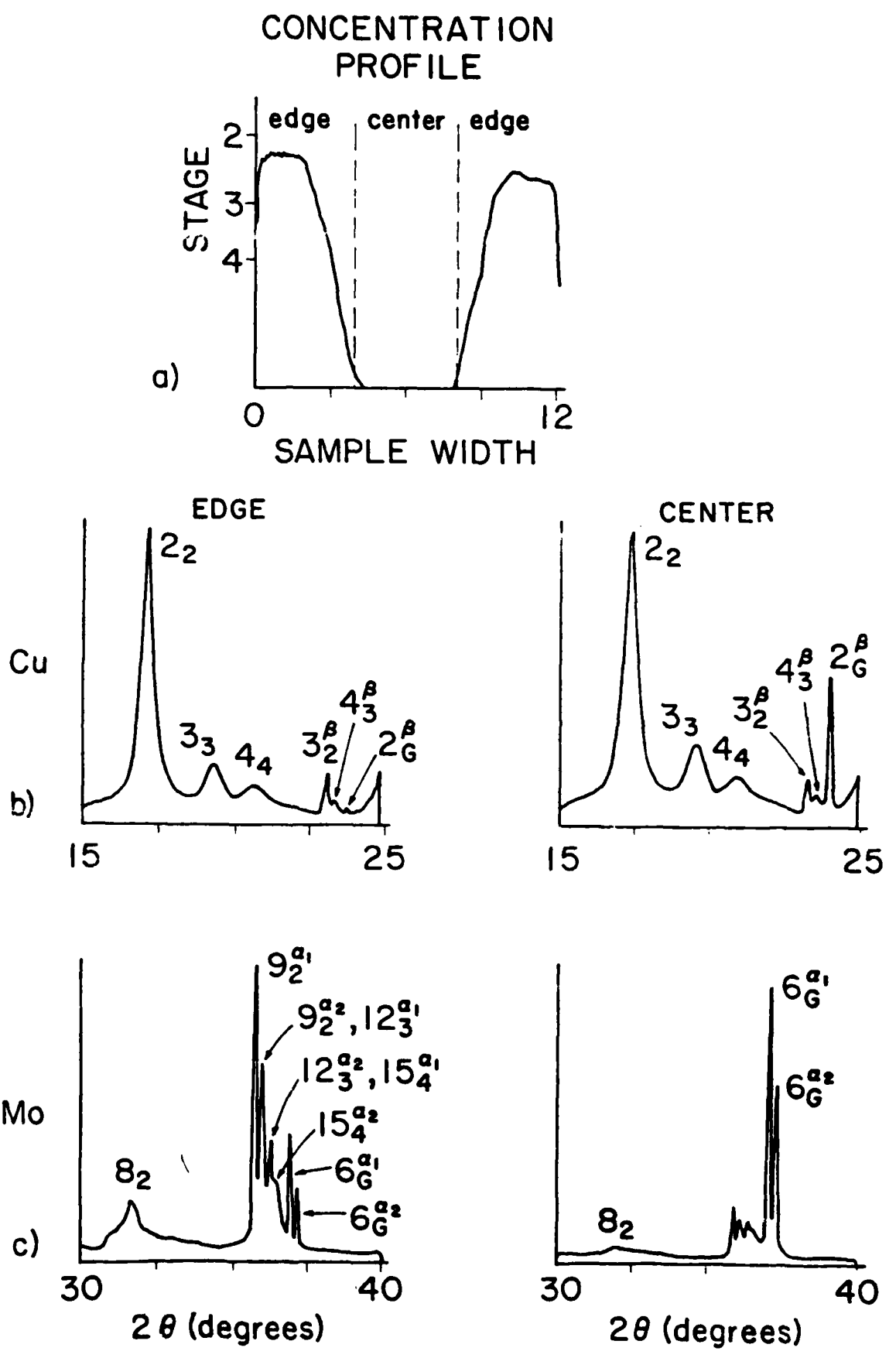
CONCENTRATION PROFILE
edge
center
edge
STAGE
2
3
4
a)
0
12
SAMPLE WIDTH
EDGE
CENTER
Cu
b)
2_2
3_3
4_4
3_2^β
4_3^β
2_G^β
15
25
Mo
c)
$9_2^{a_1}$
$9_2^{a_2}, 12_3^{a_1}$
$12_3^{a_2}, 15_4^{a_1}$
$15_4^{a_2}$
$6_G^{a_1}$
$6_G^{a_2}$
8_2
30
40
2θ (degrees)

Fig. 4

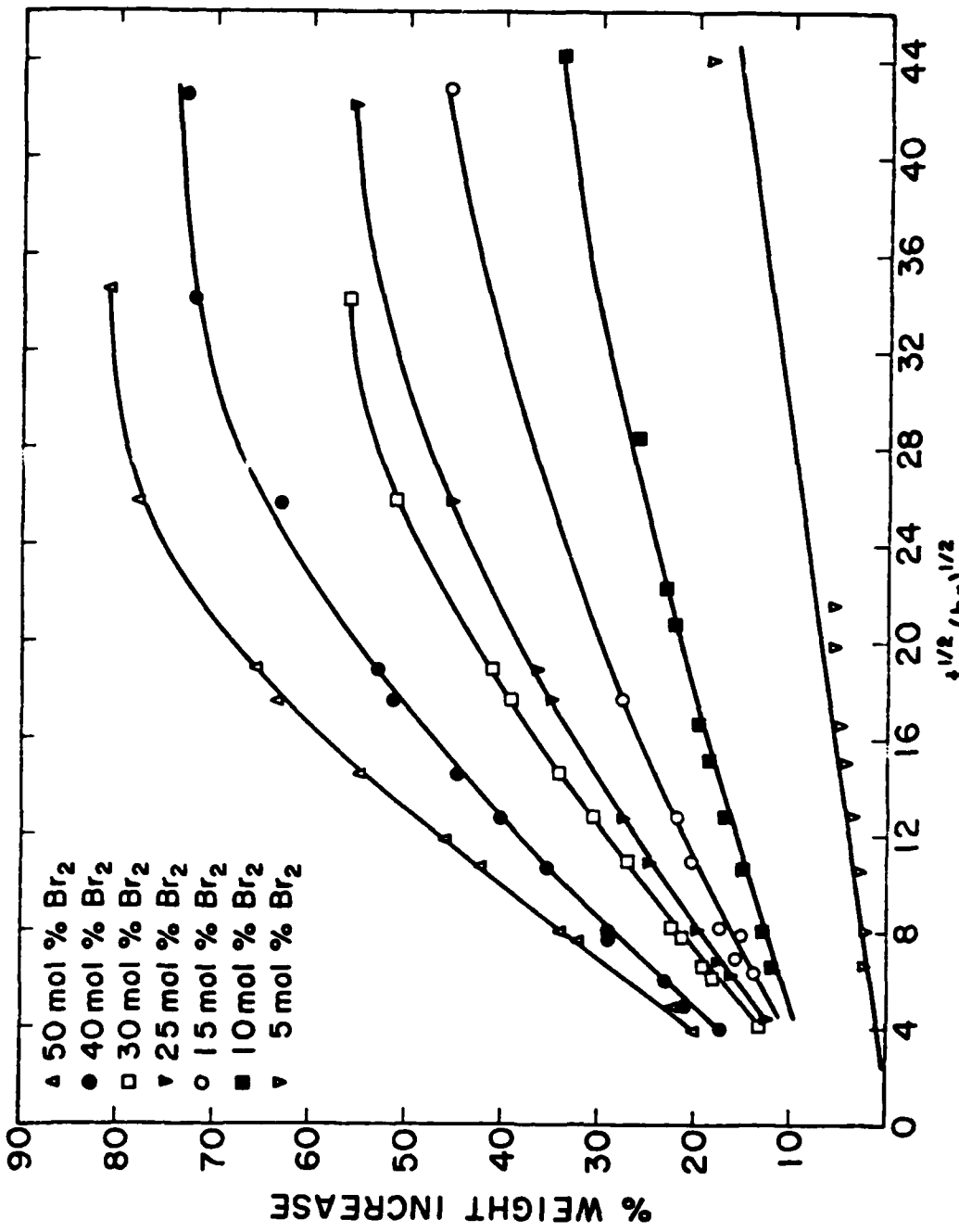
% WEIGHT INCREASE
$t^{1/2}$ (hr)$^{1/2}$
50 mol % Br_2
40 mol % Br_2
30 mol % Br_2
25 mol % Br_2
15 mol % Br_2
10 mol % Br_2
5 mol % Br_2
0
4
8
12
16
20
24
28
32
36
40
44
10
20
30
40
50
60
70
80
90

Fig. 5

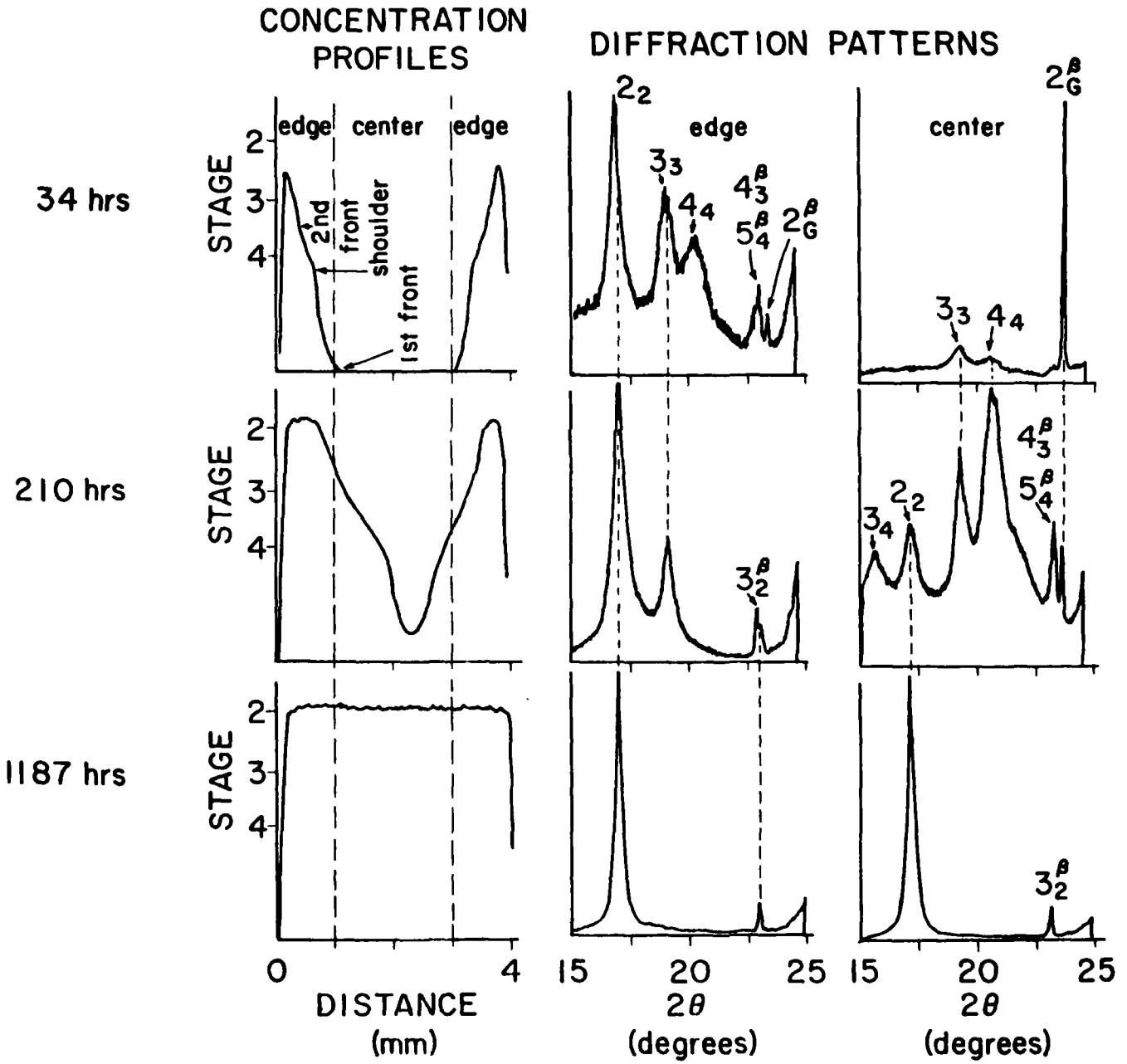
CONCENTRATION PROFILES
DIFFRACTION PATTERNS
34 hrs
210 hrs
1187 hrs
STAGE
edge
center
edge
2nd front shoulder
1st front
2_2
3_3
4_4
4_3^β
5_4^β
2_G^β
3_2^β
3_4
5_4^β
0
4
DISTANCE (mm)
15
20
25
2θ (degrees)

Fig. 6

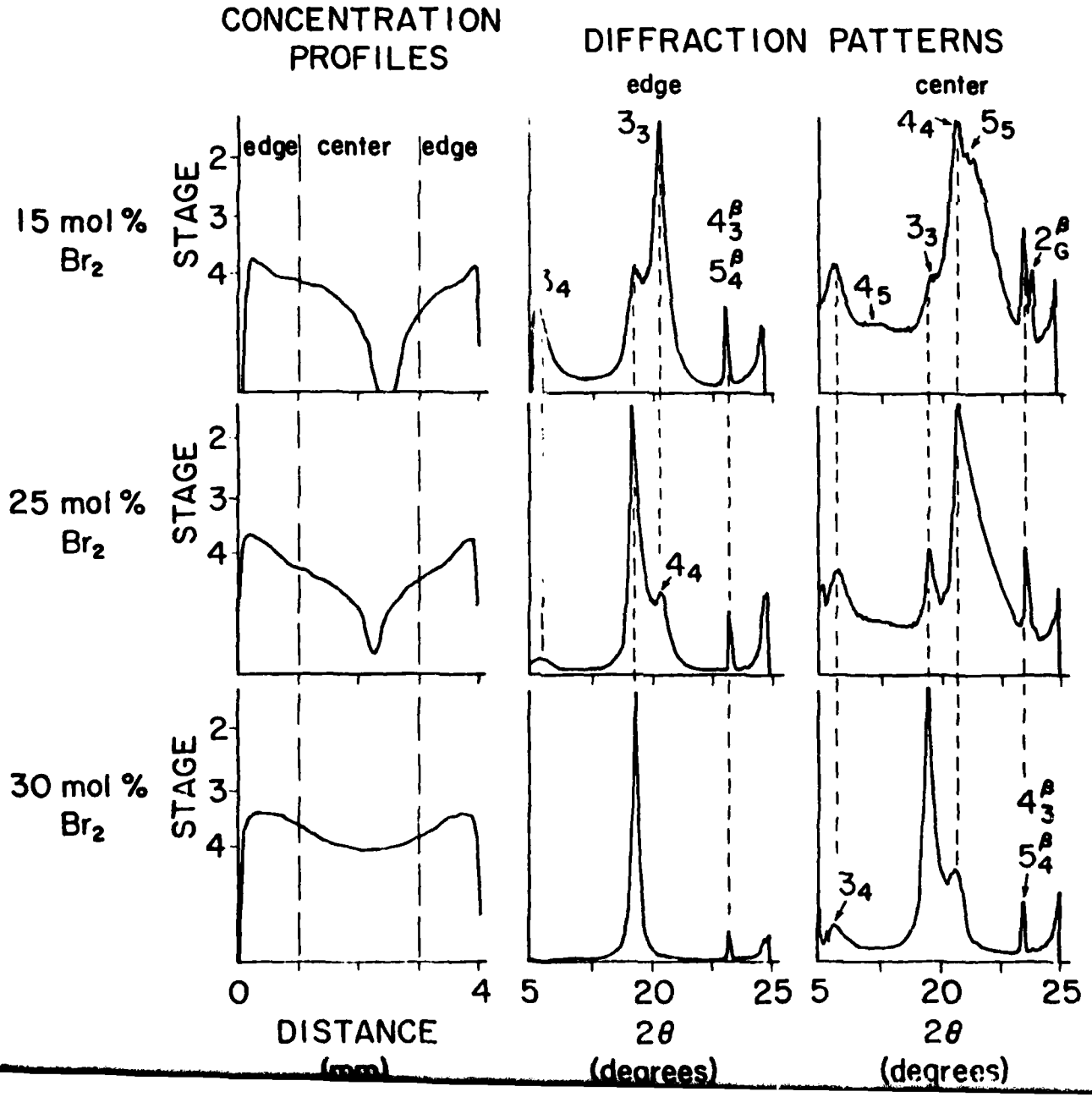
CONCENTRATION PROFILES
DIFFRACTION PATTERNS
edge
center
edge
15 mol % Br2
25 mol % Br2
30 mol % Br2
STAGE
2
3
4
0
4
DISTANCE (mm)
5
20
25
2θ (degrees)
3 3
4 3 β
5 4 β
3 4
4 4
5 5
2 G β
4 5

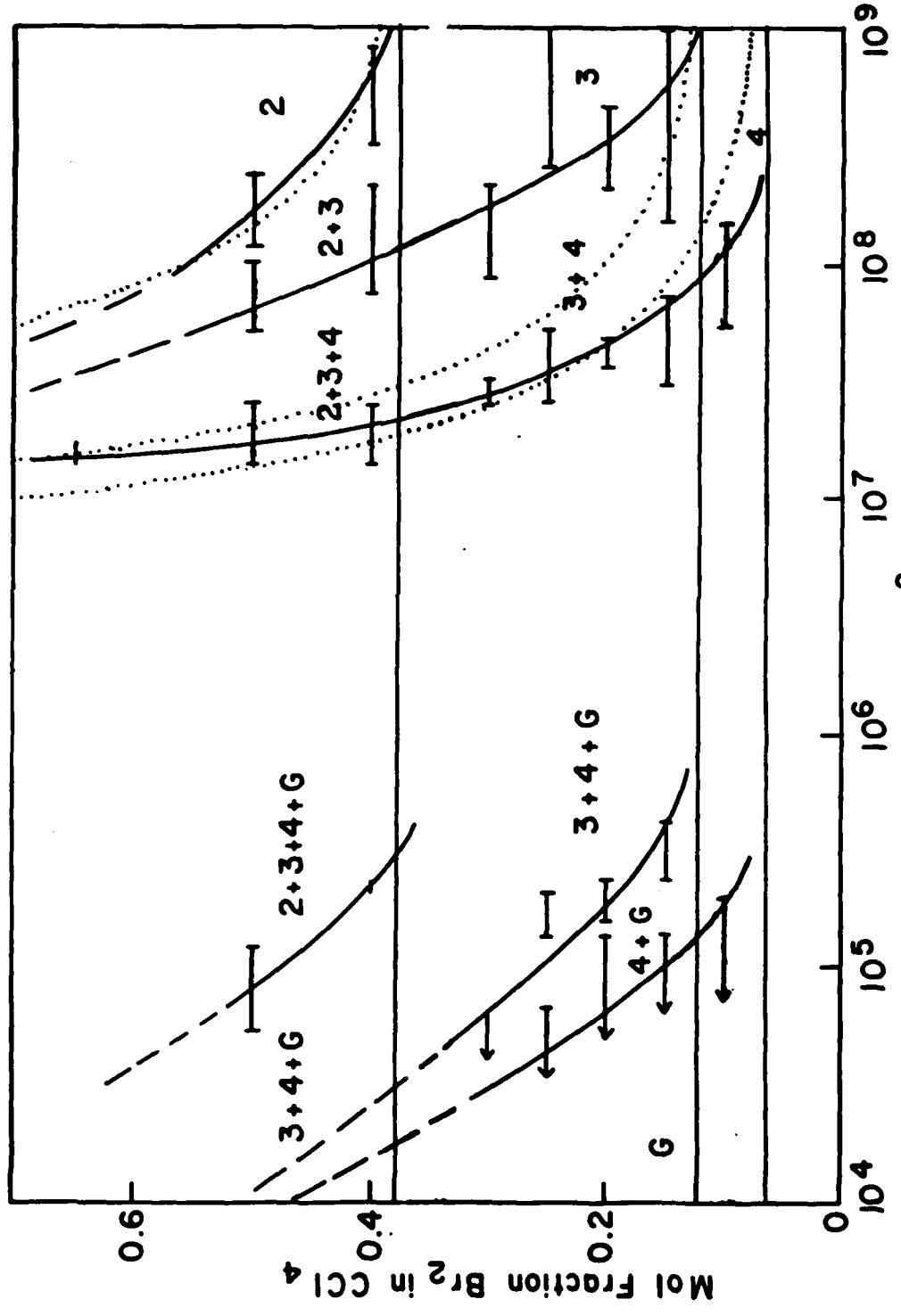
Mol Fraction Br_2 in CCl_4
0.6
0.4
0.2
0
10^4
10^5
10^6
10^7
10^8
10^9
(s/cm²)
2
2+3
2+3+4
3
3+4
4
2+3+4+G
3+4+G
4+G
3+4+G
G

Fig. 8

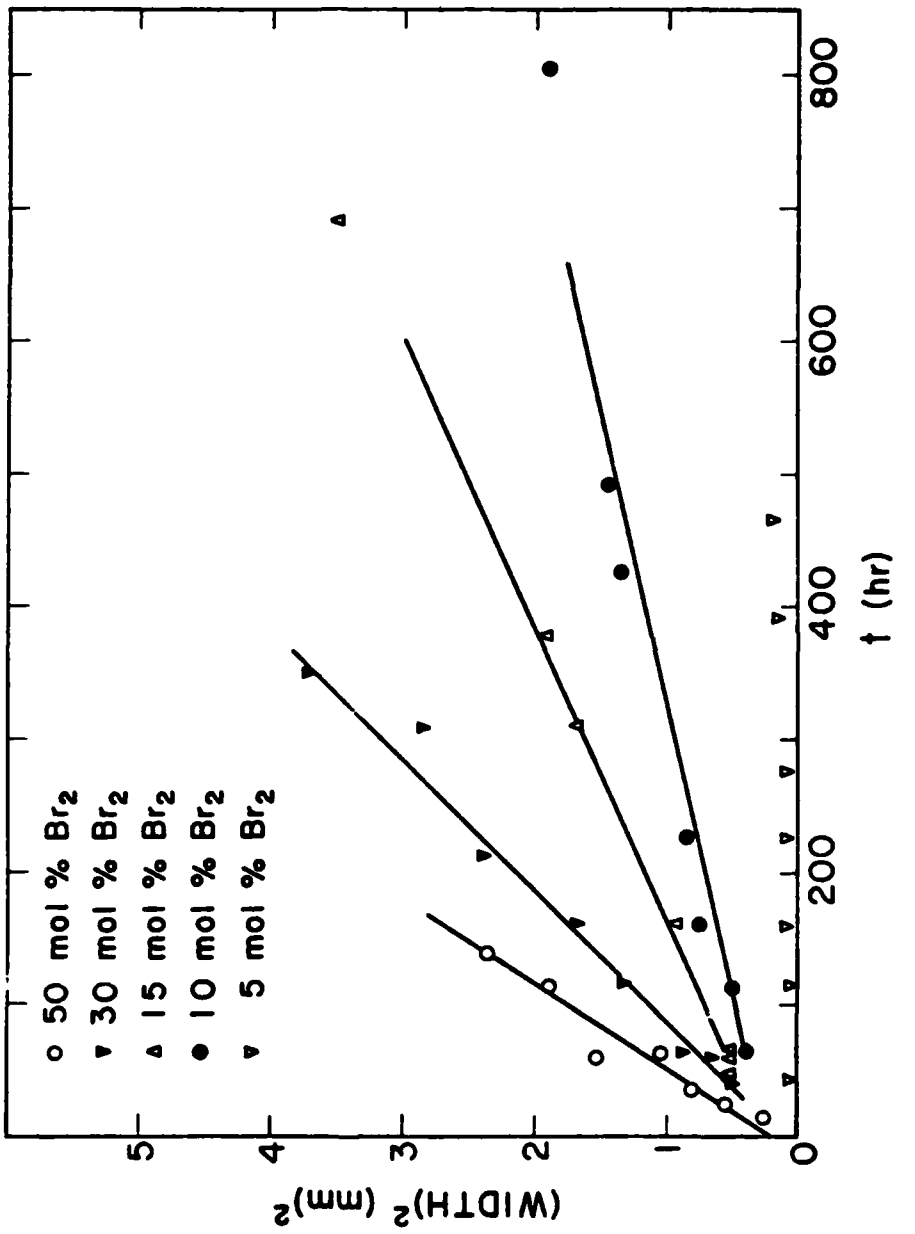
(WIDTH)² (mm)²
t (hr)
0
1
2
3
4
5
200
400
600
800
○ 50 mol % Br₂
▼ 30 mol % Br₂
▲ 15 mol % Br₂
● 10 mol % Br₂
▼ 5 mol % Br₂

Fig. 9

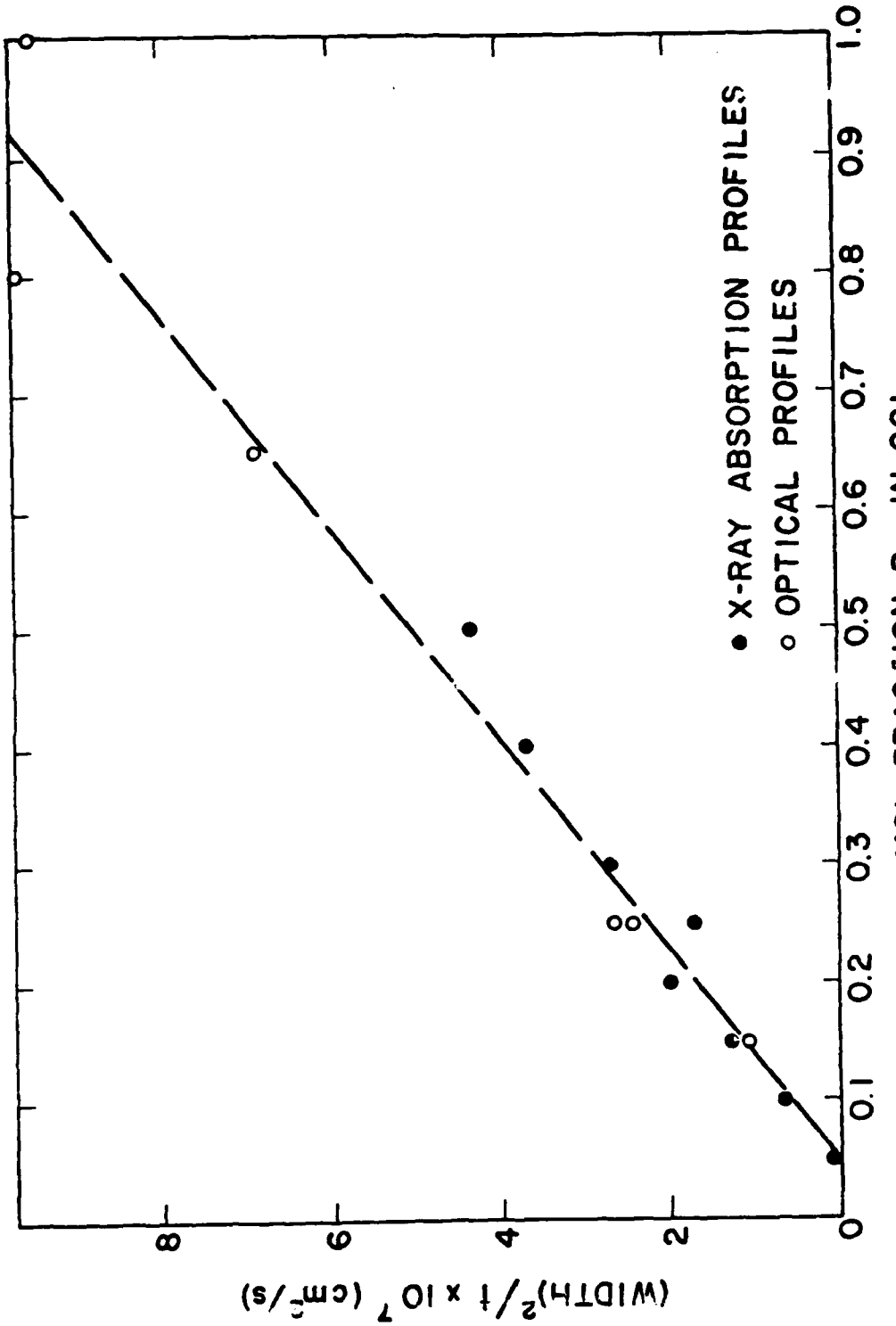
(WIDTH)²/t x 10⁷ (cm²/s)
0
2
4
6
8
0
0.1
0.2
0.3
0.4
0.5
0.6
0.7
0.8
0.9
1.0
MOL FRACTION Br₂ IN CCl₄
• X-RAY ABSORPTION PROFILES
o OPTICAL PROFILES

Fig. 10

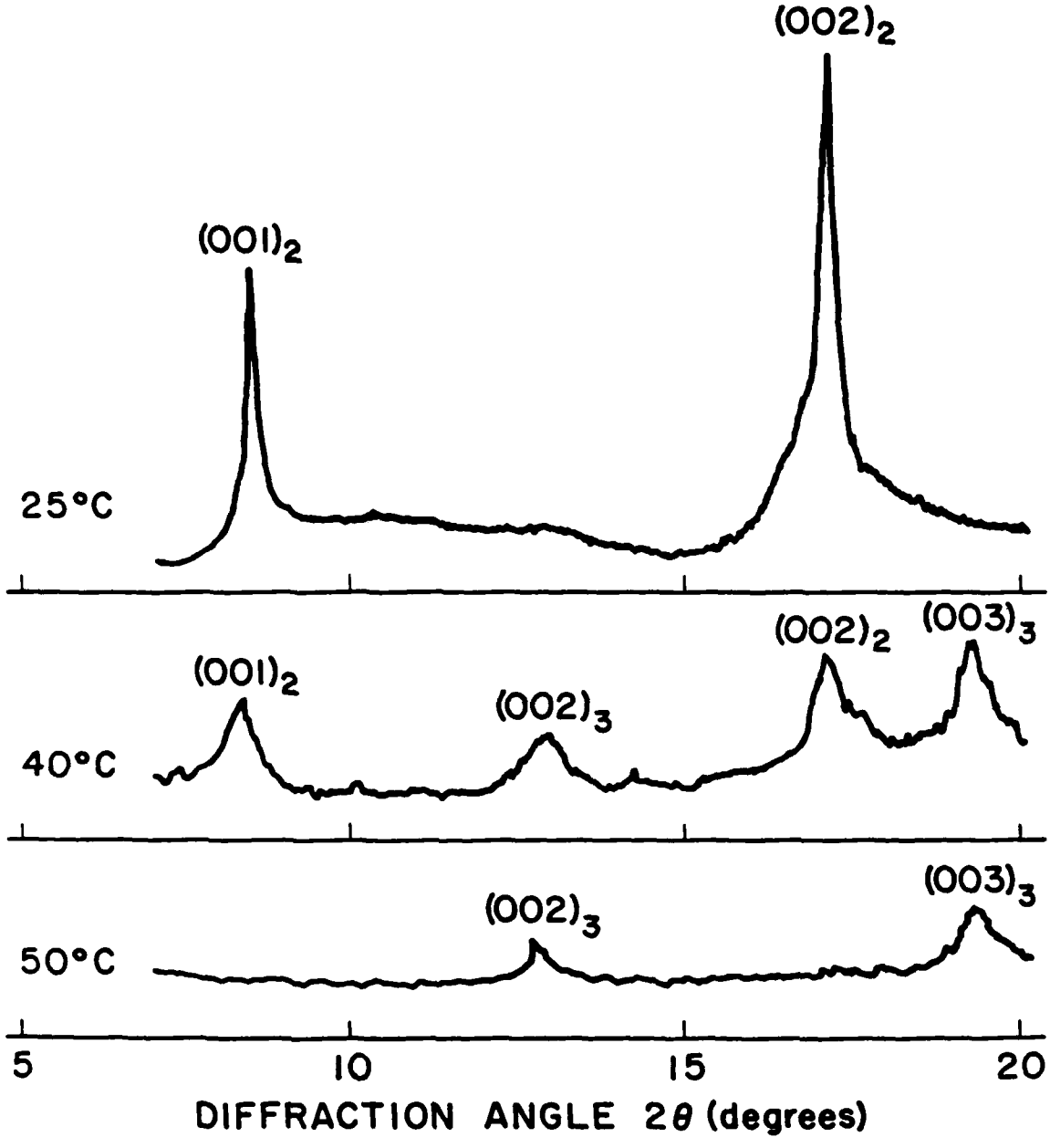
(002)2
(001)2
25°C
(002)2
(003)3
(001)2
(002)3
40°C
(003)3
(002)3
50°C
5
10
15
20
DIFFRACTION ANGLE 2θ (degrees)

Fig. 11

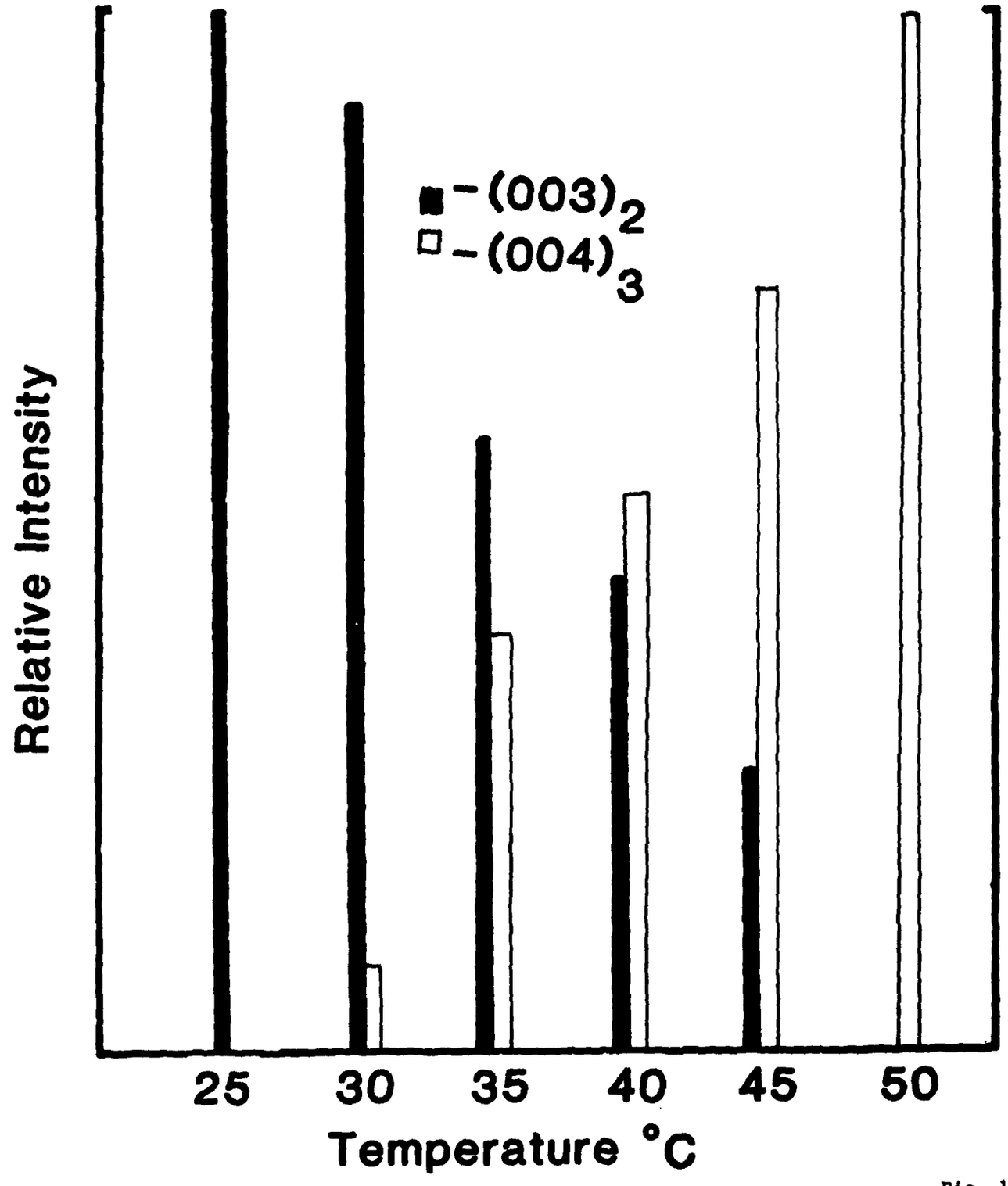

Fig. 12

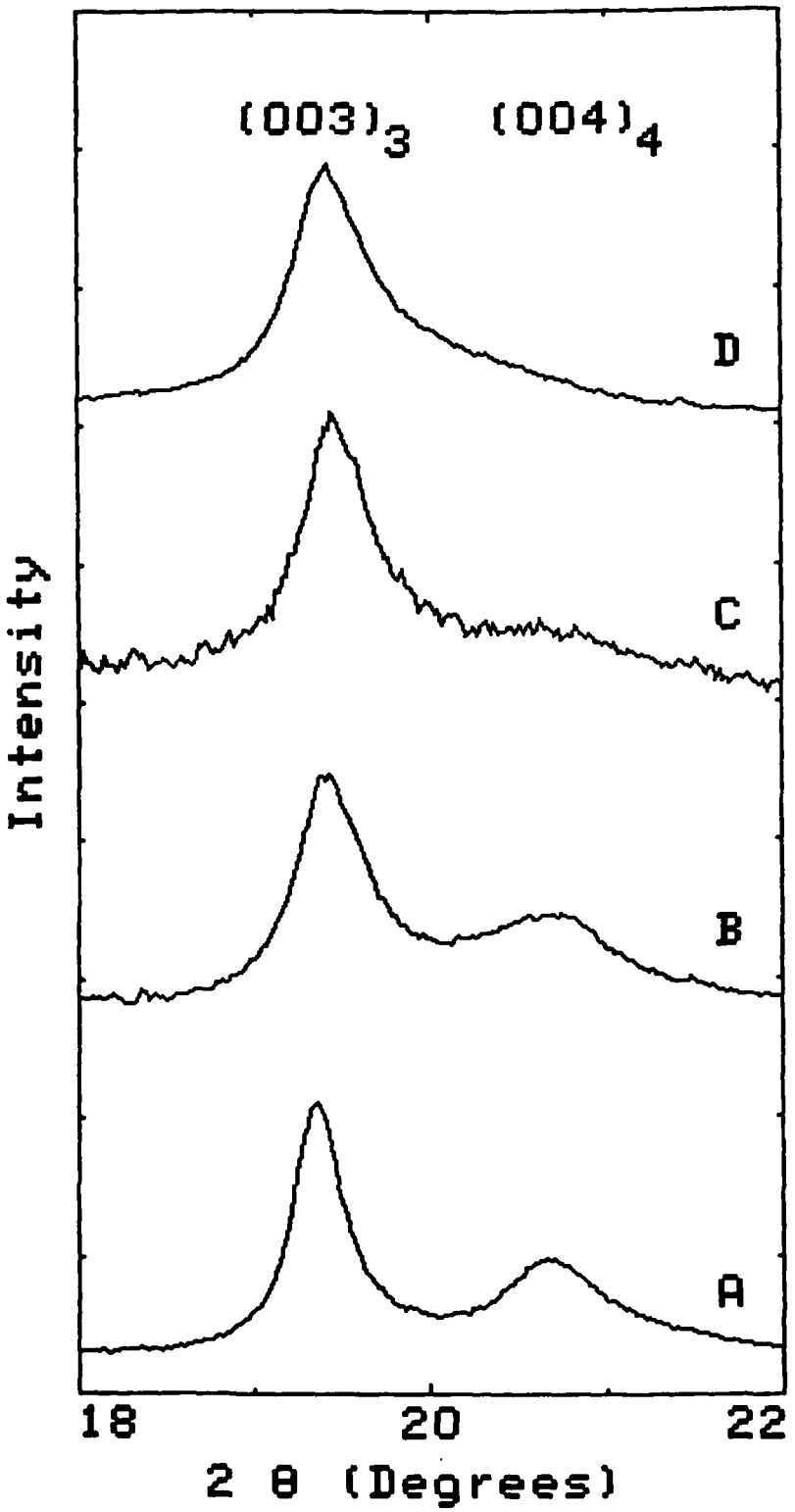

Fig. 1

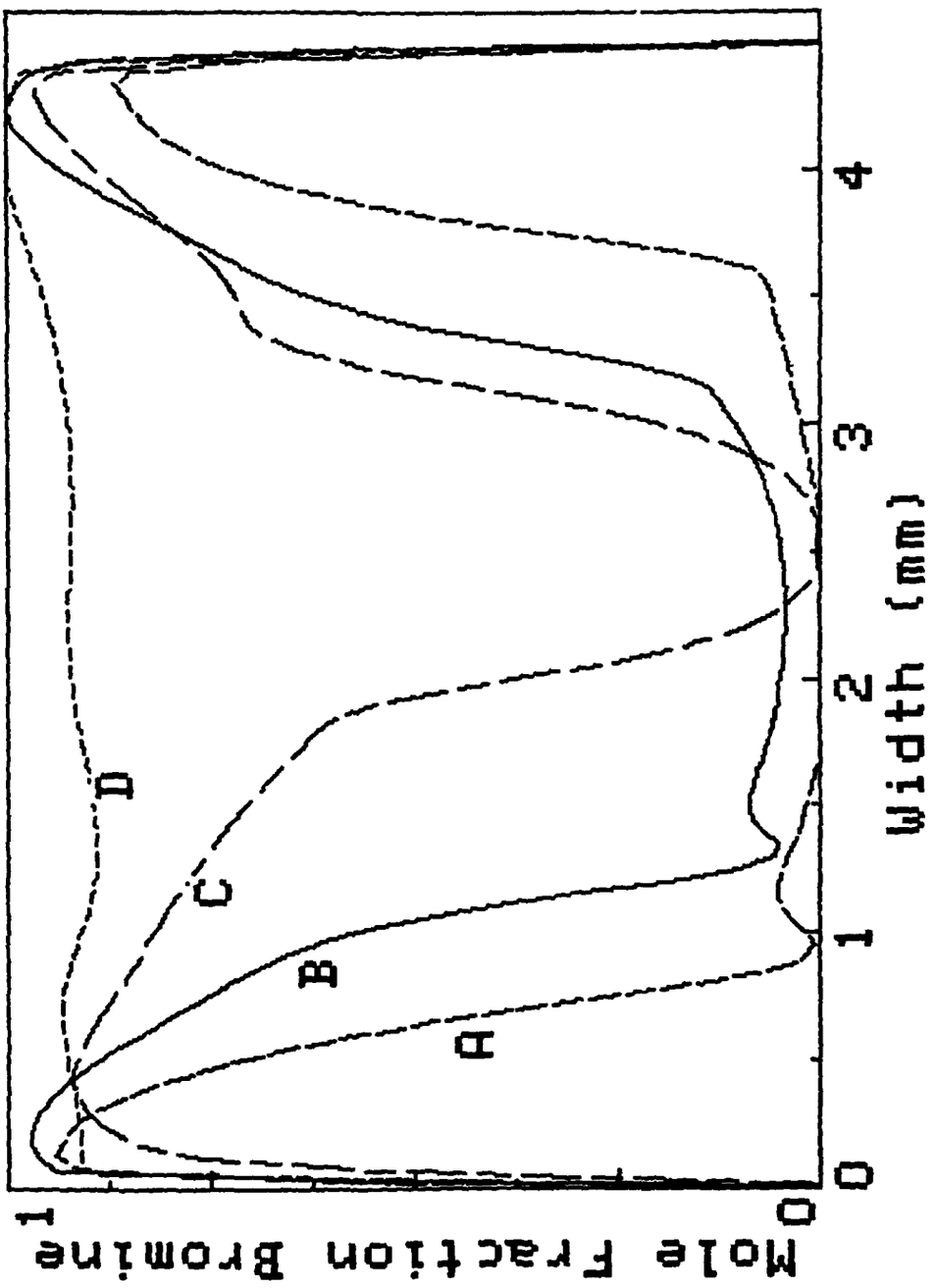

Fig. 14

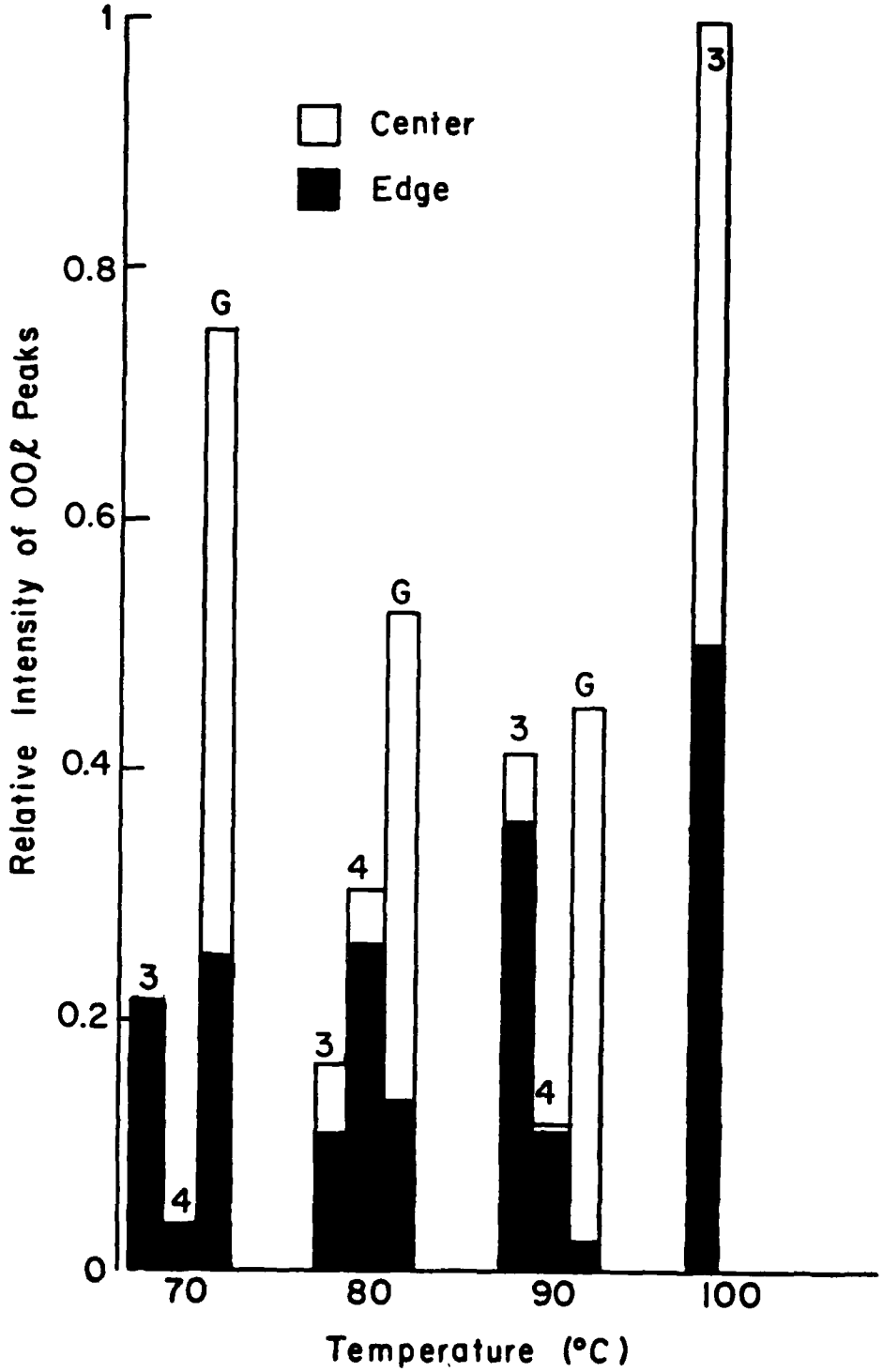
Center
Edge
Relative Intensity of 00ℓ Peaks
1
0.8
0.6
0.4
0.2
0
G
3
4
70
80
90
100
Temperature (°C)

Fig. 15

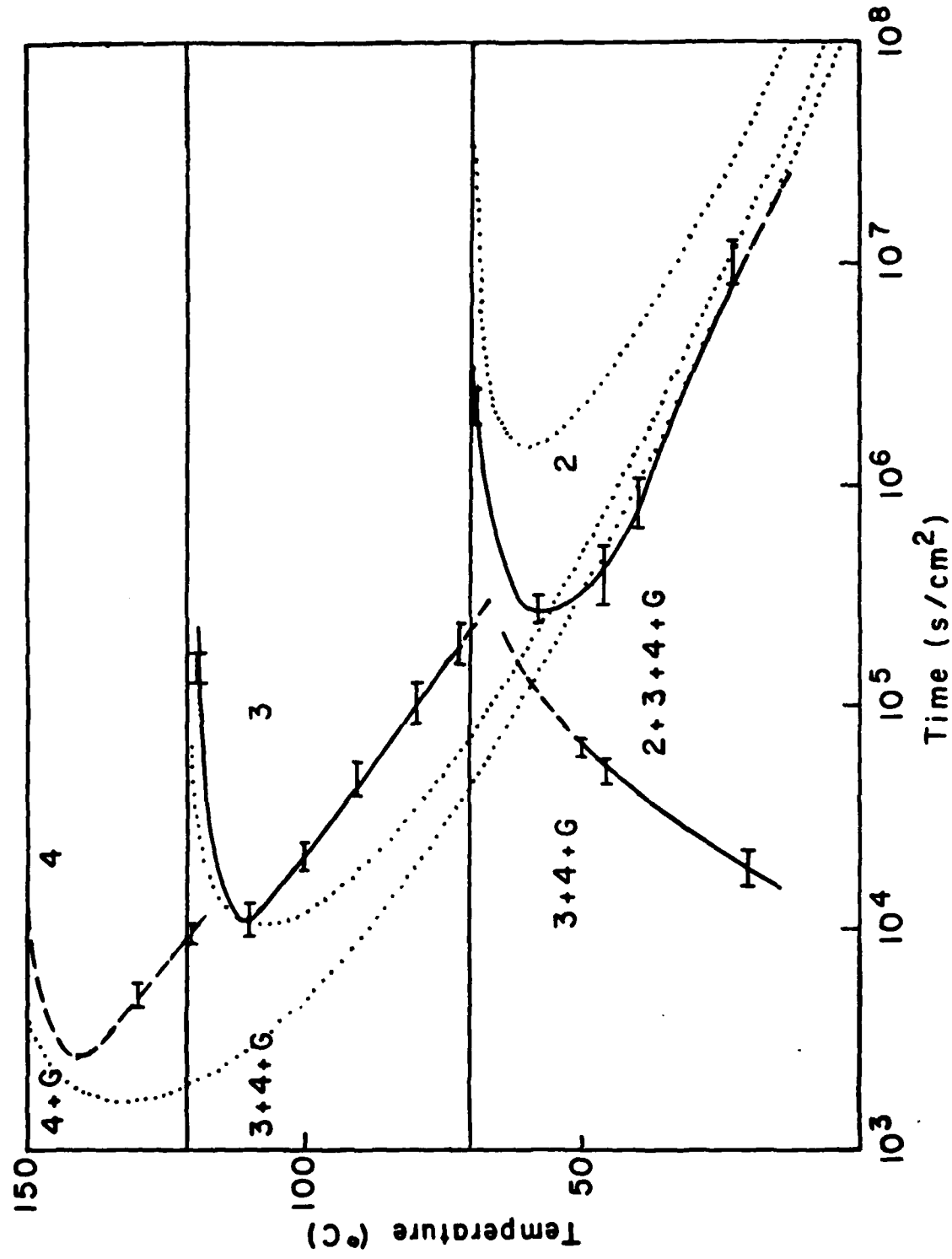
4
4+G
3
3+4+G
2
3+4+G
2+3+4+G
150
100
50
Temperature (°C)
10^3
10^4
10^5
10^6
10^7
10^8
Time (s/cm^2)

Fig. 16

APPENDIX 3

THERMODYNAMICS OF INTERCALATION OF BROMINE IN GRAPHITE*

Proceedings of Symposium on Intercalat graphite, Annual Meeting of Materials Research Society, Boston, 1982, accepted for publication.

S. H. ANDERSON AND D. D. L. CHUNG
Department of Metallurgical Engineering and Materials Science,
Carnegie-Mellon University, Pittsburgh, PA 15213, USA

ABSTRACT

The thermodynamics of intercalation of bromine in highly oriented pyrolytic graphite had been studied by determining the pressure-temperature equilibrium diagram for stages 2-4. The standard heat and entropy of reaction for the transformation from stage n to stage n-1 (n=5, 4, 3) were found to be roughly the same, though the enthalpy of reaction became slightly more negative as the stage number increased. The heat and entropy of formation from pure graphite were thus found to be -10.9 kcal mol^{-1} Br_2 and -30.4 cal mol^{-1} Br_2 K^{-1} respectively for stage 2, -11.3 kcal mol^{-1} Br_2 and -30.6 cal mol^{-1} Br_2 K^{-1} respectively for stage 3, and -11.5 kcal mol^{-1} Br_2 and -30.6 cal mol^{-1} Br_2 K^{-1} respectively for stage 4.

INTRODUCTION

The thermodynamics of intercalation of alkali metals in graphite had been studied for stages 1-5 by vapor pressure measurement [1-4], solid-state emf measurement [5], calorimetry [6] and stage-2-to-stage-1 transformation temperature measurement [7]. On the other hand, the thermodynamics of intercalation of bromine in graphite had only been studied by decomposition vapor pressure measurement of stage 2 [8-10], which gave the standard heat of reaction of -10.2 ± 0.3 kcal mol^{-1} and the standard entropy of reaction of -29.9 ± 1.2 cal mol^{-1} K^{-1} for the stage-3-to-stage-2 transformation [10]. In this paper, by determining the pressure-temperature equilibrium diagram for stages 2-4 of graphite-bromine, we have obtained the standard heats of reaction and the standard entropies of reaction for the transformations from stage 5 to stage 4, from stage 4 to stage 3, and from stage 3 to stage 2. Using these data, the heats of formation of stages 2-4 were calculated.

INTERCALATION METHODS

Four methods of intercalation have been investigated. They differ in the parameter(s) used to control the eventual stage, as listed in Table 1 and also described below.

1. Temperature method (two-bulb). In this method, the sample temperature is varied to control the eventual stage, while the intercalate vapor pressure resulting from a reservoir of pure intercalate is fixed. The sample temperature should be kept higher than the intercalate reservoir temperature to avoid condensation of the intercalate on the sample. This method is popular and was originally developed for the intercalation of alkali metals [7].

*Research sponsored by the Air Force Office of Scientific Research, Air Force Systems Command, USAF, under Grant No. AFOSR-78-3536. The United States Government is authorized to reproduce and distribute reprints for Governmental purposes notwithstanding any copyright notation hereon.

TABLE 1 Intercalation Methods

Method	Parameters	
	Intercalate vapor pressure	Sample temperature
Temperature method (two-bulb)	-	X
Temperature method (one-bulb)	X	X
Solution method	X	-
Temperature-solution method	X	X

X Varied to control the stage - Not varied

2. Temperature method (one-bulb). In this method, the sample and the pure intercalate are at the same temperature. Thus an increase in sample temperature necessarily increases the intercalate vapor pressure. This method is experimentally simpler than the two-bulb method because it requires only one temperature. It was used by Bach et al. to prepare various stages of graphite-bromine, as shown by weight measurement [11].

3. Solution method. In this method, the intercalate is dissolved in a certain solvent which does not intercalate. The concentration of the intercalate in the solvent is used to control the eventual stage. Intercalation takes place at room temperature. This method was first used by Hennig to prepare graphite-Br_2 with Br_2-CCl_4 solution [12]; it was also used by Saunders et al. [13].

4. Temperature-solution method. In this method, the intercalate is dissolved in a solvent as in the solution method, but the temperature method (one-bulb) is also involved. In other words, the sample and the intercalate solution are at the same temperature, such that this temperature and the intercalate concentration in the solution are both varied to achieve a given eventual stage. In this work, this method was used for the first time to prepare graphite-bromine.

It should be noted that the temperature method (one-bulb) and the solution method are special cases of the temperature-solution method. In this paper, the use of the temperature-solution method enabled the determination of the pressure-temperature equilibrium diagram for various stages of graphite-bromine. The temperature method (two-bulb) was also used for the same purpose, though to a smaller extent. The consistency of the pressure-temperature data obtained by the two methods gave additional support for the validity of the temperature-solution method. Shown in Fig. 1 are 00ℓ x-ray diffraction patterns obtained with CuKα radiation on stage 4 highly oriented pyrolytic graphite (HOPG) samples prepared by (a) the temperature method (two-bulb), (b) the temperature method (one-bulb), (c) the solution method, and (d) the temperature-solution method. These diffraction patterns show that all four methods yield well-staged compounds.

EQUILIBRIUM DIAGRAM

Figure 2 shows the equilibrium diagram, which is a map of the pressure-temperature combinations that yield a given eventual stage. The pressure refers to the bromine vapor pressure; the temperature refers to the sample temperature. The vapor pressure P_{sol} above the Br_2-CCl_4 solution is related to the vapor pressure P_{Br_2} of pure bromine and the mole fraction X of Br_2 in the solution by the relation [14]

$$\ln\left(\frac{P_{sol}}{P_{Br_2}\,X}\right) = 1.197\,(1-X)^2 - 0.493\,(1-X)^3, \qquad (1)$$

where P_{Br_2} is pressure in mm Hg. The validity of Eq. (1) is confirmed by the consistency between data points obtained by the temperature-solution method and those obtained by the two-bulb temperature method. The vapor pressure P_{Br_2} of pure bromine is given by [15]

$$\log_{10} P_{Br_2} = \begin{cases} 5.82 - \dfrac{638.25}{T+158.006} & -48°C<T<58.2°C \\ 7.583 - \dfrac{1562.26}{T+273.78} & 70°C<T<110°C \end{cases} \quad (2)$$

where T is temperature in C°.

The intercalation reaction between bromine and pure graphite for a final stage of n can be written as

$$7n\ C(s) + Br_2\ (g) = C_{7n}\ Br_2\ (s) \quad (3)$$

The transformation from stage n+1 to stage n can be written as

$$n\ C_{7(n+1)}\ Br_2\ (s) + Br_2\ (g) = (n+1)\ C_{7n}\ Br_2 \quad (4)$$

In Eq. (3) and (4), the in-plane stoichiometry is such that stage 2 is C_7Br (or $C_{14}Br_2$), as indicated by the recently determined in-plane structure of stage 2 [16]. For either reaction (Eq.(3) or (4)), the equilibrium bromine vapor pressure P (in atmospheres) is related to the change in free energy of the reaction by the relation

$$\ln P = \Delta H°/RT - \Delta S°/R, \quad (5)$$

where $\Delta H°$ is the standard heat of reaction and $\Delta S°$ is the standard entropy of reaction. Hence, the slope of the straight line separating regions of different final stages in the ln P vs. 1/T diagram gives $\Delta H°$ for the change from one stage to the next, whereas the intercept gives $\Delta S°$. Such boundaries between stages 4 and 5, 3 and 4, and 2 and 3 are shown in Fig. 2, which was obtained by allowing intercalation to occur under conditions represented by a number of pressure-temperature combinations and then determining the final stage for each combination by x-ray diffraction. The values of $\Delta H°$ and $\Delta S°$ for the change of one stage to the next lower one are listed in Table 2. It may be pointed out that these values are independent of the actual in-plane stoichiometry used in writing Eq. (4).

The values of $\Delta H°$ and $\Delta S°$ for the change from stage 3 to stage 2 are in close agreement with those reported by Sasa [10]. Table 2 indicates that $\Delta H°$ increases slightly with increasing stage, while the variation in $\Delta S°$ is much less marked. These characteristics are similar to those reported on graphite-alkali metals [5].

Salzano and Aronson [17] proposed a model for the change in enthalpy during intercalation due to electrostatic interactions between the intercalate layer and the graphite layers. In this model, the change of enthalpy $\Delta H°$ for the transformation from stage n_2 to stage n_1 was given by

$$\Delta H° = -aH + M + I\left(\frac{n_1}{n_2} - \frac{n_2}{n_1}\right), \quad (6)$$

where a indicates the in-plane stoichiometry (a=7 for $C_{7n}Br_2$), H is the interlayer bonding energy between two adjacent carbon layers in graphite, less the interlayer bonding energy between two adjacent graphitic layers with the same spacing as in the compound, M is the attractive interaction energy between the graphite layers and adjacent intercalate layers, and I is a measure of the repulsive interaction between adjacent intercalate layers. Following their analysis [1], we have calculated the standard heats and entropies of formation of various stages from pure graphite (i.e., Eq. (3)), as listed in Table 3. The standard heat of formation $\Delta H_f°$ of stage 4 was approximated by plotting the experimental values of $\Delta H°$ versus $[(n_1/n_2) - (n_2/n_1)]$, thereby obtaining $-aH + M$ as the intercept and I as the slope, and then taking $\Delta H_f°$ as $-aH + M + \frac{I}{n}$, where n = 4. The standard entropy of formation $\Delta S_f°$ of stage 4 was taken as equal to the value of $\Delta S°$ for the change of stage 5 to stage 4. The values of $\Delta H_f°$ and $\Delta S°$ for other stages were then calculated by summing the experimental heats and entropies of progressive stage changes.

Since the in-plane structure of graphite-bromine is the same for different stages, it is not surprising that there is little difference in $\Delta S°$ from stage to stage. Compared with the values for the intercalation of the alkali metals [5], these values are relatively high. This may be due to the two-phase nature

TABLE 2 Heats and Entropies of Changes of Stage

Change of Stage	Equilibrium Reaction	$\Delta H°$ (kcal mol^{-1} Br_2)	$\Delta S°$ (cal mol^{-1} Br_2 K^{-1})
3→2	$2C_{21}Br_2$ (s) + Br_2 (g) →3 $C_{14}Br_2$(s)	-10.0 ± 0.5	-29.9 ± 0.5
4→3	$3C_{28}Br_2$ (s) + Br_2 (g) → 4 $C_{21}Br_2$ (s)	-10.8 ± 0.2	-30.8 ± 0.3
5→4	$4C_{35}Br_2$ (s) + Br_2 (g) → 5 $C_{28}Br_2$ (s)	-11.0 ± 0.2	-30.6 ± 0.3

of the in-plane structure, where one phase is less ordered than the other [16]. It may be noted that $\Delta S°$ of bromine intercalation is about one and a half times that of alkali metal intercalation for stages ≥ 2 [5].

To the extent that an electrostatic model is suitable for bromine, it is interesting to compare the enthalpies obtained in bromine with those observed in the alkali metals. $\Delta H_f°$ in bromine are about a third less than those observed in the alkali metals, suggesting that there is much less electrostatic interaction in graphite-bromine.

CONCLUSION

The thermochemical data for the intercalation of bromine in HOPG have been determined. The standard heats and entropies of reaction reported are expected to be of use to graphite-bromine concentration cells [18].

TABLE 3 Heats and Entropies of Formation

Stage	Reaction	$\Delta H_f°$ (kcal mol^{-1} Br_2)	$\Delta S_f°$ (cal mol^{-1} Br_2 K^{-1})
2	14 C (s) + Br_2 (g)→ $C_{14}Br_2$ (s)	-10.9	-30.4
3	21 C (s) + Br_2 (g)→ $C_{21}Br_2$ (s)	-11.3	-30.6
4	28 C (s) + Br_2 (g)→ $C_{28}Br_2$ (s)	-11.5	-30.6

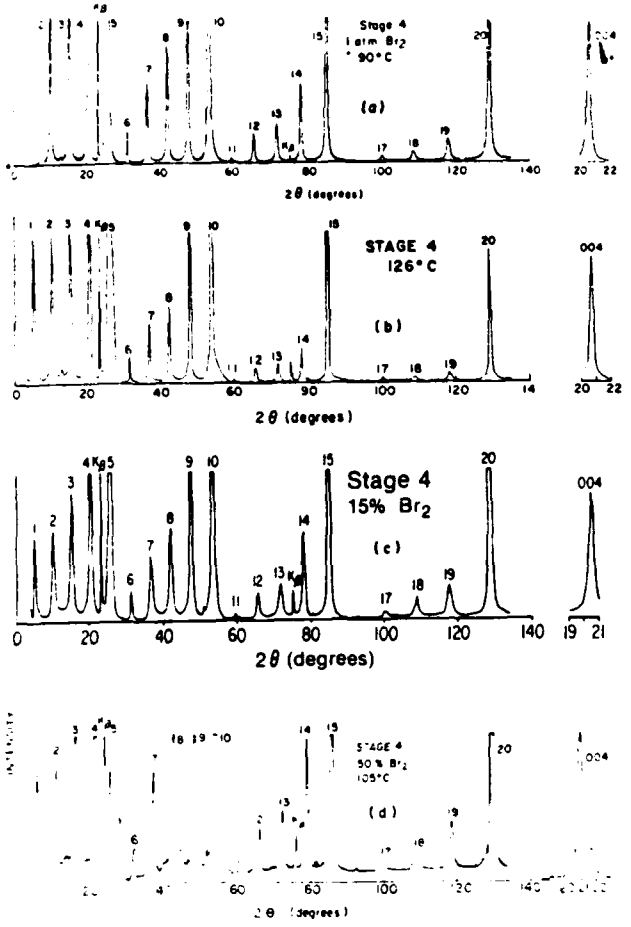

Fig. 1. 00ℓ x-ray diffraction patterns of stage 4 prepared by (a) two-bulb temperature method, (b) one-bulb temperature method, (c) solution method, and (d) temperature-solution method. Each peak is labeled by its ℓ index.

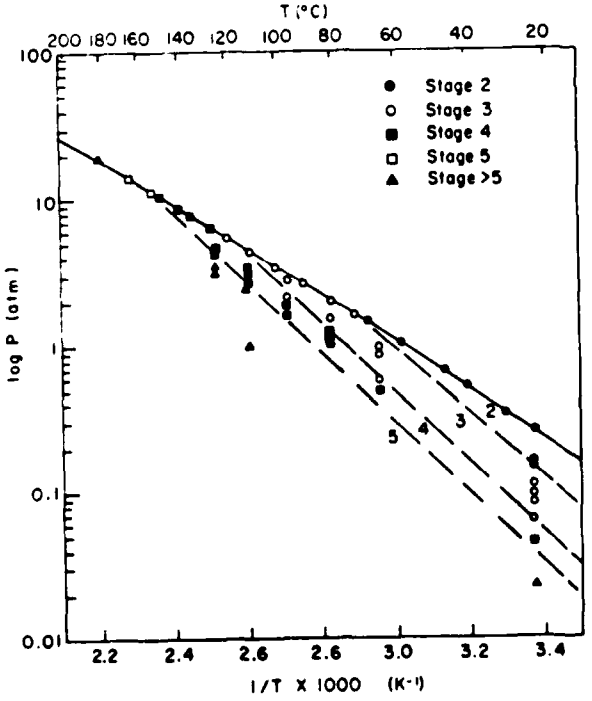

Fig. 2. Equilibrium diagram of bromine vapor pressure P vs. 1/T.

ACKNOWLEDGMENT

Division of Materials Research of NSF for the x-ray diffraction equipment grant (DMR-8005380). Materials Research Laboratory Section, Division of Materials Research of NSF (DMR 76-81581 A01) for central research facility support.

REFERENCES

1. F. J. Salzano and S. Aronson, J. Chem. Phys. 43, 149 (1965).

2. F. J. Salzano and S. Aronson, J. Chem. Phys. 45, 4551 (1966).

3. F. J. Salzano and S. Aronson, J. Chem. Phys. 46, 4169 (1967).

4. F. J. Salzano and S. Aronson, J. Chem. Phys. 47, 2978 (1967).

5. S. Aronson, F. J. Salzano and D. Bellafiore, J. Chem. Phys. 49, 434 (1968).

6. D. Saehr, Bull. Soc. Chim. France 1287 (1964).

7. A. Herold, Bull. Soc. Chim. France 999 (1955).

8. A Herold and R. Setton, Les Carbones, Vol. 2, Masson, Paris (1965) p.606.

9. G. A. Saunders, A. R. Ubbelohde and D. A. Young, Proc. Roy. Soc. Ser. A, 271, 499 (1963).

10. T. Sasa, Carbon 11, 497 (1973).

11. B. Bach, M. Bagouin, F. Bloc and A. Herold, Compte Rend., Acad. Sci. (Series C) 257, 681 (1963).

12. G. R. Hennig, J. Chem. Phys. 20, 1438 (1952).

13. G. A. Saunders, A. R. Ubbelohde and D. A. Young, Proc. Roy. Soc. Ser. A, 271, 499 (1963).

14. C. Barthel and M. Dode, Bull. Soc. Chim. 21, 1312 (1954).

15. S. Ohe, Computer Aided Data Book of Vapor Pressures, Data Book Publishing Company, Tokyo, Japan (1976).

16. D. Ghosh and D. D. L. Chung, submitted for publication.

17. F. J. Salzano and S. Aronson, J. Chem. Phys. 45, 2221 (1966).

18. J. M. Lalancette and R. Roussel, Can. J. Chem. 54, 3541 (1976).

APPENDIX 4

Ext. Abstr. Program - Bienn. Conf. Carbo
16 (1983).

MODEL OF INTERCALATION OF BROMINE IN GRAPHITE*

S.H. Anderson and D.D.L. Chung
Department of Metallurgical Engineering and Materials Science
Carnegie-Mellon University, Pittsburgh, Pennsylvania 15213, U.S.A.

1 Introduction

Any of several steps may be rate controlling in the formation of an intercalation compound--the transport of the intercalating species to the surface of the graphite, adsorption on the surface, transport of the intercalate within the graphite and staging within the graphite. In the case of bromine, we have assumed, largely on the basis of the relatively high pressures needed for the intercalation of bromine, that the processes occurring on the surface are likely to be fast and not rate-controlling.

2 Model of Intercalation

We have calculated the time to intercalate to a given stage as

$$t = (x/v) + (x^2/4\eta^2 D), \quad (1)$$

where x is the width of the part of the sample intercalated at time t; v is the velocity of the intercalation reaction given by

$$v = A_o \exp(-E_i/RT)[P(act)-P(eq)]. \quad (2)$$

The first pair of terms in Eq. (2) indicate the probability of a jump across the interface, with E_i being the activation energy for such a jump. E_i was approximated by the activation energy for the movement of an interstitial between graphite planes, i.e., 690 cal/mol [1]. A_o =1 x 10^{-3} cm/sec and was chosen to position the nose of the calculated time-temperature-transformation (TTT) curve with the experimentally observed nose (Fig. 1). The last term represents the driving force for the reaction. P(act) = the actual vapor pressure of bromine at a given temperature and CCl_4 concentration; P(eq) = the bromine pressure at which two stages are in equilibrium. It may be observed that the resultant equation is fairly temperature insensitive until the actual pressure is very close to the equilibrium pressure, at which time the reaction rate will decrease.

The second term in Eq. (1) is due to the time required for bromine to diffuse to the intercalation front. For the diffusion coefficient, D, we have used the form

$$D = D_o \exp[(-Q+P(act)V_a)/RT], \quad (3)$$

where D_o =1.1 x $10^5 cm^2/sec$ and Q = 18 kcal/mol were determined by thermogravimetric measurements. In Eq. (3), V_a represents the dependence of the activation energy on pressure, and was found to be 0.3±0.1 cal/mol-atm. The term η represents a measure of the driving potential for diffusion and is determined by the relation

$$\eta\, \mathrm{erf}(\eta) \exp(\eta^2) = [(P(act)-P(eq)]\pi^{1/2}. \quad (4)$$

3 Experimental

The correlation between the model and experimental results is shown in Fig. 1. The solid squares indicate the times at which intercalation to second stage was complete in a 4 mm HOPG sample; the open squares indicate the times needed to complete third stage intercalation; the solid triangles indicate the times needed to intercalate to fourth stage; the open triangle indicates the time needed to intercalate to fifth stage. These points were determined by observing the stage and distribution of the intercalate as a function of time during intercalation using x-ray diffraction and absorption. The short horizontal lines in Fig. 1 are an approximation of the minimum times at which no pure graphite was left. (HOPG samples, 4 mm wide, were exposed to pure bromine at the given temperature for 10 min., quenched, and the position of the intercalate/graphite interface was determined by x-ray absorption. The time at which no graphite remained was estimated assuming first a growth rate linear in time, and then a growth rate proportional to the square root of time. These estimates represent interface reaction control and diffusion control, respectively.) The curves were drawn using free energy relations determined from the experimental phase diagram [2]. Free energy values for the 7th and 100th stage compounds were extrapolated using the method of Salzano and Aronson [3], where it is assumed that the enthalpy of intercalation decreases with decreasing stage due to an increase in the electrostatic repulsion between intercalate layers.

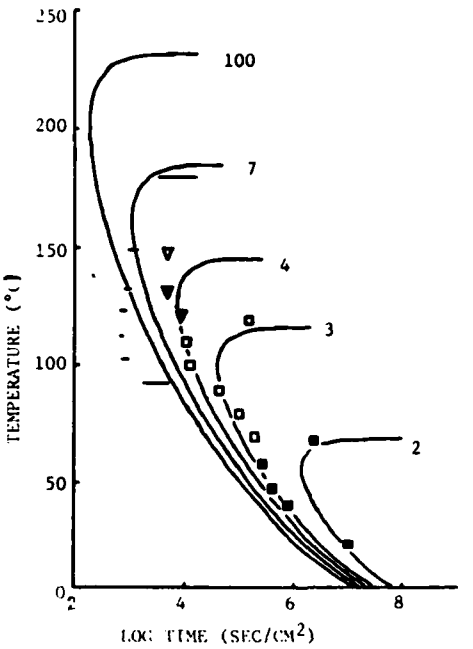

Fig. 1 Time-temperature-transformation curves for graphite bromine intercalation compounds. The solid lines are theoretical curves for the times required to complete intercalation of a 4 mm sample to stage 2, 3, 4, 7, and 100. The experimentally observed times to complete intercalation are given by solid squares for stage 2; open squares for stage 3; solid triangles for stage 4; the open triangle for stage 5. The short horizontal lines indicate the approximate times at which no pure graphite remained.

4 Discussion

In general the rate of intercalation of bromine in graphite appears to be controlled by the rate of diffusion. However, this generalization fails at phase boundaries, i.e., when the change in free energy of an n^{th} stage is only slightly less than that of an $(n+1)^{th}$ stage, the kinetics are

controlled by the rate of the $(n+1)^{th}$ to n^{th} stage reaction. The shape of the TTT-curves is due to the increase in the diffusion rate with increasing temperature until the diffusion rate is larger than the solid state reaction rate. With further increase in temperature, the rate of formation of the final stage decreases as $|\Delta G|/RT$ when ΔG approaches zero.

The most noticeable difference between the theory and data is the maximum intercalation rate (i.e., the nose of the TTT-curves). The theory consistently predicts a maximum rate lower than that actually observed. This may be due to errors in the values for D and Q. The 100^{th} stage curve is drawn to approximate the kinetics of a near infinite stage, and it predicts that a $C_{n\geq 4}Br_2$ compound cannot be stable at high temperatures, namely in the neighborhood of 250°C. This may be understood as a consequence of the decrease with increasing temperature of the free energy change associated with the intercalation of bromine.

Another possible factor in the decrease in rate with increase in temperature is the effect of the hydrostatic pressure due to the bromine vapor pressure. Saunders et al. [4] observed that a uniaxial load of up to 300 atm. applied to HOPG decreased the bromine intercalation rate. Moran et al. [5] observed in the intercalation of nitric acid that the intercalation rate was quite sensitive to an argon overpressure, with a reduction in the reaction rate by a factor of ~50 in the presence of an argon pressure of 5 atm. This raised the question of the effect of pressure on the reaction rate, since there was a rate decrease with increasing temperature and the bromine vapor pressure increased to tens of atmospheres, well above the pressures observed by Moran et al. To test the possibility that the decrease in reaction rate at high temperatures may be due to the hydrostatic pressure of the bromine vapor, a piston-type, teflon-lined copper pressure cell was constructed and the rate was measured for different pressures. The results (Fig. 2), indicated a pressure dependence of the diffusion coefficient of 0.3 cal/mol-atm, which, while in keeping with an estimated activation volume for the viscosity of bromine, was far less than that required to account for the observed decrease in rate with temperature.

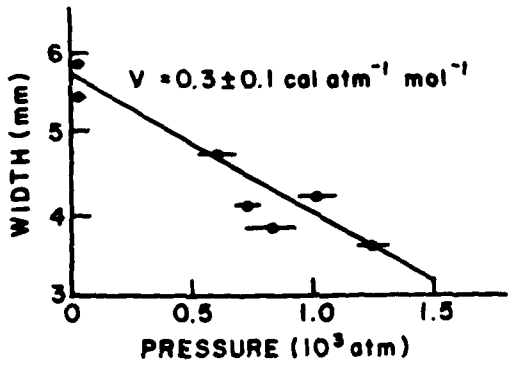

Fig. 2 The width of intercalated graphite in liquid bromine for 10 min. at 113°C as a function of hydrostatic pressure.

5 Conclusion

The kinetics of intercalation of bromine in graphite were modeled on the basis of the change in free energy from stage to stage and the diffusion rate of bromine. The overall reaction rate showed no appreciable pressure dependence in the range of pressures corresponding to the vapor pressure of bromine up to 180°C. The model predicts that graphite-bromine is unstable at temperatures above ~250°C. Satisfactory agreement was found between the model and the experimental TTT-curves.

*Research sponsored by the Air Force Office of Scientific Research, Air Force Systems Command, USAF, under Grant No. AFOSR-78-3536. The United States Government is authorized to reproduce and distribute reprints for Governmental purposes notwithstanding any copyright notation hereon.

1. P.A. Thrower and R.T. Loader, *Carbon*, 7, 467 (1969).
2. S.H. Anderson and D.D.L. Chung, *Proc. of Symposium on Intercalated Graphite, Materials Research Society Annual Meeting, Boston, 1982*, Ed. M.S. Dresselhaus, Elsevier (1983).
3. F.J. Salzano and S Aronson, *J. Chem. Phys.*, 45, 2221 (1966).
4. G.A. Saunders, A.R. Ubbelohde and D.A. Young, *Proc. Roy. Soc.,London*, A271, 512 (1963).
5. M.J. Moran, J.W. Milliken, C. Zeller, R.A. Grayeski and J.E. Fischer, *Synth. Met.*, 3, 269 (1981).

Synthetic Metals, 2 (1980) 57 - 84

KINETICS OF INTERCALATION AND DESORPTION IN GRAPHITE*

K. K. BARDHAN
Department of Physics,
J. C. WU and J. S. CULIK**
Department of Electrical Engineering,
S. H. ANDERSON and D. D. L. CHUNG***
Department of Metallurgy and Materials Science, Carnegie-Mellon University, Pittsburgh, PA 15213 (U.S.A.)
(Received June 7, 1980)

Summary

The kinetics of intercalation was studied by measuring the surface profile on the *c*-face and the expansion at the edge during intercalation. A phenomenological model of interface-controlled intercalation is presented and agreement between the model and various experimental results is shown. The kinetics of desorption was studied by using surface profilometry, gas detection and thermogravimetry. These experimental results suggest a phenomenological model of desorption, which considers the out-diffusion of the intercalate.

1. Kinetics of intercalation

1.1. Introduction

Graphite intercalation compounds are currently being investigated for use in such diverse applications as catalysts, batteries, and electrical conductors due to the attractive properties of intercalation compounds and the variety of intercalation compounds which form. While investigation of the structure and properties of intercalation compounds is important, it is valuable to gain an understanding of the kinetics of intercalation and desorp-

*Research sponsored by the Air Force Office of Scientific Research, Air Force Systems Command, USAF, under Grant No. AFOSR-78-3536. The United States Government is authorized to reproduce and distribute reprints for Governmental purposes notwithstanding any copyright notation hereon.
**Present Address: Solarex Corp., 1335 Piccard Dr., Rockville, MD 20850, U.S.A.
***Also in the Department of Electrical Engineering.

tion in order to provide a guide to determining the optimum conditions for producing a particular type of intercalation compound.

Intercalation is the process which results in a lamellar compound. However, a lamellar compound tends to desorb its intercalate once it is removed from the equilibrium with the intercalate vapor. Although a fraction of the intercalate is still retained in the graphite after desorption has ended, the desorbed compound has a much lower intercalate concentration than the parent lamellar compound. Therefore, understanding the kinetics of desorption is essential for practical uses of graphite intercalation compounds.

In this paper, Section 1 addresses the kinetics of intercalation and Section 2 addresses that of desorption.

The *c*-direction thickness expansion characteristic of intercalation lends itself to investigation of the kinetics of intercalation. Hooley *et al.* [1 - 3], by measuring the thickness at the sample edge and *c*-face center, demonstrated that intercalation begins at the edges of *c*-face surfaces and proceeds to the center. Saunders *et al.* [4, 5] used thickness measurements to calculate the internal constraints on expansion.

The shape deformation known as the "ashtray effect" or "window pane effect" [6] offers a simple and direct means of observing the position of the intercalated region as a function of time. For example, this effect has been used to observe the intercalation of lithium in transition metal dichalcogenides [7]. In this work the topographical profile of the *c*-face was measured during the intercalation of bromine into highly oriented pyrolytic graphite (HOPG) in order to elucidate the intercalation process. Furthermore we have measured the edge expansion of HOPG during intercalation with Br_2, ICl, and HNO_3 in a more rapid and precise manner than has hitherto been done.

1.2. Experimental techniques

1.2.1. Surface profilometry

Specimens used in profilometry were all based on HOPG (Grade ZYA) kindly provided by Union Carbide Corporation. They were cut into cylindrical discs by using a spark cutter, such that the *c*-axis was parallel to the thickness. Disc diameters vary from 4.5 to 8 mm and disc thicknesses vary typically from ~ 0.1 to 0.4 mm. Cleaving by using adhesive tape was performed to improve the smoothness of the *c*-face surface. Samples of large thickness could not be obtained due to the tendency of splitting during spark cutting. Square specimens obtained by using a wire saw were also used.

Profilometry was performed during intercalation with Br_2. Intercalation was achieved by exposing the sample to the vapor of the particular intercalate species. Various Br_2 vapor pressures were achieved by varying the temperature of the Br_2 liquid using a water bath. To obtain the variation of the surface profile during intercalation, the sample was removed from the intercalation vessel at regular intervals and its surface profile was measured at room temperature. Each measurement took, typically, about half an hour.

Occasional interruptions of the intercalation process are believed to have a negligible effect on the experimental results reported here.

The surface profile on the *c*-face was measured by the Tallysurf method using a surface profilometer (Dektak, Sloan Technical Corp.) which had a diamond stylus of radius 0.0005 in. at the tip. The stylus was allowed to move along several diameters of each disc with a pressure of 50 mg/cm^2, which is fixed by the manufacturer. The maximum range of the profilometer was 0.01 cm, which is, in most cases, less than the maximum expansion possible along the *c*-direction (55% of the sample thickness for the case of Br_2 intercalation). As a result, complete surface profiles during the entire intercalation process could not be obtained.

1.2.2. Edge expansion

The apparatus used to measure the edge thickness is similar to that used by Hooley [3]. The sample was supported with glass wool in a glass tube, which was put in a glass weighing bottle containing the chosen intercalate liquid. A cover glass was quickly placed over the greased open end of the bottle, which had air inside. Time was measured from the moment the sample was introduced in the bottle. The liquid was almost 1 cm high and the sample was about 3 cm above the liquid surface. The edge of the sample was then observed by using a travelling microscope equipped with an X–Y micrometer stage and a digital readout. The system enabled readings to be taken once every 20 s on the average, except for the first reading which was taken after about 40 s from the start. The uncertainty in a single reading was about ± 5 μm. The samples were based on highly-oriented pyrolytic graphite (Grade ZYA) supplied by Union Carbide Corp. and were cut by means of a wire saw into pieces of approximately 7 × 7 mm and were cleaved to thicknesses in the range 0.05 - 0.3 mm.

Bromine, ICl, and HNO_3 were the intercalate species chosen because they are known to cause crack formation in order of increasing severity. A further motivation for the choice of these intercalate species was to investigate the possible effects of the intercalation mechanism on the edge expansion; nitration is known to be accompanied by a progressive change in stage during intercalation to a given eventual stage [8] whereas bromination is not [9].

1.3. Experimental results

1.3.1. Surface profilometry

The sequence of surface profiles obtained at four different times during Br_2 intercalation is shown in Fig. 1. The sample was of diameter 4.5 mm and thickness 0.3 mm. An advancing intercalate front was clearly observed. In the early part of intercalation, the profile was bucket shaped. Later, the profile became V-shaped such that the region outside the V-shaped part of the profile was roughly flat. As intercalation further progresses, the V-shaped part of the profile decreases in size and eventually leaves a rough, flat surface.

60

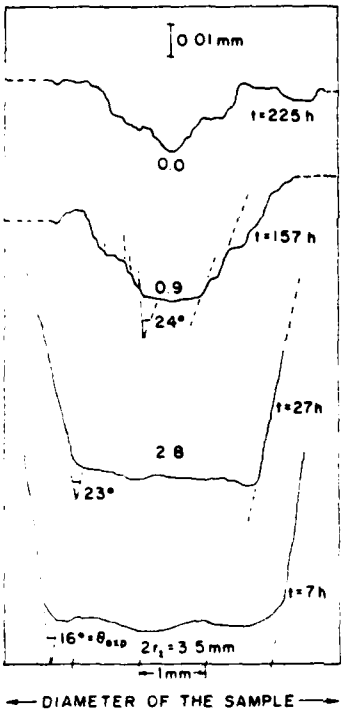

Fig. 1. Sequence of *c*-face surface profiles of a cylindrical HOPG sample (diameter 4.5 mm, thickness 0.3 mm) as bromination proceeds at room temperature.

Of importance is the linearity of the slanted portions of the profile, *i.e.*, the sides of the "bucket". The angle between these sides is indicated for three profiles in Fig. 1. Due to the difference in scale between the vertical and horizontal axes in Fig. 1, the measured angles indicated are not the actual angles. Corresponding to the measured angle θ_{exp} (Fig. 1), the actual slope of the slanted portion is 1/50 cot ($\theta_{exp}/2$). The trend in slope variation, as shown in Fig. 1, is quite representative. This is also shown in Fig. 2, where the actual slope is plotted against the time of intercalation for samples of different diameters and thicknesses. In spite of the scatter in the data points, it is evident that the slope is steep at the beginning and then decreases quickly to a steady value. It should also be noted that the large scatter in the slope data obscures the effect of the size of the sample, if an effect is present. The steady value of the slope is about 0.08. Extrapolation to zero time is quite uncertain, given the time scale shown in Fig. 2.

An interesting feature is the appearance of rings, as seen visually, and of corresponding ledges, as seen in the profiles (*e.g.*, at t = 157 h) in Fig. 1 after some time of intercalation. In many cases, the parallel nature of the ledges is remarkable and simplifies the determination of the slope, as illustrated by the dashed lines in the third profile from the bottom of Fig. 1. The

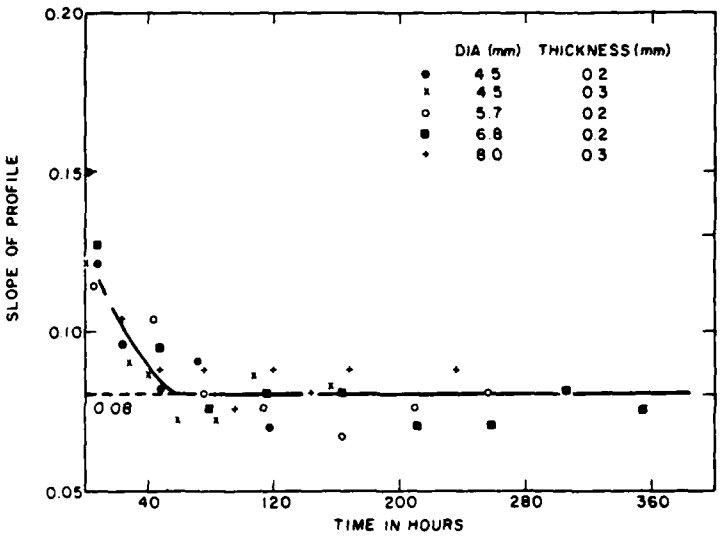

Fig. 2. Plot of the actual slope of the surface profile *vs.* time for samples of various diameters and thicknesses.

number of occurrences of the ledges appears to increase with time, but decrease with increasing sample diameter. Moreover, it is insensitive to the thickness. Although the height of the ledges tends to increase with diameter, the width apparently is independent of size and is of the order of 100 - 150 μm. The origin of the ledges is presently not clear.

The variation in the diameter of the contour of the intercalate front during intercalation is shown in Fig. 3 for samples of different diameters but of the same thickness, and is shown in Fig. 4 for samples of different thicknesses but of the same diameter. The slope of this plot yields the velocity of the front. The general features of the plot are noted below.

(1) Each curve is dominated by a linear portion which indicates that the velocity is constant for the most part of the intercalation process. This means that the intercalation process is interface-controlled. However, the initial portion is characterized by a steeply falling curve, implying that the velocity decreases rapidly from a large, average, initial value ($\sim 5 \times 10^{-6}$ cm/s) to a steady value which is at least an order of magnitude less. The magnitude of the steady velocity is shown for each curve.

(2) Irrespective of diameter or thickness, all the curves approach linearity at approximately the same time ($\sim$44 h), which is close to the time at which the slope becomes steady (Fig. 2). Moreover, the amount of decrease in the intercalate front contour diameter ($\sim$2.3 mm) in this period is apparently independent of the sample diameter or thickness.

(3) There is apparently no correlation between the magnitude of the steady velocity and the sample thickness (Fig. 4). For a given thickness (Fig. 3), the steady velocity appears to be fairly independent of the dia-

62

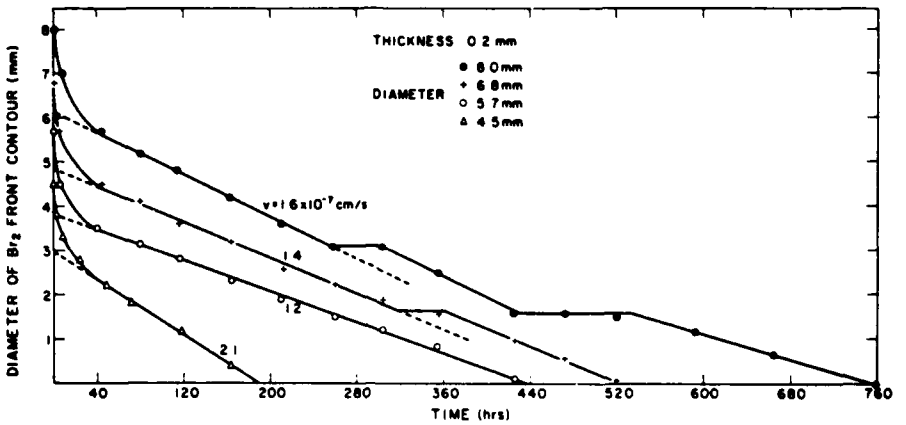

Fig. 3. Plot of the Br_2 front contour diameter *vs.* time for samples of the same thickness but of different diameters. The magnitude of the steady velocity is indicated for each curve.

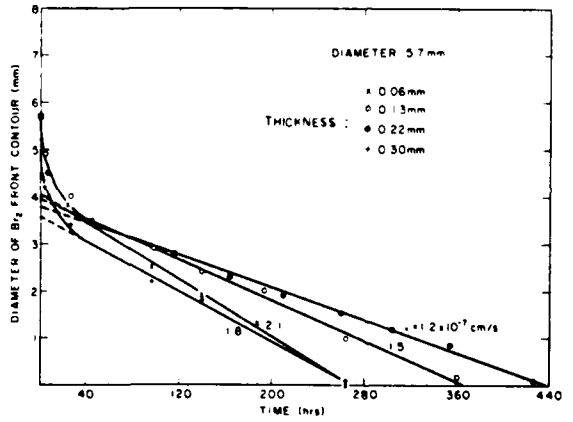

Fig. 4. Plot of the Br_2 front contour diameter *vs.* time for samples of the same diameter but of various thicknesses. The magnitude of the steady velocity is indicated for each curve.

meter, as long as the sample diameter is large compared with ~2.3 mm. However, as the diameter becomes comparable with 2.3 mm, as for the 4.5 mm diameter case, the steady velocity increases with decreasing diameter, though the applicable region decreases in extent.

(4) In Fig. 3, the two curves corresponding to large diameters for the same thickness show "steps" (drawn as a guide to the eyes), whereas the other two curves corresponding to smaller diameters do not. As seen in Fig. 4, for the same diameter, no steps appear as the thickness increases.

An interesting conjecture about the last mentioned feature is that, as the sample diameter increases, the steps may become more numerous so as to

cause considerable decrease in intercalate absorption rate. The step may even assume an indefinite width so that intercalation stops. It is interesting to note contrasting effects of the diameter and thickness found by Hooley [3] in the intercalation of natural graphite flakes of dimensions generally smaller than those used in this work.

The above experimental results were obtained with the sample at room temperature and the bromine vapor pressure at 200 mmHg (corresponding to that in equilibrium with room temperature liquid Br_2). In addition, we have performed surface profilometry for various sample temperatures and various intercalate vapor pressures. With the sample at 22 °C, the speed of intercalation was found to increase with increasing Br_2 vapor pressure; with the Br_2 vapor pressure at 200 mmHg, the speed of intercalation was found to decrease with increasing sample temperature. Shown in Fig. 5 is the variation of the intercalate front position with time during intercalation at various intercalate vapor pressures.

The variation of intercalate vapor pressure provides an investigation of the dependence of the kinetics of intercalation on the final stage. It is also of interest to investigate the dependence of the kinetics of intercalation on the initial stage. All of the results discussed above were obtained with the initial stage being ∞ (*i.e.*, pristine graphite). To investigate the dependence on the initial stage, we have performed surface profilometry during Br_2 intercalation from stage 4 to stage 2. Figure 6 shows the evolution of half of the surface profile during this intercalation. The sample was initially intercalated with the Br_2 vapor pressure at 120 mmHg. X-ray diffraction showed that the compound formed was stage 4, together with a small amount of stage 3. At this vapor pressure, the intercalate front moved at a speed of $v_1 = 9 \times 10^{-8}$ cm s^{-1}. After a certain time period, the Br_2 vapor pressure was changed from 130 mmHg to 200 mmHg, because the compound formed at 200 mmHg is stage 2. A stage 2 compound has a thickness increase of 55% over the pristine graphite, whereas

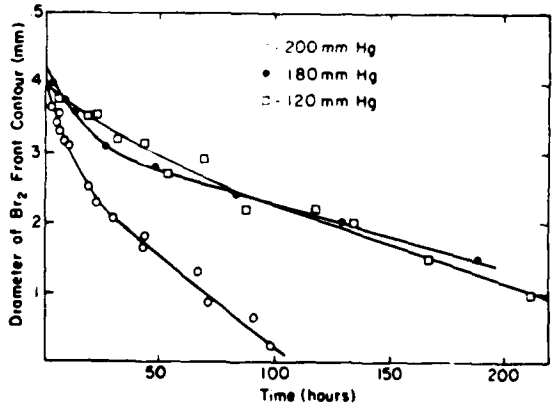

Fig. 5. Plot of the Br_2 front contour diameter vs. time for intercalation at different intercalate vapor pressures.

64

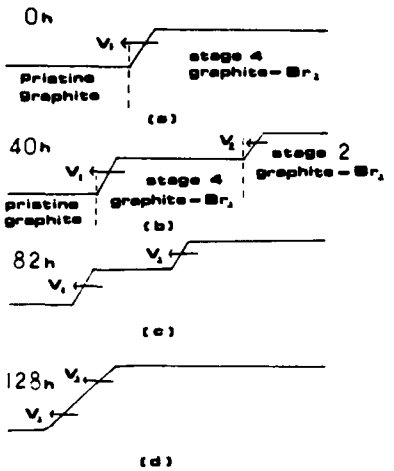

Fig. 6. Schematic diagram showing the evolution of half of the surface profile during two-step intercalation. The first step was vapor phase intercalation at a Br_2 vapor pressure of 130 mmHg, giving stage 4 in the intercalated region. The second step was vapor phase intercalation at a Br_2 vapor pressure of 200 mmHg, giving stage 2 near the edge of the profile. (a) Shows the profile during the first step; (b), (c) and (d) show the second step. $v_1 = 9 \times 10^{-8}$ cm s^{-1}; $v_2 = 2.5 \times 10^{-7}$ cm s^{-1}.

a stage 4 compound has a thickness increase of only 27%. Because of this difference in thickness expansion, the movement of the intercalate fronts of both stage 4 and stage 2 components in the sample could be observed, as shown in Fig. 6(c). The intercalate front of the stage 2 component was found to move at a speed of $v_2 = 2.5 \times 10^{-7}$ cm s^{-1}, while that of the stage 4 component still moved at a speed of v_1. Since $v_2 > v_1$, the stage 2 intercalate front finally caught up with the stage 4 intercalate front and the two fronts became one.

1.3.2. Edge expansion

Figure 7 shows the typical expansion *versus* time curves during the intercalation of the three intercalate species in samples of approximately the same size. In the case of Br_2 intercalation, the expansion approaches a limiting value of 55%, which is indicated by an asterisk in Fig. 8 and is equal to the calculated value, based on X-ray diffraction data, of the lattice expansion. In the cases of ICl and HNO_3 intercalation, the expansion curves exceed the theoretical limits. In particular, nitration caused expansion several times larger than the theoretical limit. This behavior was due to cracks which gradually became visible. In addition, in the case of ICl intercalation, a sharp decrease in the expansion rate characteristically occurred at an expansion corresponding to the theoretical value for a first stage compound. Given a sufficiently thick sample, bromination also causes cracks. Thus, apart from showing the expansion behavior with and without cracks, the comparison of the three curves in Fig. 7 demonstrates that the minimum thickness for cracking, in the presence of saturated intercalate vapor at a

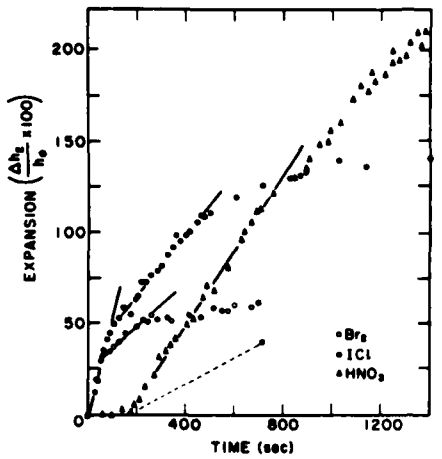

Fig. 7. Variation of the percent. expansion with time during the intercalation of Br_2, ICl, and HNO_3. The theoretical limits in expansion are indicated by *.

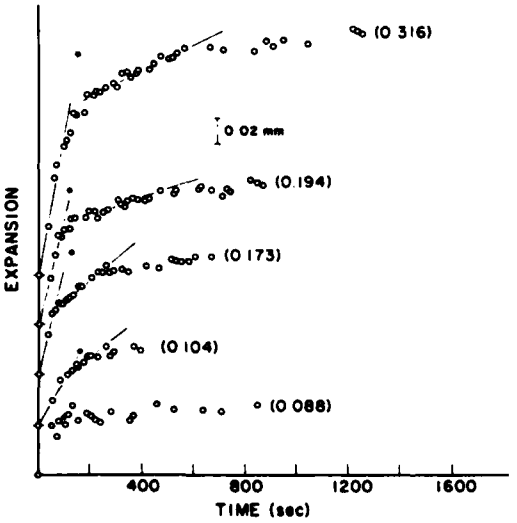

Fig. 8. Variation of expansion with time during Br_2 intercalation of samples of various initial thicknesses, indicated in units of mm in parentheses. The theoretical limits in expansion are indicated by *.

given temperature, decreases in the order Br_2, ICl and HNO_3, as will be expected from comparison of their respective layer spacing expansions d'.

The expansion curves for Br_2 and ICl are rather similar to each other in shape, as expected. For each intercalate, the curve below the theoretical limit, marked by an asterisk in Fig. 7, exhibits two dominant linear portions distinguished by different slopes. This is illustrated in Figs. 8 and 9 with data

for various initial thicknesses. This feature has not been previously reported. The initial slope is always greater than the later one; the ratio seems to increase with the initial thickness in the case of bromination. In fact, the expansion curve for the thinnest sample used (0.088 mm thick) for bromination appeared to be a single, straight line within the experimental uncertainties. Interestingly, the expansion at which the change of slope occurred was neither constant nor a definite fraction of the sample thickness.

The expansion curves for nitration are dominated by an initial linear portion followed by a nonlinear expansion of generally lower expansion rate (Fig. 7). The expansion curve provides no obvious indication of changes in stage during intercalation. Expansion during HNO_3 intercalation differs from that during Br_2 or ICl intercalation by the presence of an "induction period" of about 2 min during which there was no expansion. Previous studies [6, 10] have found that no mass uptake occurred in similar induction periods, though the periods were longer.

On the basis of Hooley's results [1], *i.e.*, that intercalation starts at the *c*-face surfaces and proceeds to the middle of the edge, one would expect the

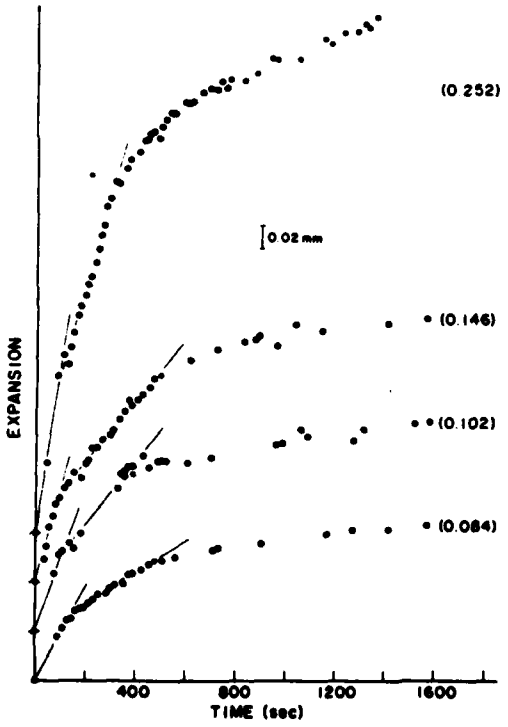

Fig. 9. Variation of expansion with time during ICl intercalation of samples of various initial thicknesses, indicated in units of mm in parentheses. The theoretical limits in expansion are indicated by *.

absolute expansion rate to be independent of sample thickness. As shown in Fig. 10, we observed that the absolute expansion rate increased with sample thickness for all three intercalate species. Furthermore, the surface cracks which appeared at early stages of ICl and HNO_3 intercalation showed no spacial preference and were distributed uniformly over the graphite surface. Both of these observations suggest that intercalation is initiated uniformly over the graphite surface. The disagreement with Hooley's results probably is due to the much thicker specimens used by Hooley than those examined in this work.

1.4. Model of interface-controlled intercalation

The proposed model is based on a mechanism of nucleation and subsequent growth, considered for simplicity in a perfect graphite structure.

According to the mechanism suggested by Hooley [1] for the intercalation of bromine in graphite, we assume that intercalation starts at the interlayer spaces at the two ends and proceeds toward the inner region in such a way that there are n graphite layers between two successive, nucleated intercalate layers for an eventual n-th stage intercalation compound*. We further assume that the nucleation of an intercalate layer occurs at the edge of the layer, and that once nucleated, the intercalate layer grows toward the inside at a velocity, v, which is, in general, a function of time. The structure of the resulting intercalate layer corresponds to that of an n-th stage compound. As the first intercalate layer grows, nucleation occurs at the inter-

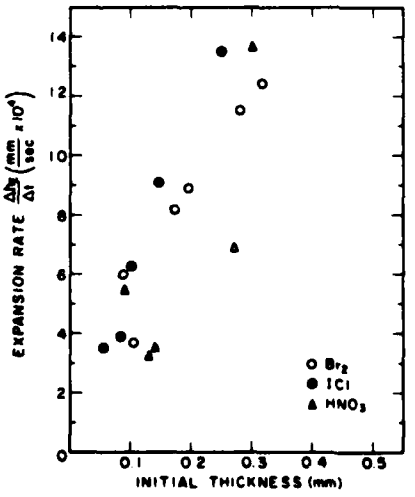

Fig. 10. Dependence of the absolute expansion rate on the initial thickness.

*This assumption implies that the system does not progressively go through different stages on the way to a given stage.

layer space separated by n graphite layers from the first intercalate layer. In this way, the nucleation and growth of an intercalate layer eventually take place at every interlayer space appropriate for the n-th stage compound. Let the time gap between the nucleation of two successive intercalate layers be ΔT, which we assume to be constant at a given pressure and temperature.

A schematic diagram of a sample at an instant of time during intercalation to a stage 2 compound is shown in Fig. 11. When the intercalate enters an interlayer space, it forces the spacing between the bounding graphite layers to expand. Thus, the thickness profile as well as the weight of the sample change as intercalation proceeds. On the basis of the above model, these changes can be expressed analytically as functions of the time of intercalation. For simplicity, we have restricted our consideration to cylindrical samples with the thickness along the c-direction, though the analysis can be extended to samples of other shapes. Let the radius of the cylinder be R_0; let there be Nn graphite layers in the cylinder, where n is the stage of the compound that eventually forms. This means that the number of intercalate layers in the cylinder after the completion of intercalation is N. The thickness of the cylinder before intercalation is Nnd, where d is the interlayer spacing in pure graphite.

The proposed model indicates the existence of several time lengths that are of importance. Let the time taken for the nucleation of all intercalate layers be t_N, which is given by

$$t_N = \left(\frac{N}{2} - 1\right) \Delta T \approx \frac{N}{2} \Delta T \tag{1}$$

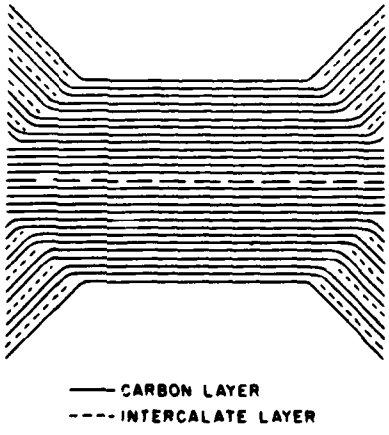

Fig. 11. Schematic diagram of a sample at an instant of time during intercalation to a stage 2 compound.

The above approximation is used in the rest of this model.

Let $r(t) = R_0\, g(vt/R_0)$ denote the radius of the advancing (inner) front of an intercalate layer at time t after its formation. If the layer grows at a steady velocity, v, g is simply given by

$$g\left(\frac{vt}{R_0}\right) \equiv 1 - \frac{vt}{R_0}\,. \tag{2}$$

In what follows, each intercalate layer is assumed to grow with the same velocity, v, in the manner described by eqn. (2). The radius of the intercalate front contour for the j-th intercalate layer at time t is given by

$$r_j = R_0 - v(t - j\Delta T)\,. \tag{3}$$

Clearly, the time of completion of growth of the outermost layers is $t_G = R_0/v$. The time when intercalation is finished corresponds to the time at which the $N/2$-th intercalate layer (the middle intercalate layer) completes its growth. This occurs at a time $t_I = t_N + t_G$ after the start of intercalation.

Depending on the ratio of the thickness to the radius of the cylindrical sample at a given pressure and temperature, one of two cases occurs during intercalation.

Case 1: $t_N < t_G$.

This means that the nucleation of all intercalate layers is completed before the growth of the outermost layers is completed.

Case 2: $t_N > t_G$.

This means that the nucleation of intercalate layers continues after the growth of the outermost layers is completed.

1.4.1. Surface profile

To follow the variation in the surface profile during intercalation for Case 1, consider, separately, three time intervals: (a) $0 < t < t_N$, (b) $t_N < t < t_G$ and (c) $t_G < t < t_I$.

Consider first the interval $0 < t < t_N$. Let $h(r,t)$ be the increase in thickness at a distance r from the center and at a time t from the start of intercalation. Note that, for a cylindrical sample, the intercalate front is circular, so that h is radially symmetrical.

Let us assume that the increase in the separation of two consecutive graphite layers at r is proportional to the concentration at r of the intercalate layer in between them. In interface-controlled intercalation, there is no intercalate concentration gradient in the intercalated region. Thus, half of the total increase in thickness is given by

$$h(r,t) = d'j, \tag{4}$$

where $2j$ is the number of intercalate layers that have progressed up to point r at time t, and d' is the change in the spacing between two adjacent graphite layers due to the insertion of an intercalate layer in between (3.7 Å for Br_2

intercalation). Putting eqn. (4) in eqn. (3) yields the equation for the thickness at r for $t \leq t_N$:

$$r = R_0 - v\left(t - \frac{h\Delta T}{d'}\right). \tag{5}$$

The intercalate front corresponds to $h = 0$ in eqn. (5) and its position $r = r_I$ is given by:

$$r_I = R_0 - vt. \tag{6}$$

Rearrangement of eqn. (4) gives

$$h(r,t) = \begin{cases} \dfrac{d'}{v\Delta T}\left[r - (R_0 - vt)\right], & r \geq r_I \\ 0, & r \leq r_I. \end{cases} \tag{7}$$

Before intercalation begins ($t \leq 0$), the profile is flat, as shown by curve 0 in Case 1 of Fig. 12. As time progresses, the profile corresponding to eqn. (8) on one of the c-faces becomes bucket-shaped, as indicated by the line abcd (curve 1) in Case 1 of Fig. 12. The slanted linear portions (ab, cd) have a slope equal to $d'/v\Delta T$ and the intercalate front (b, c) moves with a constant velocity equal to v. As intercalation proceeds further, the straight lines ab or cd translate parallel to themselves toward the center.

The edge thickness increases to the maximum value, $h_{\infty} = Nd'$, at a time $t = t_N$. After time $t = t_N$, the lines ab and cd continue to translate parallel to

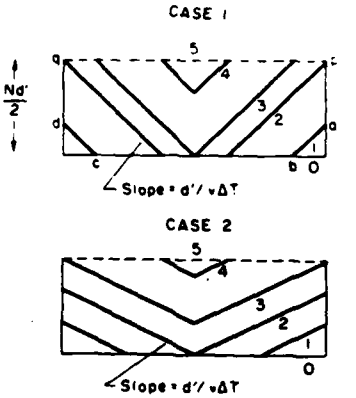

Fig. 12. Schematic diagram of the sequence of surface profiles as interface-controlled intercalation proceeds with time.
Case 1 ($t_N \leq t_G$). Curve 0: $t = 0$; 1: $t < t_N$; 2: $t = t_N$; 3: $t = t_G$; 4: $t > t_G$; 5: $t = t_I$;
Case 2 ($t_N > t_G$). Curve 0: $t = 0$; 1: $t < t_G$; 2: $t = t_G$; 3: $t = t_N$; 4: $t > t_N$; 5: $t = t_I$.

themselves until time $t = t_G$, when these lines meet at the center of the sample and result in a V-shaped profile, as shown by curve 3 in Case 1 of Fig. 12. At this time, the formation of the first intercalate layers is completed. After this, the V-shaped part of the profile becomes smaller as more intercalate layers are completely formed, as shown by curve 4 in Case 1 of Fig. 12. When intercalation is completed ($t = t_I$), the V-shaped part of the profile vanishes, leaving a flat surface, as shown by the line pq (curve 5) in Case 1 of Fig. 12. This line is parallel to line bc and is at a height of $Nd'/2$ from line bc.

Similar arguments give the evolution of the surface profile for Case 2 ($t_N > t_G$), as illustrated in Fig. 12.

The evolution of surface profiles as predicted for Case 1 of the model of interface-controlled intercalation is in excellent qualitative agreement with the experimental results in Fig. 1. In particular, the change of a "bucket" shape to a "V" shape, as discussed in the model, is well confirmed. All experimental results belong to Case 1, in which the time of nucleation of all layers (t_N) is less than the time of completion of the outermost layers. This is not unexpected in view of the fact that the samples used had the thickness much less than the diameter.

As indicated already in Figs. 2 - 4, the slope of the profiles and the velocity of the intercalate front remain constant for the most part of the growth period, as was assumed in the model. However, the initial period is apparently marked by changing slope and velocity. This can possibly be attributed to an edge effect for the following reasons. The fact that the velocity decreases from a large value at the edge to a smaller, steady value after the intercalate layers have moved a certain distance inside the sample is consistent with a smaller resistance to deformation at the edge than inside. Moreover, the distance the intercalate front moves inside until the steady state is reached is independent of the sample diameter. This means that steady state can be considered to correspond to an infinite sample.

Since, in the model, the slope is equal to $d'/v\Delta T$, where d' is the expansion of the graphite layer spacing and ΔT is the time gap between the formation of two successive intercalate layers, it might seem that the initial decrease in slope may be explained by an increase in ΔT with time. However, the explanation might be applied only up to time t_N, which is also the time required for completing the edge expansion. For the HOPG samples used in the present work, t_N is of the order of a few minutes, as determined by edge expansion measurement (Section 2.4.2), whereas the slope continues to decrease for a much longer time (~44 h). Alternatively, the simple assumption of constant ΔT, with the velocity of growth of the intercalate layers decreasing with increasing distances from the surfaces, can explain the decrease in slope. Indeed, it is quite reasonable to assume that the further away from the c-face surface an intercalate layer is, the smaller is the velocity due to the increasing rigidity until the steady state is reached. Since the time of the first measurement is a few hours after the start of intercalation, a rigorous determination of the parameter ΔT used in the model cannot be made. This is because the determination of ΔT requires the evaluation of the

slope by extrapolation to zero time. Due to the scatter in the data, this extrapolation is quite rough. However, this difficulty does not necessarily exist in the case of samples which have large values of t_N. It must be noted that using the value of the steady slope yields only a redefined value of ΔT, which is about 3 s, as compared with the value of 10^{-3} s obtained from edge expansion results.

1.4.2. Edge expansion

It follows from eqn. (7) that at the edge, where $r = R_0$ the total expansion $h_E = 2h$ is given by

$$h_E(t) = \begin{cases} 2d' \dfrac{t}{\Delta T}, & 0 \leq t \leq 1/2(N\Delta T) \\ \\ Nd', & t \leq 1/2(N\Delta T). \end{cases} \tag{8}$$

Edge expansion is finished when all the intercalate layers are nucleated, *i.e.*, at a time equal to $1/2(N\Delta T)$. Thus the model predicts that the expansion is linear in time and that ΔT is inversely proportional to the rate of expansion.

The edge expansion results obtained during Br_2 and ICl intercalation can be described fairly well by the model if the quantity ΔT is allowed to increase to a larger value after some expansion. This appears plausible because the middle layers may be constrained in such a way as to cause a change in the rate of nucleation. Let ΔT_1 be the value of ΔT corresponding to the first slope; let ΔT_2 be the value of ΔT corresponding to the second slope. The ratio of ΔT_2 to ΔT_1 is always equal to, or greater than, unity, as mentioned earlier. Considered in the light of the model, the graphite (natural flakes)–$FeCl_3$–nitromethane system investigated in detail by Hooley [3] seems to provide an interesting example of a situation in which ΔT_2 is infinite; *i.e.*, there is no further expansion. The data indicate that the edge expansion of the flakes is initially quite linear in time and then it stops at an expansion which is generally less than the maximum possible. However, there is a difference between the $FeCl_3$ intercalation of Hooley and our Br_2 and ICl intercalation in that the initial rate of expansion appears to decrease with increasing initial thickness in the case of the former, whereas the opposite is true for the latter. For comparable thicknesses, ΔT_1 for $FeCl_3$ intercalation is of the order of 0.1 s, which is about two orders of magnitude greater than the corresponding value for Br_2 or ICl intercalation. This is not surprising in view of the low molarity of $FeCl_3$ in the $FeCl_3$–nitromethane solution used.

The sensitivity of ΔT_1 to the partial pressure of an intercalate at a fixed temperature can be seen in Fig. 13, when $\log \Delta T_1$ is plotted against $p_o/(p - p_{th})$, where p_o is the vapor pressure of Br_2 at the fixed temperature, p is the Br_2 pressure and p_{th} is the threshold pressure. The ΔT_1 values were calculated using eqn. (8) from the data obtained by Saunders *et al.* [5] with

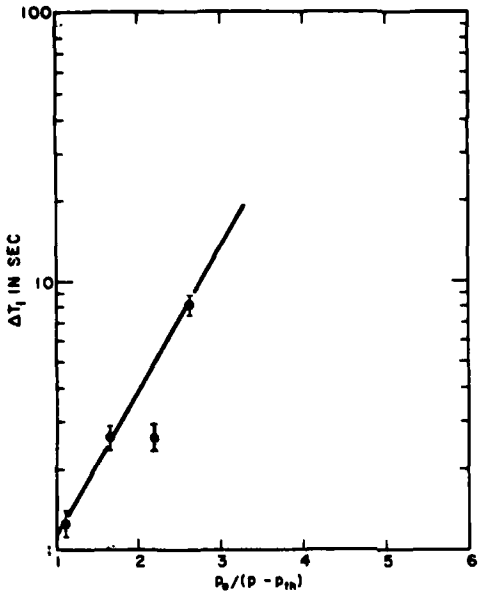

Fig. 13 Log ΔT_1 *vs.* $p_o/(p - p_{th})$, where p_o is the vapor pressure of Br_2 at the fixed temperature, p is the Br_2 pressure and p_{th} is the threshold pressure.

an uniaxial load on the sample at 20 °C. On the basis of the linearity of the plot, which is based on limited data points, the dependence of ΔT_1 on Br_2 pressure, p, may be written in the following empirical form:

$$\Delta T_1 = A \exp [B/(p - p_{th})] (p \geq p_{th}), \quad (9)$$

where A and B are functions of temperature. In Fig. 13, p, corresponding to a certain mole fraction of Br_2 in the Br_2–CCl_4 solution, was obtained from the table in ref. 6. At $p = p_{th}$, ΔT_1 is infinite, indicating that no intercalation takes place. For the case of pure bromine, Fig. 13 shows that $\Delta T_1 = 1.2$ s, which is very large compared with the first value given in Table 1. This is due to the fact that a load of 95 kg/cm^2 was applied to the sample in the work of Saunders *et al.* [5].

The perfection of the graphite material also has a large influence on the rate of expansion or ΔT_1, as shown in Table 1, where the samples are listed in order of increasing perfection of the graphite material. In particular, the results of Hooley *et al.* [5] on samples of equal thickness clearly show the trend that the higher is the perfection of the graphite material, the smaller is ΔT_1 or the higher is the rate of expansion. A similar trend applies to the electrical resistivity and threshold pressure [11]. In the absence of sufficient relevant data, it is difficult to establish an absolute correspondence between ΔT_1 and the variables mentioned above. However, ΔT might prove to be equally as good as resistivity or threshold pressure in determining the per-

TABLE 1

Values of ΔT_1 for intercalation of different types of graphite at a Br_2 pressure of 145 mmHg at 20 °C

Source	*Sample*	*Dimensions* * (cm)	ΔT_1 (s)
Saunders *et al.* [5]	A	0.4 × 0.4 × 0.1	7×10^{-2}**
Hooley *et al.* [1]	PG1	0.26 (dia.) × 0.6	1.9×10^{-2}***
	PG3	0.26 (dia.) × 0.6	4.2×10^{-4}***
	PG6	0.45 × 0.45 × 0.6	1.5×10^{-4}***
Present work	HOPG	0.7 × 0.7 × 0.03	6.8×10^{-4}

*The last dimension listed is the thickness.

** This value is obtained by extrapolating the curve of ΔT_1 *vs.* load at 20 °C, to zero load.

***These values are based on the data given in Table 1 of ref. 1; they are rough estimates only. Disc production tends to underestimate the values by enhancing the rate of expansion.

fection of the graphite material, especially since ΔT_1 has the advantage of being easily measurable. However, ΔT_1 has the disadvantage of being dependent on the size, particularly the thickness, as shown by comparison of the data in the last two lines in Table 1. ΔT_1 for HOPG is expected to be smaller than that for PG6, but, due to a difference in thickness, it is not.

The stage of an intercalation compound is best determined by X-ray diffraction. The stage number as well as the layer spacing expansion should ideally agree with the macroscopic expansion along the *c*-axis. Conversely, the stage number can ideally be ascertained from the macroscopic expansion [12] with the help of only the knowledge of the layer spacing expansion. From eqn. (8), the theoretical maximum macroscopic expansion is Nd'. The initial thickness can be written as Nnd, where n is the stage number and d is the pure graphite layer spacing (3.35 Å). Thus, the theoretical fractional expansion is d'/nd. For the first stage ($n = 1$) graphite–ICl compound, $d' =$ 3.89 Å, so that the theoretical fractional expansion is 116%, as indicated by asterisks in Fig. 9. It is clear that the presence of cracks will lead to misleading results, as is evident in the review of different previous results for ICl intercalation [13]. Therefore, measurement of the final expansion is not as revealing as that of the expansion during the whole course of intercalation.

The model is applied to nitration by assuming that ΔT_1 is an overall rate determining quantity, since an initial linear portion is obtained in the experimental data of expansion *vs.* time (Fig. 6). We further assume that the time at which the lattice expansion is finished corresponds to the time when the curve deviates from linearity in Fig. 6. In this context, the dashed line in Fig. 6 represents the true lattice expansion. It should be mentioned that the concentration of fuming nitric acid used in this work was such that a third stage graphite nitrate resulted, as verified by X-ray diffraction. Accordingly, ΔT_1 for nitration is 8.0×10^{-3} s.

There has not been much experimental data which can yield clues to the relationship between ΔT_1 and temperature. From the data of Saunders *et al.* [5], it is evident that the rate of expansion falls with increasing temperature. This is consistent with the fact that the velocity of the intercalate front decreases with temperature (Section 2.3.1) and with the interpretation of ΔT given in terms of the velocity (Section 2.4). If the distance an intercalate layer has to move inward before the next layer is nucleated does not vary much with temperature, the decrease in velocity means a longer time gap (ΔT_1) between successive nucleation events. The threshold pressure also increases with temperature [4, 5]. This is not unexpected if we assume that the threshold pressure represents the pressure for the initiation of nucleation.

The decrease in the expansion rate during Br_2 intercalation is consistent with the discrepancy found in the later period of expansion between the model prediction and the experimental curve of fractional expansion *vs.* fractional mass uptake (Section 2.4.3). The calculated curve based on a single ΔT rises faster than the data beyond 80% of the expansion. Taking into account a slower rate of expansion will obviously reduce the discrepancy. It may be noted that the stage number n need not be an integer as has been tacitly implied in the model. In fact, n can be defined just as the ratio of the number of graphite layers to the number of intercalate layers. This is in accordance with the finding that the equilibrium expansion under a certain pressure is proportional to the mass uptake [4, 5]. A similar view has also been adopted in connection with the interpretation of X-ray diffraction patterns [14]. This, of course, means that ΔT should be considered as an average time gap between two successive nucleation events.

2. Kinetics of desorption

Desorption is due to the thermodynamic instability of lamellar compounds. This instability results from the relatively weak bonding between carbon and the intercalate and between adjacent intercalate atoms or molecules, as evident in graphite–Br_2. Surface profilometry, described in Section 2.1, has been performed to study the kinetics of desorption, with further information obtained through isothermal and scanning thermogravimetry, as well as detecting the effluent gas during desorption.

2.1. Experimental techniques

2.1.1. Gas detection

The detection of desorbed intercalate from a sample upon heating was achieved by using an effluent gas analyzer incorporated in a differential scanning calorimeter (Perking-Elmer DSC-1B). The analyzer consisted of a two-thermistor bridge circuit which monitored the thermal conductivity of the DSC sample holder purge gas relative to the gas which bypassed the sample holder. The system was purged at 30 cm^3/min with dry nitrogen. A weighed graphite–Br_2 sample was placed in a platinum pan and mounted in

the DSC sample holder which was purged for about 10 min at room temperature. The sample temperature was increased at either 5 or 10 °C/min. A Columbia Scientific Industries integrator was used to record the effluent analyzer output; the acquisition rate was 5 or 10 per min.

2.1.2. Thermogravimetry

The thermal gravimetric measurement was performed by using a Perkin-Elmer electronic microbalance (Autobalance Model AD-2Z), which has a maximum sensitivity of 0.1 μg. The sample was placed on a pyrex pan which was suspended by a pyrex hangwire. A 19 mm i.d. pyrex tube enclosed the hangwire and the sample pan. During the measurement, the tube was slowly purged with argon at approximately 20 cm^3/min. A low mass furnace surrounded the sample pan and was controlled by a Theall Engineering Model TP-2000 temperature programmer, which was capable of either isothermal or scanning temperature control. The sample temperature was measured by placing a chromel–alumel thermocouple immediately below (within 2 mm) the sample pan. During isothermal measurements, the controller kept the sample temperature within 1 °C from the programmed temperature. All temperature scans were performed at a heating rate of 2 °C/min.

2.2. Experimental results

2.2.1. Gas detection

Typical effluent gas analyzer response is shown in Figs. 14 and 15. A graphite–Br_2 sample, which had been allowed to desorb at room temperature from 83 to 43.3 wt.% Br_2, was heated from room temperature to 107 °C at 10 °C/min, as shown in Fig. 14. Little evolved bromine was detected until 101 °C. At this point a considerable amount of intercalate was detected and is interpreted as being an effect of intralayer intercalate position disordering at 100 °C.

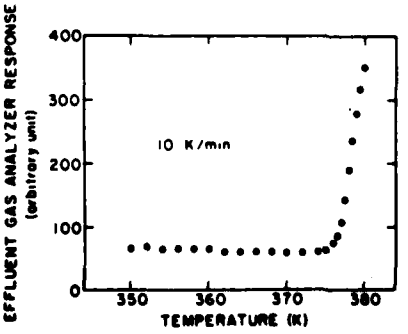

Fig. 14. Effluent gas detector response as a function of temperature, showing desorption commencing at the intralayer order–disorder transformation temperature in graphite–Br_2 (100 °C). The sample contained 43.3 wt.% Br_2 before heating.

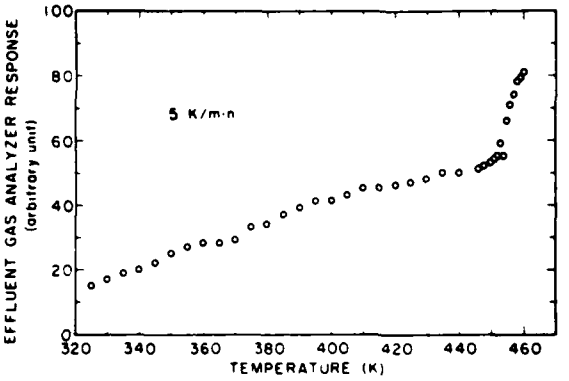

Fig. 15. Effluent gas detector response as a function of temperature, showing desorption associated with exfoliation near 177 °C. The sample contained 21.5 wt.% Br_2 before heating.

Figure 15 shows the effluent gas analyzer response for a less concentrated graphite–Br_2 sample at a higher temperature range and sensitivity. The sample was originally a saturated lamellar compound (83 wt.% Br_2); prior to this temperature scan, it had been desorbed at room temperature and by heating to about 117 °C, and it contained 21.5 wt.% Br_2. The temperature of the sample was scanned from room temperature to 187 °C at 5 °C/min. In Fig. 15, the analyzer trace increases slowly (probably due to baseline drift at this high sensitivity) until about 177 °C, where the amount of desorbed intercalate increased sharply. This increase is attributed to extensive exfoliation, which was visually confirmed at 176 °C for this sample.

The amount of vapor desorbed near 101 °C has been found to increase significantly with increasing intercalate concentration. At low intercalate concentration, as for the sample of Fig. 15, this increase at ~102 °C was too small to be observed, By contrast, at relatively high intercalate concentrations, as for the sample of Fig. 14, a large increase was observed at ~102 °C.

By using the gas detection technique, we have found that the intralayer order–disorder transformation and exfoliation greatly affect the rate of intercalate desorption. However, the effect of the order–disorder transformation on desorption is small at low intercalate concentrations. In order to study these effects more precisely and to obtain information on the kinetics of intercalate desorption, we have used thermogravimetry, as described in Section 2.2.2.

2.2.2. Thermogravimetry

2.2.2.1. Isothermal desorption. Isothermal desorption was studied on graphite–Br_2 prepared by exposing pristine, highly-oriented pyrolytic graphite (HOPG) to bromine vapor at room temperature for a sufficient amount of time to produce saturated stage 2 graphite–Br_2 (83 wt.% Br_2). The sam-

ples were approximately 4 × 4 × 0.5 mm in size and weighed between 9 and 18 mg before intercalation. The uncertainty in sample weight was ± 10 μg.

Figure 16 shows the intercalate concentration (in wt.% Br_2) as a function of time for samples desorbed at 50, 60, 70, 80 and 90 °C. During the early part of the desorption process, the desorption rate increases as the temperature increases. However, complete desorption does not occur, as a significant portion of the original intercalate (~19 wt.% of parent graphite) is retained by the parent graphite even after a long desorption time. This behavior is clearly shown by the 90 °C desorption curve. In a similar manner, samples desorbed at lower temperatures also approached this minimum concentration, given sufficient time. Since ~19 wt.% Br_2 is strongly retained by the graphite at these temperatures (for desorption below 100 °C), this amount is subtracted from the total amount intercalated to yield the "desorbable" portion of the intercalate. The weight fraction of desorbable intercalate remaining is thus defined as

$$\frac{M}{M_\infty} = \frac{M - M_\infty}{M_0 - M_\infty}, \tag{10}$$

where M_0 is the mass of intercalate before desorption, M_∞ is the mass of intercalate after an infinitely long desorption time, and M is the instantaneous mass of intercalate.

Desorption curves for desorption at temperatures above the intralayer order–disorder transformation temperature are shown in Fig. 17. Due to the anomalously high desorption rate at the intralayer order–disorder transformation temperature, it was impossible to maintain a high intercalate concentration above the order–disorder transformation temperature. As a result, measurements above the order–disorder transformation temperature could only be performed on relatively dilute compounds. The temperatures chosen for the isothermal measurements were 110, 120, 130 and 140 °C. As shown in Fig. 17, desorption at these temperatures led to intercalate concentrations less than 18 wt.% Br_2. However, the minimum concentration has not been determined and the effect of the order–disorder transformation on the con-

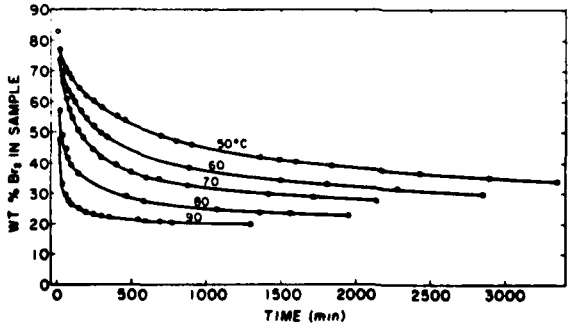

Fig. 16. Isothermal desorption curves of initially saturated graphite–Br_2 at temperatures below the intralayer order–disorder transformation temperature.

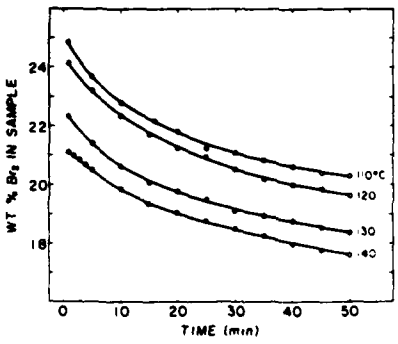

Fig. 17. Isothermal desorption curves of relatively dilute graphite–Br_2 at temperatures above the intralayer order–disorder transformation temperature.

centration has not been quantitatively studied. Nevertheless, like desorption below the order–disorder transformation temperature, the desorption rate above the order–disorder transformation temperature increases as the temperature increases.

2.2.2.2. Scanning thermogravimetry. Because the desorption rate is very high at high temperatures for high concentration samples, measurement during temperature scanning was performed on samples of starting concentration less than 30 wt.% Br_2. The uncertainty in the sample weight was ± 10 μg at low temperatures and increased as the temperature increased, since disturbance caused by violent desorption or exfoliation occurred at high temperatures.

Figure 18 is a plot of intercalate concentration *vs.* temperature for three samples which were obtained by desorbing saturated graphite–bromine compounds at various temperatures, to the starting concentration. The samples were heated at 2 °C/min, and held isothermally at 120, 130, or 140 °C for 50 min before being heated to higher temperatures. The sample associated with curve 1 was initially desorbed at 60 °C and was held at 120 °C. The samples yielding curves 2 and 3 were desorbed at 50 and 70 °C, respectively, and were held at 130 and 140 °C, respectively.

As shown in Fig. 18, the sample weight decreases sharply at two distinct temperatures. The first decrease occurs at approximately 98 °C and corresponds closely to the temperature associated with the intralayer intercalate position order–disorder transformation. The desorption rate below this temperature is negligible compared with that above this temperature. The second decrease occurs at ~165 - 170 °C and is associated with exfoliation. The desorption rate and the equilibrium intercalate concentration above the exfoliation temperature have not been determined in this work. However, it was observed that the sample weight did not decrease smoothly but jumped, indicating perhaps that desorption above the exfoliation temperature occurred in spurts. Moreover, the exfoliation temperature appeared to depend on the desorption temperature prior to the temperature scan, such that the lower

80

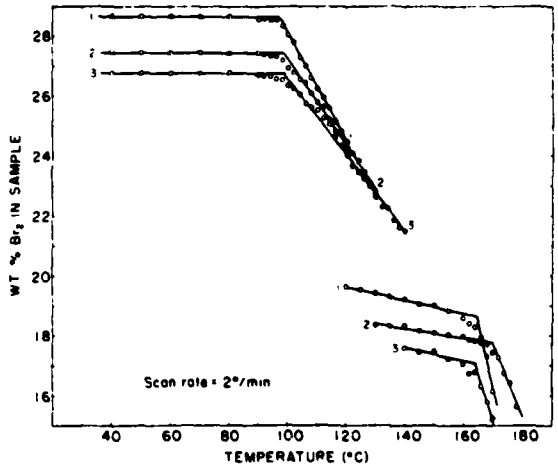

Fig. 18. Scanning thermogravimetric curves taken at 2 °C/min for three relatively dilute graphite–Br_2 samples. The scan was interrupted for 50 min at 120 °C for Sample No 1, at 130 °C for Sample No. 2, and at 140 °C for Sample No. 3.

the initial desorption temperature, the higher the exfoliation temperature. These observations on exfoliation are consistent with our thermal mechanical analysis results [15].

2.3. Discussion

2.3.1. Model of desorption

We propose to model the desorption process as out-diffusion of the intercalate. The intercalate concentration $C(x,t)$ is assumed to be uniform throughout the sample prior to desorption ($t \leq 0$). Let

$$C(x,0) = C_0 , \tag{11}$$

i.e., C_0 is the initial intercalate concentration. The out-diffusion process is governed by the continuity equation

$$\frac{\partial C}{\partial t} = D\frac{\partial^2 C}{\partial x^2} . \tag{12}$$

To simplify the solution, the sample is assumed to be infinitely large along the x-axis. This gives the boundary condition

$$C(\infty, t) = C_0 . \tag{13}$$

If D is assumed to be constant, eqn. (12) can be solved to give

$$\frac{C(x,t)}{C_0} = \mathrm{erf}\left(\frac{x}{2\sqrt{Dt}}\right). \tag{14}$$

Equation (14), in turn, can be used to determine the weight fraction of desorbing species remaining as ref. 16

$$\frac{M}{M_\infty} = \left(\frac{2Dt}{\pi l^2}\right)^{1/2} \tag{15}$$

where t is the desorption time, D is the diffusion coefficient and l is the width of the sample [16]. The sample is of finite size, so the boundary condition expressed in eqn. (13) does not hold exactly. However, this boundary condition can be assumed in the beginning of the desorption process and eqns. (14) and (15) are applicable.

Since the thickness of an intercalation compound is proportional to the concentration, eqn. (14) also indicates the c-face surface profile during desorption. Figure 19 shows the evolution of the concentration profile along the c-face according to eqn. (14). The experimental c-face surface profiles shown in Fig. 20, obtained during room temperature desorption in air of $C_{16}Br_2$ based on HOPG, are in qualitative agreement with those predicted in Fig. 19. In contrast to intercalation, no sharp intercalate front was observed during desorption.

Figure 21 is a plot of ln D *vs.* $1/T$, where D is determined by the initial slope of the M/M_∞ *vs.* $(t/l^2)^{1/2}$ curves shown in Figs. 22 and 23. If the diffusion coefficient is written as

$$D = D_0 \exp\left(-\frac{E_D}{RT}\right), \tag{16}$$

where E_D is the activation energy (per mol) for diffusion, the slope of a plot of ln D *vs.* $1/T$ is equal to $-E_D/R$. By this relation the activation energy for diffusion is found to be 17 kcal/mol below 100 °C, the order–disorder transformation temperature, and 4 kcal/mol above the order–disorder transformation temperature. The value of 17 kcal/mol is in agreement with the 11 - 14 kcal/mol activation energy determined by Aronson [17] for the self-dif-

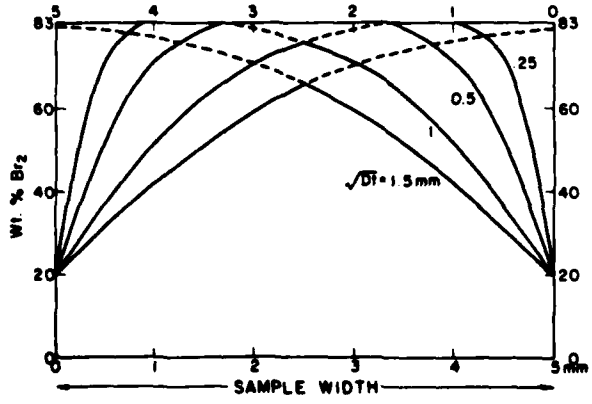

Fig. 19. Evolution of the concentration profile along the c-face according to the proposed model of desorption.

82

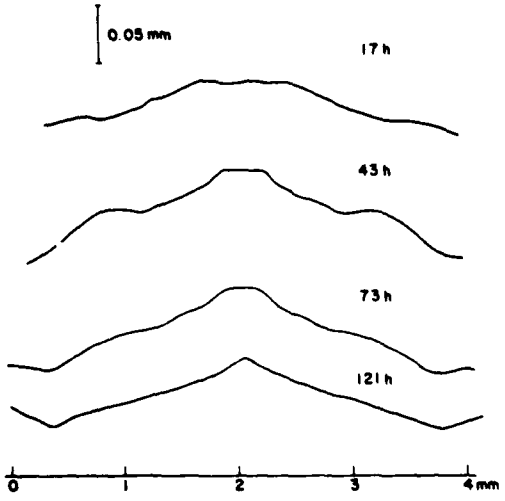

Fig. 20. Experimental *c*-face surface profiles obtained at different times during room temperature desorption in air of $C_{16}Br_2$ base on HOPG.

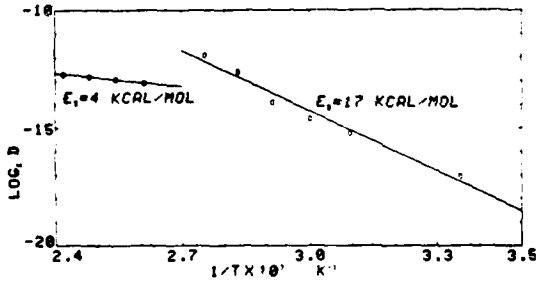

Fig. 21. A plot of ln D *vs.* $1/T$, where D is determined by the initial slope of the M/M_∞ *vs.* $(t/l^2)^{1/2}$ curves shown in Figs. 22 and 23.

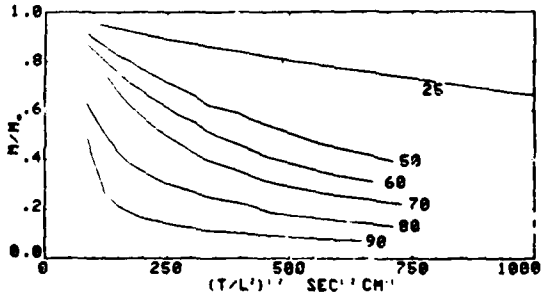

Fig. 22. A plot of M/M_∞ *vs.* $(t/l^2)^{1/2}$ *for desorption at temperatures* below the intralayer order–disorder transformation temperature of graphite–Br_2.

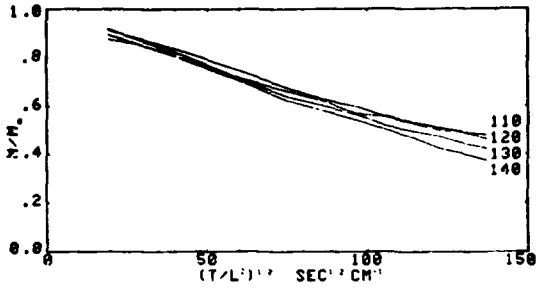

Fig. 23. A plot of M/M_∞ *vs.* $(t/l^2)^{1/2}$ for desorption at temperatures above the intralayer order–disorder transformation temperature.

fusion of bromine within an intercalate layer in the temperature range 30 - 50 ℃. The lower activation energy above the order–disorder transformation temperature is consistent with the intuitive notion that diffusion should be easier in a disordered material. For example, the activation energy for diffusion in a liquid is lower than in a solid. In the case of β-brass [18], the activation energy for diffusion is lower in the high temperature β than in the ordered β'.

As the concentration of bromine within a layer is apparently independent of stage, a bulk concentration gradient indicates a succession of stages. As the diffusion coefficient within a layer is likely to be constant, and interlayer diffusion is unlikely, the flux through a given area should be related to the stage in that area, that is, the bulk diffusion coefficient should be concentration dependent, perhaps inversely proportional to the stage number. While M/M_∞ would still be proportional to $t^{1/2}$ at short times, such a concentration dependence would cause increasing deviation from proportionality as desorption progresses, as is evident in Fig. 22. Such a dependence is also indicated by the diffusion coefficients measured above the order–disorder transformation temperature. To avoid exfoliation the high temperature samples were desorbed to a nominal concentration of 28 wt.% Br_2 at room temperature before being heated and weighed at high temperatures. Consequently, the diffusion coefficient can be smaller at high temperatures though the activation energy is less at these temperatures.

3. Conclusion

The kinetics of intercalation and desorption have been studied by following the physiochemical changes during these processes. In particular, surface profile measurement was used for the first time to study these processes. In addition, thermogravimetric analysis was performed to study the kinetics of desorption. Phenomenological models have been formulated to describe the kinetics of intercalation and desorption. The model of intercalation describes interface-controlled intercalation and allows for the first

time a coherent explanation of the various physiochemical changes that accompany intercalation. The model of desorption considers the out-diffusion of the intercalate and gives the first quantitative description of the desorption process. The activation energy for desorption was determined to be 17 kcal/mol below the intralayer order-disorder transformation temperature and 4 kcal/mol above this temperature.

Acknowledgments

Support from the Materials Research Laboratory Section, Division of Materials Research, National Science Foundation, under Grant No. DMR76-81561 A01 is gratefully acknowledged

References

1 J. G. Hooley, W. P. Garby and J. Valentine, *Carbon*, *3* (1965) 7.
2 J. G. Hooley and J. L. Smee, *Carbon*, *2* (1964) 135.
3 J. G. Hooley, *Carbon*, *10* (1972) 155.
4 G. A. Saunders, A. R. Ubbelohde and D. A. Young, *Proc. R. Soc. London, Ser. A*, *271* (1963) 499.
5 G. A. Saunders, A. R. Ubbelohde and D. A. Young, *Proc. R. Soc. London, Ser. A*, *271* (1963) 512.
6 G. A. Saunders, *Ph. D. Thesis*, University of London, 1962.
7 R. R. Chianelli, *J. Cryst. Growth*, *34* (1976) 239.
8 D. E. Nixon, G. S. Parry and A. R. Ubbelohde, *Proc. R. Soc. London, Ser. A*, *291* (1966) 324.
9 T. Sasa, Y. Takahashi and T. Mukaibo, *Carbon*, *9* (1971) 407.
10 M. B. Dowell, *Mater. Sci. Eng.*, *31* (1977) 129.
11 I. L. Spain, A. R. Ubbelohde and D. A. Young, *J. Chem. Soc.*, (1964) 920.
12 G. R. Hennig, in F. A. Cotton, (ed.), *Progr. Inorg. Chem.*, *1* (1959) 125.
13 J. G. Hooley, *Chem. Phys. Carbon*, *5* (1969) 321.
14 W. Metz and D. Hohlwein, *Carbon*, *13* (1975) 87.
15 S. H. Anderson, J. S. Culik and D. D. L. Chung, *Ext. Abstr. Program-Bienn. Conf. Carbon*, *14* (1979) 262.
16 J. Crank, *Mathematics of Diffusion*, Oxford Univ. Press, London, 1957.
17 S. Aronson, *J. Inorg. Nucl. Chem.*, *25* (1963) 907.
18 A. B. Kuper, D. Lazarus, J. R. Manning and C. T. Tomizuka, *Phys. Rev.*, *104* (1956) 1536.

APPENDIX 6

Carbon, submitted.

EXFOLIATION OF INTERCALATED GRAPHITE *

S.H.Anderson and D.D.L.Chung

Department of Metallurgical Engineering

and Materials Science

Carnegie-Mellon University

Pittsburgh, PA 15213

* Research sponsored by the Air Force Office of Scientific Research, Air Force Systems Command, USAF, under Grant No. AFOSR-78-3536. The United States Government is authorized to reproduce and distribute reprints for governmental purposes notwithstanding any copyright notation hereon.

Abstract

By x-ray diffraction, exfoliated graphite-Br_2 was found to exhibit the same in-plane superlattice ordering as intercalated graphite prior to exfoliation. This ordering persisted even after heating for an hour at 1700°C. Furthermore, an intercalated single crystal flake retained its orientation throughout exfoliation and collapse. By dilatometry, a single exfoliation event was found to consist of multiple expansion spurts, which occurred at ~150°C and ~240°C for first exfoliation, and ~100°C and ~240°C for subsequent cycles. The amount of expansion was found to increase with decreasing intercalate activity during intercalation. With exfoliation cycles to higher temperatures or longer times, the amount of residual expansion after the collapse on cooling increased until no second exfoliation was observed on reheating. Due to intercalate desorption, the amount of expansion for concentrated samples increased with increasing sample width; desorbed samples showed little width dependence. Acoustic emission was observed before appreciable expansion during the first exfoliation cycle; it was not observed during the collapse or subsequent exfoliation cycles. A model of exfoliation involving intercalate islands is proposed.

Introduction

When intercalated graphite is heated past a critical temperature, a large expansion along the c-direction occurs, giving the compound a puffed-up appearance. This phenomenon is known as exfoliation.

Brocklehurst [1] observed by dilatometry that desorbed graphite-Br_2 based on polycrystalline artificial extruded graphite began exfoliation at ~300°C upon heating, resulting in an expansion of up to ~2.1 % at 500°C. By similar dilatometric measurement on desorbed graphite-Br_2 based on pyrolytic graphite, Martin and Brocklehurst [2] found that

1. first exfoliation occurred at ~170°C upon first heating,
2. subsequent exfoliation occurred at ~120°C in subsequent heating cycles,
3. collapse occurred at ~110°C upon cooling,
4. second and subsequent exfoliation cycles were reversible,
5. the expansion was up to 380 % at 500°C,
6. the exfoliation temperature increased linearly with increasing load.

In contrast to the relatively small amount of expansion observed by Martin and Brocklehurst, Ubbelohde [3] observed an expansion of ~1000 % at 350°C for graphite-Br_2 based on well-oriented graphite. By using differential thermal analysis, optical microscopy and gaseous pycnometry, Mazieres et al. [4] found that desorbed graphite-Br_2 based on pyrocarbons underwent first exfoliation at 160-200°C on heating, second exfoliation at 100-120°C on heating, and collapse at 70-100°C on cooling. Furthermore, they found that thermal cycling decreased the exfoliation tendency progressively and that this effect was more pronounced when the heating was carried out in air. Mazieres et al. [5] observed irreversible exfoliation after heating desorbed graphite-Br_2 based on pyrocarbons to 1000°C and cooling in an argon atmosphere. In addition, they demonstrated that it was possible to intercalate the irreversibly exfoliated material.

Other than graphite-Br_2, exfoliation had also been observed in graphite-ferric chloride [6],

graphite-aluminum chloride [7], and graphite intercalated with a mixture of nitric and sulfuric acids [7].

The tendency for exfoliation depends on the extent of stacking order of the graphite basal planes [8]. Dowell [9] showed that possession of a basal plane stack height, L_c, greater than $\sim$450 Å was necessary for exfoliation.

The exfoliation phenomenon is of technological importance as well as scientific interest. The exfoliation of graphite-ferric chloride has been used to manufacture Grafoil [10], a high temperature thread sealant tape. The exfoliation of graphite-HNO_3-H_2SO_4 has been used for making a thermal insulator for molten metals [11]. The exfoliation of graphite-$FeCl_3$-NH_3 has been used for making blankets for the extinction of metal fires [12]. In addition, exfoliated graphite is being investigated by the U.S. Army for use as a battlefield obscurant [13]. The surface area increase resulting from irreversible exfoliation is attractive for catalytic applications of graphite intercalation compounds [14]. In addition, exfoliation is a phenomenon that affects the thermal stability of graphite intercalation compounds, so understanding of this phenomenon is necessary for the use of graphite intercalation compounds at elevated temperatures.

We have reported that the exfoliation behavior depends more strongly on the parent initial stage than on the intercalate concentration in graphite-Br_2 [15]. This paper supports this contention and offers further insight into the exfoliation process. The key issues which are addressed include the following. Is exfoliated graphite intercalated? How does exfoliation affect the structure of the parent graphite or the intercalation compound? How reversible is exfoliation? How can the reversibility or irreversibility of exfoliation be controlled? What is the mechanism of exfoliation?

In this work, we have used dilatometry to investigate the dependence of multiple exfoliation and collapse on

1. the stage,

2. the intercalate concentration,

3. the intercalation temperature,

4. the annealing time and temperature after the first exfoliation,

5. the sample size,

6. the intercalate species.

Particular attention was given to the reversibility of exfoliation. In addition, acoustic emission was used to investigate the nature of the exfoliation process and x-ray diffraction was used to study the crystal structure of the exfoliated material.

The main findings of this work are the following.

1. Exfoliated graphite exhibits the same in-plane superlattice ordering as intercalated graphite prior to exfoliation. This ordering persists even after heating for an hour at 1700°C.

2. Intercalated single crystal graphite exhibits the same orientation before and after exfoliation, with well defined (hk0) directions in both the graphite and the intercalate layers.

3. Acoustic emission was observed before appreciable expansion during the first exfoliation cycle. It was not observed during the collapse or subsequent exfoliation cycles.

4. A single exfoliation event consists of multiple expansion spurts, which occur at ~150°C and ~240°C for first exfoliation, and at ~100°C and ~240°C for subsequent cycles.

5. The expansion was found to increase with decreasing intercalate activity during intercalation, such that it increased with decreasing Br_2 concentration in the Br_2-CCl_4 solution and with increasing intercalation temperature.

6. With exfoliation cycles to higher temperatures or longer annealing times, the amount of residual expansion after the collapse on cooling increased until no second exfoliation was observed on reheating, i.e., exfoliation became irreversible.

7. Due to intercalate desorption, concentrated intercalated graphite shows more expansion after first exfoliation than after second exfoliation. However, desorbed intercalated graphite shows less expansion after first exfoliation than after second exfoliation.

8. On repeated exfoliation cycles, concentrated samples show a decrease in the amount of expansion due to desorption during exfoliation, while desorbed samples show little decrease in the amount of exfoliation.

9. Due to intercalate desorption, the amount of expansion for concentrated samples increases with increasing sample width. However, desorbed samples show little width dependence.

Experimental Techniques

Samples were prepared from highly oriented pyrolytic graphite (HOPG) kindly provided by Union Carbide Corporation. Most samples were cut to a size of 4mm x 4mm x 0.5mm and then placed in liquid bromine for intercalation. Samples which were intercalated above room temperature were placed in a constant temperature bath. Times of the order of a minute were required to place a sample in a sample holder, add bromine, seal the sample holder and place it in the water bath. A similar amount of time was necessary to remove the sample from the bath, quench it to room temperature, and remove the sample from the bromine. Fourth stage samples were prepared by placing the samples in a 15 mol% Br_2 bromine-carbon tetrachloride solution. A 12mm x 12mm x 1mm sample of graphite was intercalated in pure bromine for intercalation to second stage and was then cleaved and cut to produce 7mm x 7mm, 5mm x 5mm and 2mm x 2mm samples. Desorption of the lamellar compounds was allowed to occur in air or nitrogen. Stage 1 graphite-ICl was prepared by immersion of HOPG in ICl liquid at room temperature. The stage was characterized by x-ray diffractometry using Cu $K\alpha$ radiation.

The effect of exfoliation on the intercalate in-plane superlattice was investigated by x-ray diffraction. For HOPG, the Transmission Laue Method was used, with Mo K_α radiation and a specimen-to-film distance of 6 cm. The HOPG samples were oriented to yield mainly the (hk0) in-plane diffraction lines. The set-up allowed d-values ranging from 0.8 Å to ~6 Å to be measured. The exposure time was ~12 hr for every sample. For single crystal graphite, the Precession Method was used, with Mo K_α radiation and a precession angle of 10°.

Exfoliation expansion was followed with a probe connected to a linear variable differential transducer (LVDT). The sample was heated by a furnace around the support extending an inch above the sample. As a consequence of active cooling of the support, the air surrounding the sample was hotter than the support surface. This had the result that when exfoliation started,

the sample temperature increased toward the ambient air temperature due to enhanced insulation from the cooler support. The sample temperature was measured by a Pt-Pt 10% Rh thermocouple bead in contact with the sample. A heating and cooling rate of 20°C/min was used in the exfoliation cycles. The weight of the probe on the sample was 28 grams. The samples were purged with nitrogen gas in the presence of air during the measurements.

Acoustic emission during exfoliation was detected by using an ultrasonic transducer (Aerotech Gamma, 1.6 MHz narrow band or 0.5MHz wideband) equipped with a high temperature delay line. The transducer signal was amplified and the acoustic emission pulses were counted by using a frequency counter.

Experimental Results

Figure 1 shows x-ray diffraction patterns obtained on graphite-Br_2 (i)after desorption from saturation and before exfoliation, and (ii) after exfoliation carried out at ~300°C. The indexing of the diffraction lines are shown in Table 1 for these samples as well as pristine graphite and graphite-Br_2 exfoliated at 1700°C. The in-plane superlattice was the same as that of stage 2 graphite-Br_2 based on single crystal graphite, as determined by Ghosh and Chung [16]. The unit cell is monoclinic and commensurate with the graphite lattice, with in-plane lattice constants a=4.26 Å, b=8.87 Å, and the angles $\alpha=\beta=90°$ and $\gamma=103.9°$. Due to the mechanical deformation resulting from exfoliation, the diffraction pattern was closer to a powder pattern after exfoliation, as indicated by the complete diffraction rings obtained after exfoliation (Fig.1). For the same reason, certain (hkl) lines not observed before exfoliation were observed afterward.

A single crystal flake was intercalated to a second stage graphite-bromine compound, desorbed, and then heated to 300°C with exfoliation occurring at ~180°C. Figure 2 shows a room temperature precession photograph taken after exfoliation and collapse. It can be observed from the graphitic spots that the material remained a fairly good single crystal, although the graphitic spots had been slightly broadened. Moreover, the graphite-Br_2 (hk0) diffraction spots were clearly present. These results suggest that exfoliation has little effect on

a microscopic scale other than a small amount of local bending of the graphite planes. It appears that the deformation which takes place during exfoliation does not appreciably affect the in-plane orientation of the superlattice in the single crystal, even though the c-axis in exfoliated HOPG shows a considerable increase in the mosaic spread [9].

Thornel P-100 fibers were intercalated by immersion in nitric acid and ICl. Evidence of intercalation was obtained by x-ray diffraction. The main diffraction peak was shifted to lower angles than that of the pristine fiber (002) diffraction peak, though too few (00/) lines were observed to determine the stage. The fibers were heated in three ways: in a flame in air, in a vacuum furnace, and by passing a current through them until they broke. Examination of the fibers by optical microscopy did not indicate any of the expansion characteristic of exfoliation in HOPG nor the rupture observed by Endo et al. [17]. The FWHM of the diffraction peaks observed in our fiber indicate crystallite stack heights (L_c) on the order of ~150 Å, much less than the 450 Å suggested by Dowell [9] as a minimum for exfoliation. Consequently one may expect that exfoliation will not occur in most fibers. Vapor-grown graphite fibers, on the other hand, tend toward higher perfection; Koyama et al. [18] reported L_c greater than 1000 Å in these fibers.

Figure 3 illustrates the general features of exfoliation which we observed in graphite-Br_2 (HOPG) by dilatometry. The sample (5 x 5 mm) was initially intercalated to 3.2 mol% Br_2 (stage 4), desorbed to 1.3 mol% Br_2, reintercalated to 6.3 mol% Br_2 (stage 2), and desorbed to 1.6 mol% Br_2. During the initial part of the first heating cycle, expansion occurred very slightly though with a thermal expansion coefficient several times that of graphite. Eventually the sample exfoliated within a relatively narrow temperature range. We have determined a first onset temperature (T_1 for the first exfoliation cycle, T_2 for the second cycle) by extrapolating the line of exfoliation expansion and taking its intersection with the horizontal base line. The expansion rate diminished to form a shoulder (first shoulder) in the curve, and then increased again to form a second shoulder, as shown in Fig. 3, where the second shoulder of the first exfoliation cycle is labeled. No shoulders were observed at higher temperatures up

to 600°C in graphite–Br_2. We designate the fractional expansion at the first shoulder as E_1 for the first cycle and E_2 for the second cycle, as determined by the intersection of the line of exfoliation expansion and the expansion line at the shoulder. The second onset temperature and the fractional expansion at the second shoulder are illustrated in Fig. 3 for the first exfoliation cycle. On cooling, a large degree of hysteresis was evident, with contraction of the exfoliated structure occurring predominantly within a narrow temperature range, resulting in a small residual fractional expansion, E_c. We designate the collapse temperature T_c as the temperature determined by the intersection of lines extrapolated from the contraction region and the linear region of the curve on cooling prior to collapse. On reheating, second exfoliation occurred at about the same temperature at which collapse occurred during cooling, i.e., $T_2=T_c$. It is interesting to note that while T_1 and T_2 were quite separate, the second shoulder was observed at about the same temperature in any exfoliation cycle. The collapse behavior was largely the same for any exfoliation cycle.

Shown in Fig. 4 is the exfoliation behavior of single crystal graphite–bromine. The graphite single crystal was a flake obtained from a New York mine, ~5 mm in diameter, which was intercalated to saturation in liquid bromine, then desorbed at 90°C in air for a day. The fractional expansion at 300°C during first exfoliation was 31 times for this single crystal graphite–bromine, whereas it was only 24 times for a similarly prepared HOPG samples with similar width (see, for example, the HOPG data in Figs. 9 and 10). The collapse temperature T_c was 210±10°C for single crystal graphite–bromine, and was 100±10°C for HOPG graphite–bromine. As a result, the hysteresis was relatively small between the collapse and the next expansion for single crystal graphite. The shoulders which were quite evident in HOPG were difficult to discern in the single crystal curves.

The exfoliation behavior of a first stage graphite–ICl (HOPG, 4 x 4 mm) is shown in Fig. 5. In general the exfoliation curve is much like that observed for graphite–Br_2. The main difference is that the exfoliation onset temperature T_1 of graphite–ICl is approximately the same as the collapse temperature T_c and the second exfoliation temperatures T_2, whereas in

graphite–Br_2, T_1 is generally higher than T_2. It may also by pointed out that T_2 in graphite–ICl is about 100°C higher than that of graphite–Br_2 .

In comparing Figures 3 and 5, it can be seen that the amount of expansion which occurred during second exfoliation of graphite–ICl was considerably less than that which occurred in graphite–Br_2. This is probably not an attribute of the intercalate species, but rather a consequence of the amount of desorption which had occurred during first exfoliation. While the graphite–ICl sample was a saturated (first stage) compound just before exfoliation was begun, the graphite–Br_2 sample was a desorbed sample prior to exfoliation. Therefore, desorption was much more significant during first exfoliation of the graphite–ICl sample than the graphite–Br_2 sample. The dependence of exfoliation on desorption is given later in this paper.

Figure 6 illustrates the dependence of expansion on the number, N, of exfoliation cycles for 5mm x 5mm graphite–Br_2 samples which were, in one case (open circles), allowed to desorb from a second stage parent compound to 1.5 mol% Br_2 before exfoliation and, in the other case (closed circles), not allowed to desorb before exfoliation (i.e., the second stage parent compound). The fractional expansion at the first shoulder (i.e.,E_N, where N is the number of exfoliation cycles) was plotted against N. At the end of five exfoliation cycles, each carried out to 290°C, the partially desorbed sample had further desorbed to 0.7 mol% Br_2. For the desorbed sample, E_2 was greater than E_1, and there was only a slight decrease from E_2 to E_5. For the second stage parent compound, the bromine concentration varied from 6.3 mol% Br_2 before the first exfoliation run to 0.6 mol% Br_2 after the fifth exfoliation cycle, each carried out to 340°C. In this case, the expansion behaved as might be expected, i.e.,$E_1 > E_2 > E_3 > E_4 > E_5$. In general, we observed $E_1 > E_2$ when samples were exfoliated without prior desorption, and $E_1 < E_2$ when samples were allowed to desorb to an approximately constant weight before exfoliation.

The extent of desorption during each exfoliation cycle was measured by gravimetry. The

results are shown in Fig. 7, where the intercalate concentration (in mol% Br_2) was plotted against the square root of the number, N, of exfoliation cycles. The sample (2 x 2 mm) had been desorbed from second stage to 1.4 mol% Br_2 prior to exfoliation. The greatest weight loss occurred during the first and second exfoliation cycles, with the concentration decreased from 1.4 to 1.2 mol% Br_2 after the first exfoliation and from 1.2 to 0.9 mol% Br_2 after the second exfoliation. A similar loss, from 0.9 to 0.7 mol% Br_2 required seventeen additional exfoliation cycles. It is this region from N=2 to N=19 which is shown in Fig. 7. The concentrations after cycles 0 and 1 are not shown because they are too far from the succeeding concentrations. The line drawn is a least square fit of the data with a correlation coefficient of −0.96. The dependence on $_v/N$ suggests that the weight loss may be treated as a diffusion process with an exfoliation cycle being analogous to a unit of desorption time. The effective overall diffusion coefficient during an exfoliation cycle is probably an average of the diffusion coefficients within the temperature range covered by the exfoliation cycle.

Figure 8 shows the dependence of E_j on the sample width (the dimension perpendicular to the c-axis) for samples which were initially second stage. The filled circles correspond to samples which were not desorbed prior to exfoliation, and the open circles correspond to samples which were allowed to desorb to ~1.5 mol% Br_2 before the exfoliation cycles. The samples were all square and of approximately the same thickness. For samples which were not allowed to desorb, E_1 increased as the width of the sample increased. The samples which were allowed to desorb did not show this size dependence. Consequently we attribute the apparent width dependence to be actually a concentration dependence, which is appearing as a consequence of desorption during the previous exfoliation cycles. This point is discussed in the next section.

Figure 9 illustrates the effect of the maximum temperature on the exfoliation behavior. The samples were HOPG (4 x 4 mm) intercalated to 6.3 mol% Br_2 (stage 2), but not allowed to desorb before heating. Plot A in Fig. 9 shows dilatometric results obtained during two exfoliation cycles carried out to ~200°C; Plot B was obtained during two cycles carried out to

~400°C; Plot C was obtained during two cycles carried out to ~600°C. The main trend indicated in Fig. 9 is that E_c (the residual fractional expansion) increased as the maximum temperature increased. Figure 10 shows similar effects due to isothermal annealing at the maximum temperature during the first heating. Contraction was observed during annealing. After annealing for 0.5 hr at ~600°C, the fractional expansion was only 90 % of the initial 600°C expansion; after a one-hour anneal, the fractional expansion was 80 % of the initial 600°C expansion; after a 3-hour anneal, the fractional expansion was 70 % of the initial 600°C expansion. However, no contraction was observed in samples annealed at 200°C or 400°C. It should be noted that a second exfoliation was not observed in the samples annealed at 600°C. The results of annealing at different temperatures for various lengths of time are summarized in Table 2, where E_c and E_2 are listed relative to E_1 to lower the effect of the error in measuring the initial sample thickness. Whereas E_c/E_1 is affected by annealing, E_2/E_1 appears independent of annealing. While most of the data were obtained at heating rates of 20°C/min, several runs were made at 10°C/min and 40°C/min. Within this range of heating rates, little or no effects were observed which could be attributed to the change in heating rate. This is most likely due to the fact that even at 40°C/min, the time spent in heating to the exfoliation temperature is long compared to the time needed for desorption.

We have previously reported that the initial stage determines the exfoliation behavior [15]. We have further evidence that the initial intercalating conditions determine the exfoliation behavior. Table 3 illustrates the effect of the initial stage on the subsequent exfoliation behavior. Some samples were allowed to be intercalated, desorbed and reintercalated. Irrespective of the stage after the second intercalation, the samples which were first intercalated to fourth stage in a Br_2–CCl_4 solution of 15 mol% Br_2 had a lower T_1, larger E_1, and larger E_2 than those which were first intercalated to second stage. Within a group of the same initial stage, the sample intercalated twice had a greater E_1 and E_2 than the sample intercalated once, though neither T_1, T_c nor T_2 were affected by reintercalation.

Table 4 is a list of E_1 for samples intercalated in pure bromine at different temperatures (80 - 110°C) to produce third stage compounds. Though all the compounds had the same initial stage, E_1 increased with increasing intercalation temperature. Thus, the initial stage is not the sole factor that determines the exfoliation behavior.

For all the intercalate species studied (Br_2 in HOPG and single crystals, ICl in HOPG, and HNO_3 in HOPG), acoustic emission occurred before appreciable exfoliation took place. Figure 11 shows the acoustic emission and expansion of graphite-bromine (HOPG, 4 x 4 mm), which had been intercalated to 3.2 mol% Br_2 (stage 4). The acoustic emission events were observed as a large number of pulses within a short period of time. Very few events were observed once marked expansion had begun. While it may certainly have been the case that once a cellular structure began to form the acoustic pulses were attenuated beyond detection, a gradual reduction in the number of pulses was not observed. Instead, emission was observed at generally one or two distinct temperatures which were separate from the exfoliation onset temperature. In the case of graphite-Br_2, acoustic emission happened to occur during heating in the first exfoliation cycle at about the temperature of the second exfoliation.

Discussion

Exfoliation is commonly considered to be due to the formation of gas bubbles within an anisotropic matrix. The phenomenon is used to produce expanded graphite products such as Grafoil [10] for gaskets, valve packing and insulation, and expanded mica in the form of vermiculite. Martin and Brocklehurst [2], and Aoki et al. [19] both modeled the exfoliation of graphite-bromine by considering the expansion of gaseous bubbles as Griffiths cracks, though Aoki et al. [19] treated intercalated bromine at room temperature as a solid which vaporized at the breakaway temperature. Both assumed the bubbles to be trapped at defects within the crystal. Setton [4] also modeled the exfoliation of graphite-bromine as the vaporization of a condensed phase, after the migration of bromine to defects. Olsen et al. [20], in a study of the exfoliation of graphite-bisulfate compounds, proposed that a bisulfate compound existed as pockets at grain boundaries, with much of the graphite remaining

unaffected. They proposed that the intercalate vaporized on heating, in effect causing the pockets to explode, leaving a low density, "isotropic" material between planar arrays of pyrolytic graphite and voids. Similarly, Stevens et al. [6] viewed exfoliation of graphite-ferric chloride as the forcible rupture of sealed or partially sealed spaces within graphite due to the fact that ferric chloride decomposed to iron and chlorine gas. Dowell [7], in discussing the structures of exfoliated graphite-bisulfate and graphite-aluminum chloride compounds, agreed that the intercalate should diffuse to defects to form three-dimensional aggregates which could vaporize, expanding the structure. He also suggested channels through which the vapor escaped from the sample. We would like to propose the following model for the exfoliation of graphite intercalation compounds, as motivated by the experimental results obtained.

We assume that the precursor of bubbles are intercalate filled penny-shaped cracks distributed within a graphite crystal. If the crystal is heated, the pressure within the cracks will increase as the intercalate takes on a more gaseous character. Higashida and Kamada [21] analyzed the stress distribution around pressurized penny-shaped cracks in graphite near a free surface and concluded that two fracture modes are available. One fracture mode is brittle fracture as a Griffiths crack, i.e., the crack diameter increases when the tensile stress in the c-direction exceeds the fracture strength. The other fracture mode is the buckling of the walls of the crack, i.e., when large bending moments exist at the crack tip, the flat crack may open to form a bubble. We propose that the latter fracture mode is responsible for the expansion observed in exfoliation. Higashida and Kamada found that the internal pressure necessary for fracture by either mode increased as the crack diameter decreased. Furthermore, the internal pressure necessary for buckling was very sensitive to the depth of the crack below a free surface due to the mechanical constraints involved in bending a thick layer. The parameter h/a, where h is the depth of the crack below a free surface and a is the crack radius, was found to be much less than one when buckling was favored over Griffiths cracking. (It may be of interest to note that, unlike in glass, where brittle fracture is typically catastrophic, the c-direction fracture stress in graphite is low enough that the strain energy is rapidly dissipated into the formation of surfaces, so that the crack growth stops rather than propagating

catastrophically to the crystal edge.) Although the analysis of Higashida and Kamada was developed for cracks near a surface, it is reasonable to assume that, due to the interaction of stress fields, an array of cracks can buckle throughout the material. That is, while buckling may initiate near a free surface, another crack a similar depth below it can also buckle. Consequently h may be restated as an average c-direction separation of cracks. In short, heating an intercalated sample increases the pressure in penny-shaped cracks. Griffiths cracking is likely to occur at a critical pressure; this will reduce both the internal pressure within the cracks and the pressure necessary to cause buckling. Eventually the internal pressure and crack diameter will be such that buckling occurs, producing the sudden large expansion characteristic of exfoliation. Our observation of acoustic emission before exfoliation is in agreement with the concept of both fracture modes being active.

If cracks buckle to form an exfoliated structure, one problem is in determining the source of the penny-shaped cracks. One possibility may be defects either pre-existing in the graphite or caused by the intercalating conditions. If pre-existing defects serve as sites for penny-shaped cracks, one might expect the exfoliation behavior to be affected mainly by differences in defect distribution due to the graphitizing process. Once the defects have become saturated with intercalate, there should be little dependence of exfoliation on stage or intercalate concentration. If the defects are not saturated, there should be an intercalate concentration dependence, i.e., with less intercalate, less expansion. If defects produced during intercalation serve as crack sites, one would expect that more severe intercalating conditions should produce more defects, hence more exfoliation. Consequently one would expect a low stage compound to be associated with more defects and a greater degree of exfoliation. Otherwise, for saturated defects only a weak dependence on concentration should be expected.

Unfortunately, none of these arguments for exfoliation from either pre-existing or induced defects is supported by what we have observed in intercalated graphite. If pre-existing defects aid exfoliation, one might expect more exfoliation in a more defective graphite. In fact, fibers, which may be expected to have the greatest density of pores and defects, appear to

exfoliate the least, while single crystal flakes, which may be considered more perfect than HOPG, exfoliate the most. On the other hand, if the defect sites are the result of the intercalation process, one might expect that a more vigorous intercalation process should produce a greater degree of exfoliation. Again, what is observed is that graphite-ICl and graphite-HNO_3 exfoliate on heating to a lesser degree than graphite-Br_2, though both intercalate to first stage and are known to cause cracking and exfoliation during intercalation. Even considering just the graphite-Br_2 system, third and fourth stage samples exfoliate to a greater degree than second stage though intercalation to either third or fourth stage may be considered milder than to second stage and certainly are slower.

We propose that the intercalate islands,suggested by Daumas and Herold [22], determine the size of the penny-shaped cracks. (The crack size is not necessarily equal to the island size; instead we expect a positive correlation between the island size and the subsequent crack size.) In turn, the size of the intercalate islands is determined by the intercalating conditions. In accordance with nucleation theory, as the reactant activity increases, competition between nucleation sites increases and the subsequent microstructure is finer. Hence, as the intercalate activity is decreased, by dilution or by heating, the intercalate island size is expected to increase. For a compound of a given concentration, increased island size means that exfoliation can occur more easily and to a greater extent. Observation of intercalate islands by electron microscopy [23, 24] shows that the intercalate islands can be treated as interstitial dislocation loops and as such are susceptible to pinning at defect sites. Nonetheless, the islands are mobile and can coalesce. Single crystal diffraction results on the incommensurate room temperature graphite-Br_2 phase indicated an island size of $\sim$2,500 Å [16].

The events leading to exfoliation can be summarized as follows. On intercalation, the intercalate island size is determined by the intercalation conditions. In cases where the reaction is limited by the rate of transfer of intercalate from the surface into the bulk, as may be the case in vapor-phase intercalation, the island size may be small as the large change in chemical energy can support a high interface energy between the intercalate island and the

graphite matrix. In the case where intercalation is limited by transport within the graphite, the island size may be relatively large as a consequence of a small chemical energy change with respect to the interfacial energy. In either case a range of island sizes exist, distributed about some average size. On heating, though there may or may not be a change in island size, the effective pressure of the intercalate within the islands increases. At some point, the pressure is large enough to cause fracture to occur. On the evidence of the presence of acoustic emission before appreciable expansion, it appears that the preferred fracture mode is propagation of the island as a crack between the basal planes. With further heating, and the possibility of desorption of intercalate from the bulk into the crack, the pressure within the crack increases until further fracture occurs either as further crack propagation, or as becomes more likely with larger diameter cracks, buckling of the penny-shaped crack to form bubbles and consequent bulk expansion. As a continuous initial size distribution of the islands exists, it may be expected that islands of different size would undergo fracture at different temperatures giving rise to a smooth expansion until the bulk of the intercalate is trapped within a bubble. In the first exfoliation cycle this was observed for single crystal graphite-bromine (Fig. 4) and for HOPG graphite-ICl (Fig. 5). The shoulders evident in HOPG graphite-bromine may be due to a coincidental interaction between the crack size and the graphite crystallite dimensions. Without a high temperature anneal, graphite-Br_2 and graphite-ICl exhibit cyclic exfoliation. On cooling the structure collapses at a low temperature and re-exfoliates when heated above that temperature. The collapse is attributed to capillary forces due to the condensed intercalate, which returns the gas bubbles to a nearly penny-shaped crack configuration. On reheating, exfoliation occurs again as the intercalate vaporizes, buckling the largest set of cracks at about the same temperature that collapse occurs on cooling. The smaller set of cracks exfoliates at higher temperatures for the same reason as before, i.e., a smaller radius requires a higher pressure. On the other hand, collapse of all cracks is concurrent as condensation occurs at only one temperature; small cracks are forced shut by the larger cracks but must re-open on their own.

The extent and reversibility of single-crystal exfoliation indicates that, as with intercalation,

the presence of defects hinders exfoliation and subsequent collapse. In single crystal graphite-bromine as compared to HOPG graphite-bromine, the increased collapse temperature (T_c) results in shrinkage of the hysteresis loop formed between heating and cooling cycles, indicating less work is involved in the expansion and contraction of the single crystal derived compound. In particular the remnants of a turbostratic structure or claw defects [25] may hinder expansion or contraction by constraining a nearby crystallite which otherwise could either crack or buckle. This probably explains the lack of exfoliation in fibers. In a pitch- or PAN-based graphite fiber the small crystallite size and the large number of pores may result in the absence of intercalate islands which are large enough to cause exfoliation to occur. In the more graphitic vapor grown fiber, the islands may be large enough that exfoliation could occur, but with concentric basal planes around the fiber axis exfoliation may occur only if in plane bonds rupture. Such rupture would consume much of the available strain energy and vent the contents of the gas cells, which produce the strain energy for either rupture or exfoliation. Hence the rupture observed by Endo [17] may in fact be the counterpart of exfoliation in graphite fibers. While basal rupture was observed along the edges of HOPG samples and single crystal flakes, it typically was associated with a rather large degree of exfoliation.

The discussion thus far tacitly assumes that the cracks are gas tight, with no net flux in or out. This is not necessarily the case. A pathological example is a crack which propagates to the ambient atmosphere. In that case, the internal pressure does not increase and the walls of such a crack can only buckle due to the buckling of surrounding cracks. A less extreme example would be the diffusion of intercalate between basal planes. If the intercalate mobility and solubility are high, the intercalate species may diffuse out of the gas bubbles and into the matrix in a short time in comparison with the length of time required for the exfoliation cycle. For exfoliation at normal pressures, the loss of intercalate from the gas bubbles may even result in the collapse of the exfoliated structure. Subsequent heating and cooling will then cause negligible expansion. Such collapse during heating in the first exfoliation cycle was observed in graphite-nitric acid, which was prepared by immersion of HOPG (4 x 4 mm) in red fuming nitric acid (Fig. 12). When diffusion is slower, as in the case of bromine, long

periods of time and high temperatures are necessary before appreciable collapse occurs (Fig. 10).

When the intercalating activity was reduced by dilution, as in the initially fourth stage samples listed in Table 3, we observed that the amount of exfoliation was greater than that of an initially second stage sample, even though the actual concentration was approximately the same for various samples. Similarly, if the activity is decreased by heating, the amount of exfoliation was observed to increase with temperature for a given stage (Table 4).

Let us consider the effect of desorption on exfoliation. Bardhan et al. [26] showed that a pronounced weight loss occurred on desorbing graphite-Br_2. This is only to be expected given the exponential temperature dependence of the diffusion coefficient. Until exfoliation occurs, bromine diffuses more and more rapidly as the temperature is increased. Isothermal gravimetric results [26] indicate that desorption reduces the concentration to a limiting value of ~1.0 - 1.5 mol% Br_2, up to the temperature where exfoliation occurs. The mass fraction of bromine lost depends on $\sqrt{(Dt/l^2)}$, where D is the diffusion coefficient and l is half the sample width. Profilometry [26] and X-ray absorption studies [27] indicate that the concentration in a desorbing graphite-Br_2 compound decreases at the edge initially while the center retains the semblance of the undesorbed sample. By the time the apparent residue compound has been achieved, the concentration profile across the sample is nearly flat, with little difference in the concentration at the edge or the center. The length of time needed for this to occur can be considered as roughly proportional to l^2/D. Hence,for the same concentration, a sample half as wide as a given sample will require roughly a quarter of the time to desorb to an equivalent concentration.

The above argument applies to exfoliation in the following manner. During exfoliation the temperature is steadily rising rather than being isothermal. Consequently the diffusion coefficient should be considered as a composite diffusion coefficient weighted by the mass loss rate at each temperature. In effect, small samples may desorb to a low or even residue

concentration during the heating cycle though they may have been concentrated or even saturated prior to heating. In this case the exfoliation behavior will be the same for an initially desorbed sample as for an initially saturated sample. Experimentally this was observed, as shown by the 3 mm sample shown in Fig. 8. For wider samples, a more and more significant amount of intercalate remains in the center of the sample by the time the exfoliation temperature is reached, with the result that the amount of exfoliation increases as the sample width increases. This is the situation described by the solid circles in Fig. 8. On the other hand, if the samples have been desorbed to a low or residue composition prior to exfoliation, this width dependence becomes negligible, as shown by the open circles in Fig. 8. For the same heating rate, as was the case for all the samples in Fig. 8, the effective (Dt) term is the same for all the samples, so that the intercalate concentration remaining in a large sample at the exfoliation temperature is greater than that in a small sample for the case of an initially concentrated samples. Therefore the amount of exfoliation increases with sample width for initially concentrated samples, as we have observed.

The mobility of the intercalate is quite high at the exfoliation temperatures, and the solubility of the intercalate appears to be quite low. Diffusion of the intercalate out of the sample through the matrix is one mechanism for the loss of excess intercalate and is suggested by the least square fit of the data in Fig. 7. However, it is not necessarily the only mechanism. The gas cells themselves may serve as sinks for the excess intercalate. Under such circumstances, the matrix would lose intercalate while the sample as a whole would not. On subsequent exfoliation cycles the enriched cells should expand to a greater degree. The latter possibility is consistent with the observation of $E_2 > E_1$ for samples which are initially desorbed. The diffusion of the intercalate out of the sample is not the only means of losing intercalate. It should be born in mind that the weight losses during the first two exfoliation cycles in Fig. 7 do not fit the least square line. There is considerably more desorption during these two cycles than can be explained by using the same diffusion coefficient which can be applied to the later cycles. It seems far more likely that a certain number of the gas bubbles present are bursting, or are forming an interconnected network which in turn opens to the outside of the

sample. The channels suggested by Dowell [7] may be such a network. If so, one would expect that a greater initial concentration would tend to rupture and/or interconnect more of the cells, as a greater concentration would serve as a source of a greater gas volume. Consequently a greater proportion of the initial concentration would be lost on the first exfoliation cycle of an initially concentrated sample than in one which had been desorbed prior to exfoliation. With such a loss of intercalate, less is available on subsequent cycles so that the amount of exfoliation is decreased as shown by the solid circles in Fig. 6.

Table 5 shows the comparison of the exfoliation temperatures (first onset temperatures) of graphite-HNO_3, graphite-Br_2, and graphite-ICl with the respective intercalate melting temperatures and the respective melting and boiling points of bulk HNO_3, Br_2, and ICl. For graphite-Br_2, the collapse temperature (which is the same as the second exfoliation temperature) is approximately the same as the intercalate melting temperature. Other than this match, the exfoliation and collapse temperatures are different from any of the corresponding critical temperatures listed. Comparison of the trends down the various columns in Table 5 shows a possible relationship between the exfoliation temperature and the bulk melting temperature.

Conclusion

The amount of exfoliation of graphite-Br_2 was found to be determined by the intercalation conditions, namely the Br_2 concentration in the Br_2-CCl_4 solution and the temperature, such that the expansion increased with increasing initial stage number and with increasing temperature. Due to intercalate desorption during heating, annealing was found to increase the amount of residual expansion until exfoliation became irreversible. Desorption also resulted in the increase of the exfoliation expansion with increasing sample width for concentrated samples and the decrease in the expansion with repeated exfoliation cycles for these samples. A single exfoliation event was found to consist of multiple expansion spurts, which occurred at ~150°C and ~240°C for first exfoliation, and at ~100°C and ~240°C for subsequent cycles. Acoustic emission was observed before appreciable expansion during the first exfoliation cycle.

In-plane intercalate ordering was observed by x-ray diffraction in exfoliated graphite-Br_2.

Furthermore, for single crystal graphite, the single crystal nature was retained after exfoliation and collapse, without noticeable bending or twisting of the intercalate layers, but with slight bending of the graphite layers. A model of exfoliation involving intercalate islands [22] is proposed.

ACKNOWLEDGMENTS

The authors are grateful to Mr. H. H. Lee of Carnegie-Mellon University for assistance in the acoustic emission measurement and to Professor Roy Clarkeof the University of Michigan for providing natural graphite flakes. The x-ray diffraction equipment grant from the Division of Materials Research of the National Science Foundation under Grant No. DMR-8005380 is acknowledged. Support from the Materials Research Laboratory Section, Division of Materials Research, National Science Foundation under Grant No. DMR 76-81561 A01 is also acknowledged.

FIGURE CAPTIONS

Fig.1 Transmission Laue x-ray diffraction patterns of graphite-Br_2 (HOPG) (a) after desorption from saturation and before exfoliation, and (b) after exfoliation carried out at ~300°C.

Fig.2 Precession camera photograph of graphite single crystal after intercalation with Br_2 and exfoliation.

Fig.3 Fractional expansion versus temperature during the first two exfoliation-collapse cycles for graphite-Br_2 (HOPG) which had been desorbed form 3.2 mol% Br_2 to 1.3 mol% Br_2, then reintercalated to 6.3 mol% Br_2 and desorbed to 1.6 mol% Br_2 prior to heating.

Fig.4 Fractional expansion versus temperature during the first two exfoliation-collapse cycles for single crystal graphite-Br_2, which had been desorbed from saturation prior to heating.

Fig.5 Fractional expansion versus temperature during the first one and a half exfoliation-collapse cycles for graphite-ICl (HOPG) which was saturated (stage 1) prior to heating.

Fig.6 Fractional expansion at the first shoulder (E_N) versus the number of exfoliation cycles (N) for graphite-Br_2 (HOPG) which (i) were not desorbed prior to heating and (ii) were desorbed prior to heating.

Fig.7 Gravimetric determination of the intercalate (Br_2) concentration in (HOPG) as a function of $\sqrt{N}$, where N is the number of exfoliation cycles.

Fig.8 Fractional expansion at the first shoulder during first exfoliation (E_1) versus the sample width perpendicular to the c-axis for graphite-Br_2 (HOPG).

Fig.9 Fractional expansion versus temperature during the first one and a half exfoliation-collapse cycles carried out to three different maximum temperatures for graphite-Br_2 (HOPG).

Fig.10 Fractional expansion of graphite-Br_2 (HOPG) versus temperature during the first one and a half exfoliation-collapse cycles in which isothermal annealing at the maximum temperature (~600°C) during the first heating cycle was carried out for various lengths of time.

Fig.11 Acoustic emission versus temperature superimposed on a curve of fractional expansion versus temperature for one exfoliation-collapse cycle of graphite-Br_2 (HOPG), which had been intercalated to 3.2 mol% Br_2.

Fig.12 Fractional expansion versus temperature during the first two exfoliation-collapse cycles of graphite-nitric acid (HOPG).

References

1. J.E.Brocklehurst, Nature, London,194 (1962) 247.

2. W.H.Martin and J.E.Brocklehurst, Carbon, 1 (1964) 133.

3. A.R.Ubbelohde, Brit. Coal Util. Res. Assoc. Gaz., 51 (1964) 1.

4. C.Mazieres, G.Colin, J.Jegoudez and R.Setton, Carbon, 13 (1975) 289.

5. C.Mazieres, G.Colin, J.Jegoudez and R.Setton, Carbon, 14 (1976) 176.

6. R.E.Stevens, S.Ross and S.P.Wesson, Carbon, 11 (1973) 525.

7. M.B.Dowell, Ext.Abs.Program-Bienn.Conf. Carbon 12 (1975) 35.

8. H.Thiele, Anorg.Allgem.Chem., 207 (1932) 340.

9. M.B.Dowell, Ext.Abs.Program-Bienn.Conf. Carbon 12 (1975) 31.

10. Union Carbide Trademark,U.S. Patent 3,404,061 (1968)

11. H.Mikami, Kokai(Japan. patent),76 96,793 (1976)

12. CECA S.A., Carbone-Lorraine S.A., Brit. Patent 1,588,876

13. W.L.Garrett, J. Sharma, J.Pinto and H.Prask, Technical Report ARLCD-TR-81008, AD-E400 617; Order No.AD-A100727. May,1981 Avail. NTIS.

14. M.A.M.Boersma, in Adv.Mater.Catal., J.Burton and R.L.Garten, eds., Academic Press 1977, pp.67-99.

15. S.H.Anderson, H.H.Lee and D.D.L.Chung, Ext.Abs.Program-Bienn.Conf. Carbon 15 (1981) 357.

16. D. Ghosh and D.D.L.Chung, submitted for publication

17. M.Endo, T.Koyama and M.Inagaki, Synth. Met.,8 (1981)177.

18. T.Koyama,M.Endo, and Y.Hishiyama, Jpn. J. Appl. Phys.,13 (1974) 1933.

19. K. Aoki, T. Hirai, and S. Yajima, J. Mat. Sci., 6 (1971) 140.

20. L.C.Olsen, S.E.Seeman and H.W.Scott, Carbon, 8 (1970) 85.

21. Y.Higashida and K.Kamada, J.Nucl.Mater., 73 (1978) 30.

22. N.Daumas and A.Herold, C. R. Acad. Sci., Ser. C268 (1969) 373.

23. M.Heerschap, P.Delavignette and S.Amelinckx, Carbon, 1 (1964) 235.

24. M.Heerschap and P. Delavignette, Carbon, 5 (1967) 383.

25. A.R.Ubbelohde and F.A.Lewis, *Graphite and its crystal compounds*, Oxford University Press, London, 1960.

26. K.K.Bardhan, J.C.Wu, J.S.Culik, S.H.Anderson, and D.D.L.Chung, Synth. Met. 2 (1980) 57.

27. S.H.Anderson and D.D.L.Chung, to be published

Table 1 X-ray diffraction lines of pristine graphite, desorbed graphite-Br_2 and exfoliated graphite-Br_2

hkℓ	Pristine graphite			Graphite-Br_2, desorbed			Graphite-Br_2, exfoliated at 300°C			Graphite-Br_2, exfoliated at 1700°C		
	d_{obs} (Å)	d_{cal} (Å)	Strength	d_{obs} (Å)	d_{cal} (Å)	Strength	d_{obs} (Å)	d_{cal} (Å)	Strength	d_{obs} (Å)	d_{cal} (Å)	Strength
023_G							0.96	0.96	VW			
016_G							0.99	0.99	VW	0.99	0.99	VW
$200_G(260)_S$	1.09	1.07	W	1.09	1.07	W						
112_G							1.15	1.13	S	1.15	1.13	M
$110_G(700)_S$	1.25	1.23	M	1.26	1.23	M	1.23	1.23	W	1.23	1.23	M
011_G							2.03	2.03	VS	2.02	2.03	S
$100_G(130)_S$	2.14	2.13	M	2.14	2.13	M	2.14	2.13	M	2.14	2.13	M
120_S							2.66	2.68	W	2.73	2.68	VW
300_S				2.85	2.87	W	2.88	2.87	W	2.86	2.87	VW
002_G							3.36	3.35	S	3.39	3.35	S
200_S				4.16	4.14	W	4.17	4.14	W			

G = graphite
S = in-plane superlattice

Table 2 Effect of annealing on exfoliation behavior

Annealing Temperature (°C)	Annealing Time (hr.)	E_c/E_1	E_2/E_1	Contraction at T_{max}
200	0	0.09	0.60	0
	0.5	0.14	0.42	0
	1	0.20	0.54	0
400	0	0.16	0.51	0
	0.5	0.20	0.61	0
	1	0.31	0.49	0
600	0	0.44	0.58	0
	0.5	0.59	0.59	10%
	1	0.67	0.67	20%
	3	0.74	0.74	30%

Table 3 Effect of staging on exfoliation behavior

Stage after 1st intercalation			4	4	2	2
Stage after 2nd intercalation			2	/	4	/
Mole % Br_2			1.60	1.39	1.55	1.53
First Exfoliation						
	Temperature T_1 (°C)					
		1st Onset	161	145	185	185
		2nd Onset	239	230	230	223
	Fractional Expansion ($\Delta L/L$)					
		1st Shoulder (E_1)	28	18	8	5
		2nd Shoulder	39	23	20	14
First Collapse						
	Temperature T_c (°C)		101	89	104	105
	Residual Fractional Expansion (E_c)		2.3	1.1	2.1	1.0
Second Exfoliation						
	Temperature T_2 (°C)		100	99	99	108
	Fractional Expansion (E_2)		30	16	15	11

Table 4

Exfoliation behavior of parent 3rd stage graphite-Br_2 prepared at various temperatures

Intercalation Temperature (°C)	Fractional Expansion $(E_1)(\Delta L/L)$
80	16 ± 5
90	24 ± 5
100	29 ± 6
110	38 ± 6

Table 5 Comparison of acoustic emission, exfoliation and collapse temperatures with other critical temperatures.

Intercalate Species	Acoustic emission temperature (±10°C)	Exfoliation temperature* (±20°C)	Collapse temperature (±10°C)	Intercalate melting temperature (°C)	Bulk melting temperature (°C)	Bulk boiling temperature (°C)
HNO_3	80	130	/	-20	-42	83
Br_2	115	170	100†/210‡	101	-7	59
ICl	140	190	190	41	14§/27**	97

* First onset temperature (T_1)

† For HOPG

‡ For single crystal graphite

§ For β-ICl

** For α-ICl

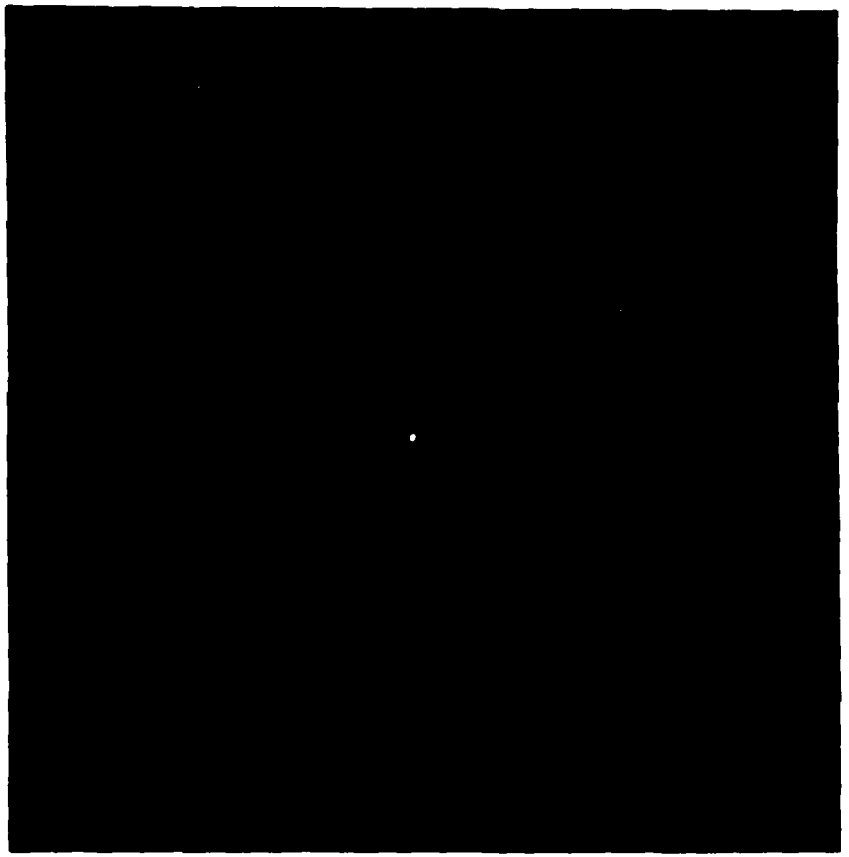

a

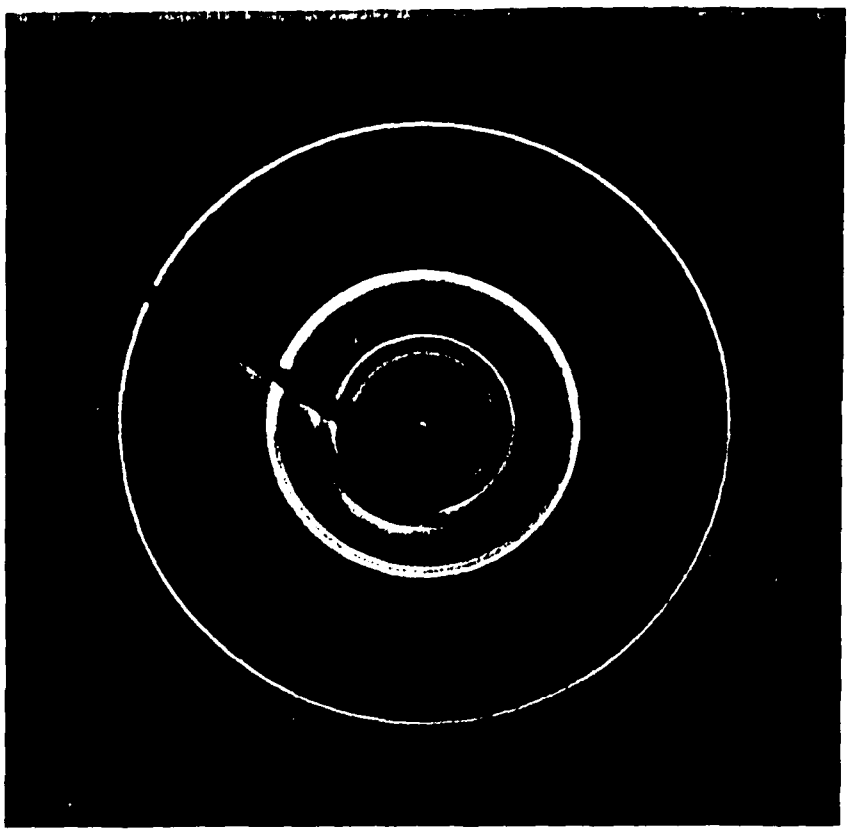

b

Fig. 1

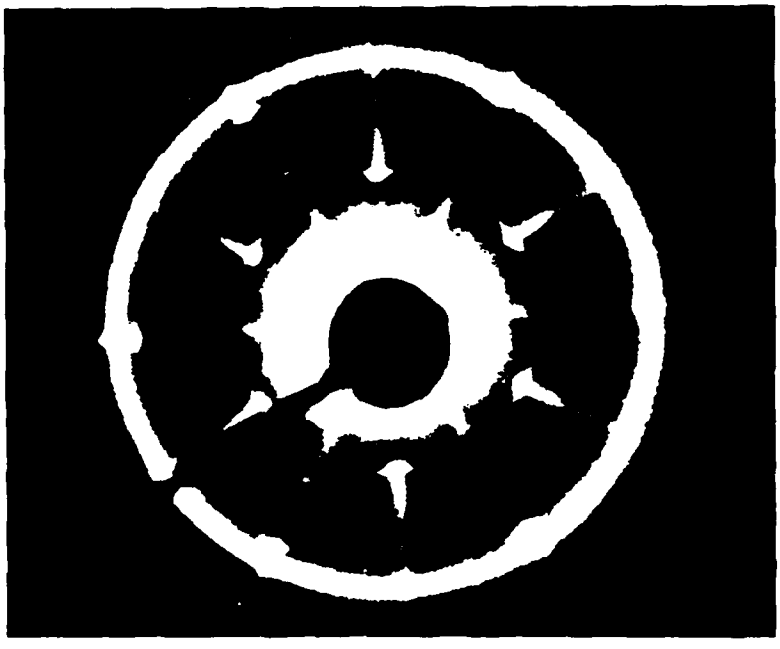

Fig. 2

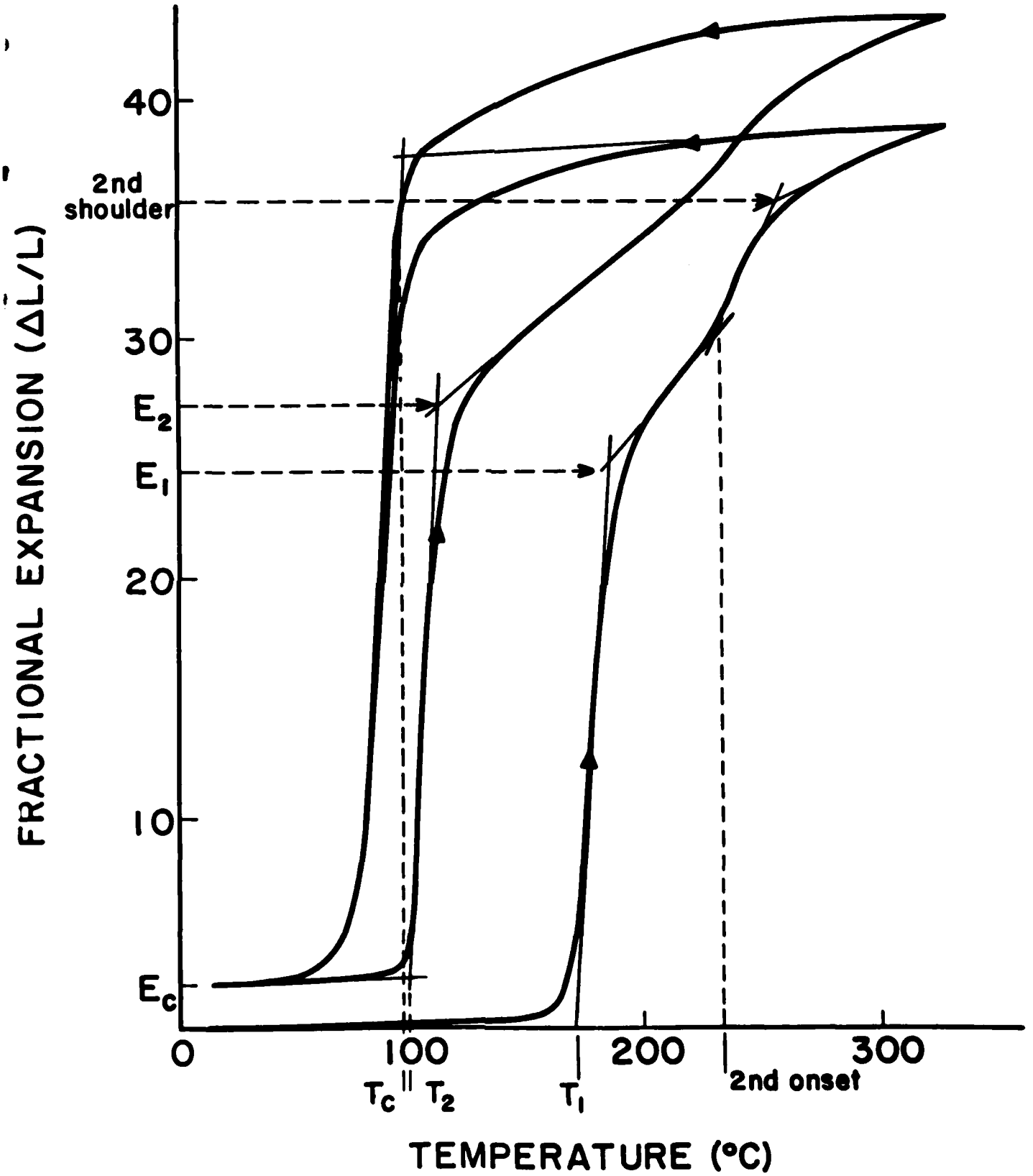
FRACTIONAL EXPANSION (ΔL/L)
40
2nd shoulder
30
E2
E1
20
10
Ec
0
100
200
300
Tc = T2
T1
2nd onset
TEMPERATURE (°C)

Fig.

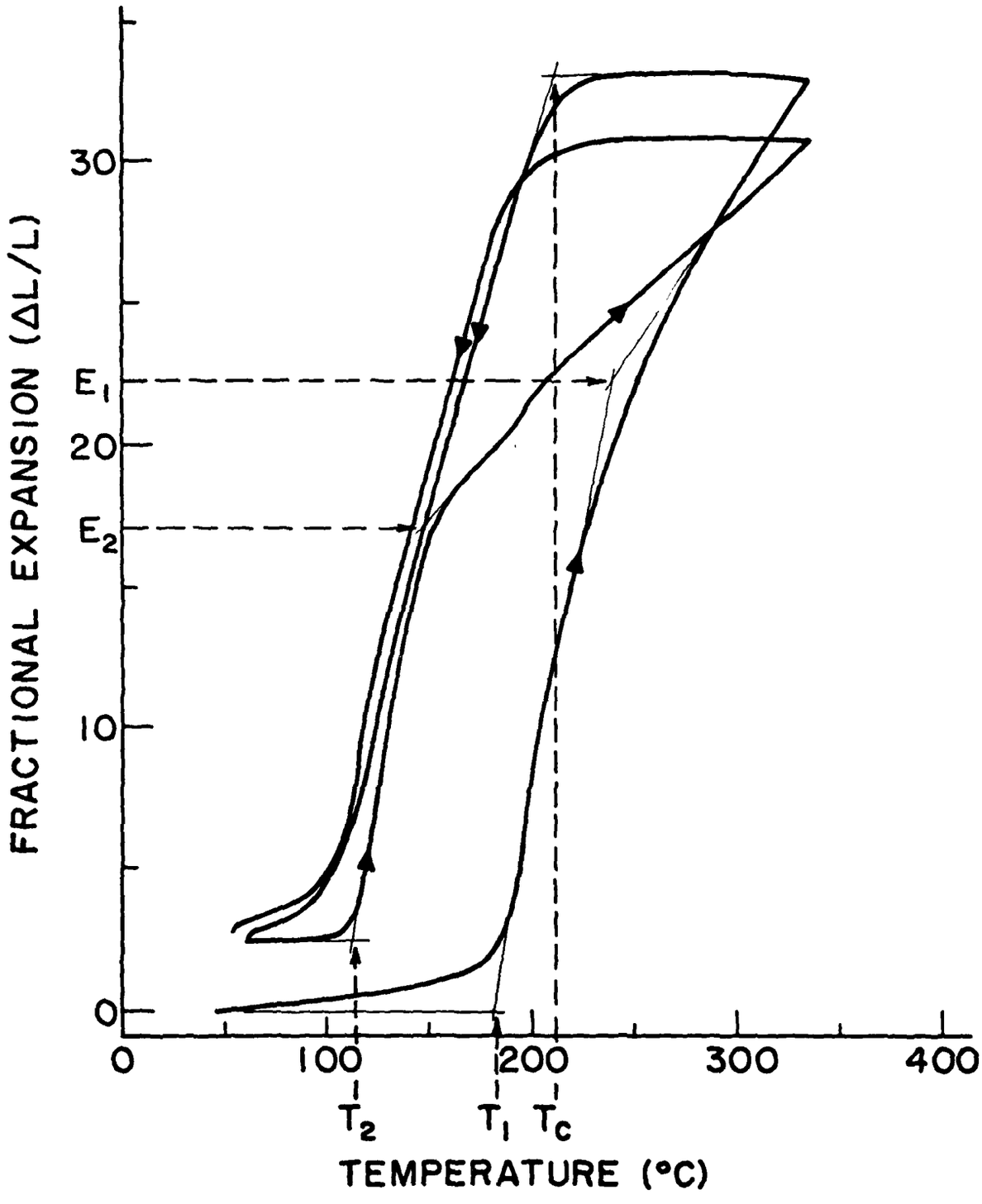
FRACTIONAL EXPANSION (ΔL/L)
30
20
10
0
E1
E2
0
100
200
300
400
T2
T1
Tc
TEMPERATURE (°C)

Fig. 4

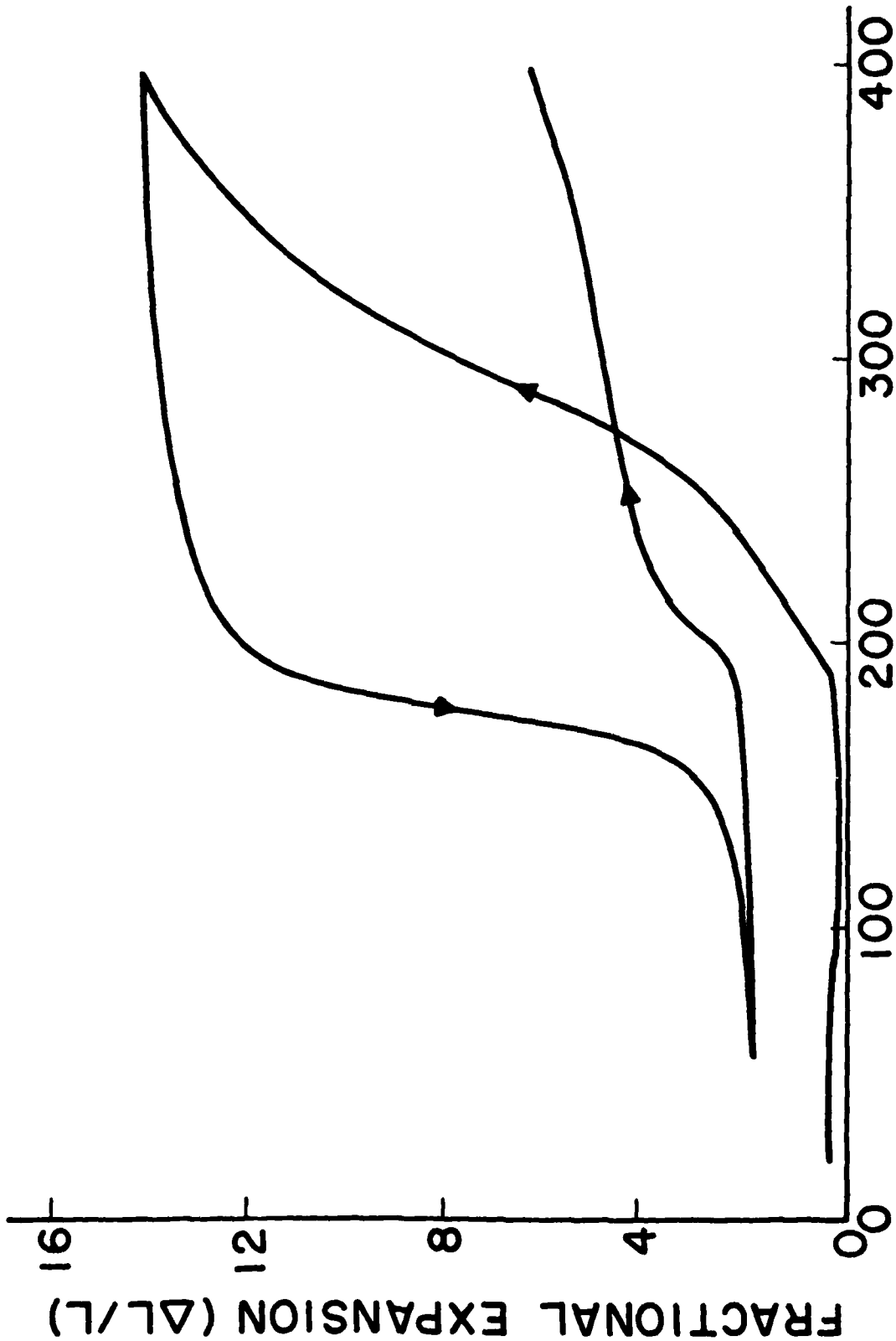
FRACTIONAL EXPANSION (ΔL/L)
0
4
8
12
16
0
100
200
300
400
TEMPERATURE (°C)

Fig. 5

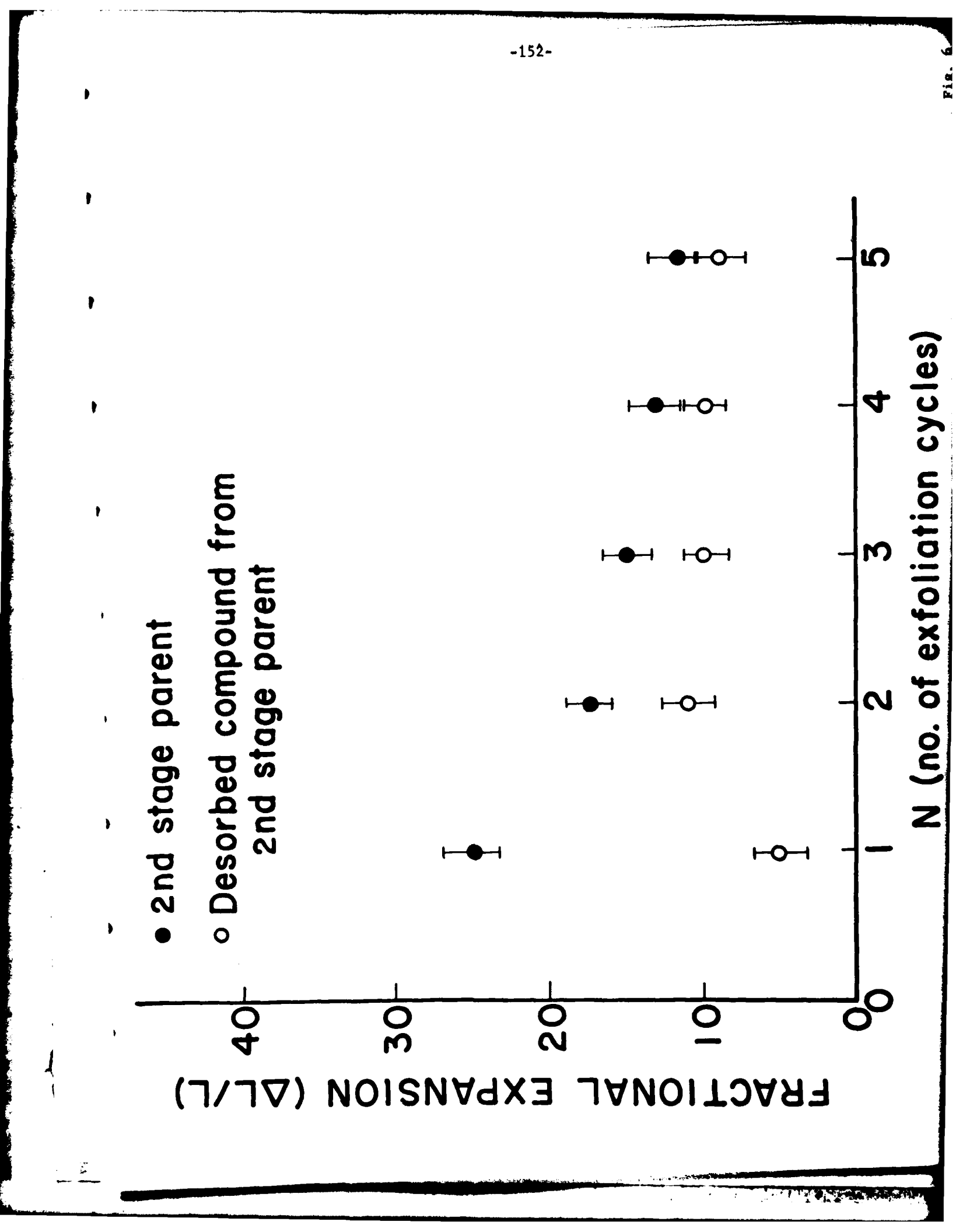
FRACTIONAL EXPANSION (ΔL/L)
0
10
20
30
40
0
1
2
3
4
5
N (no. of exfoliation cycles)
● 2nd stage parent
○ Desorbed compound from 2nd stage parent

Fig. 6

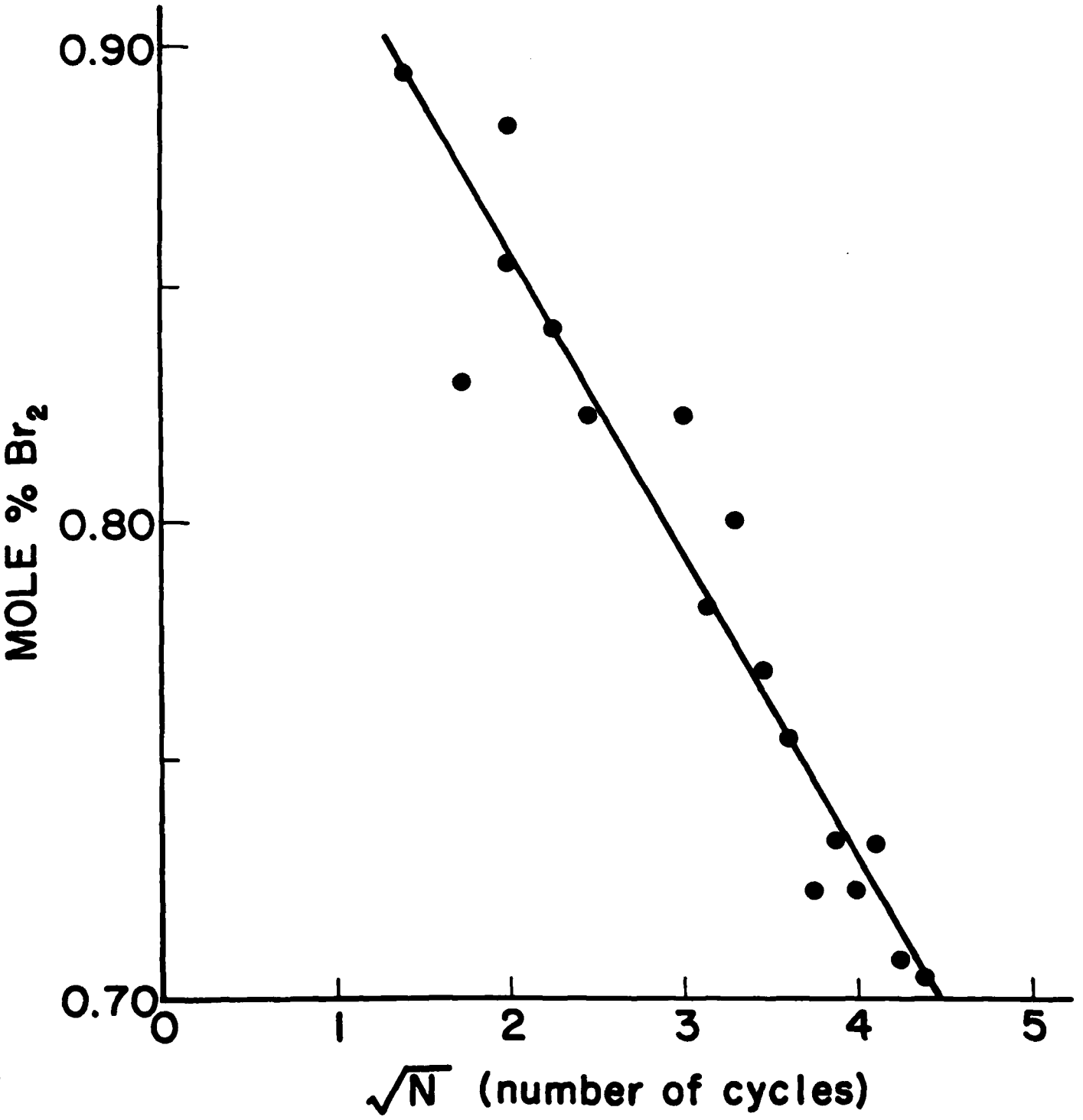

Fig.

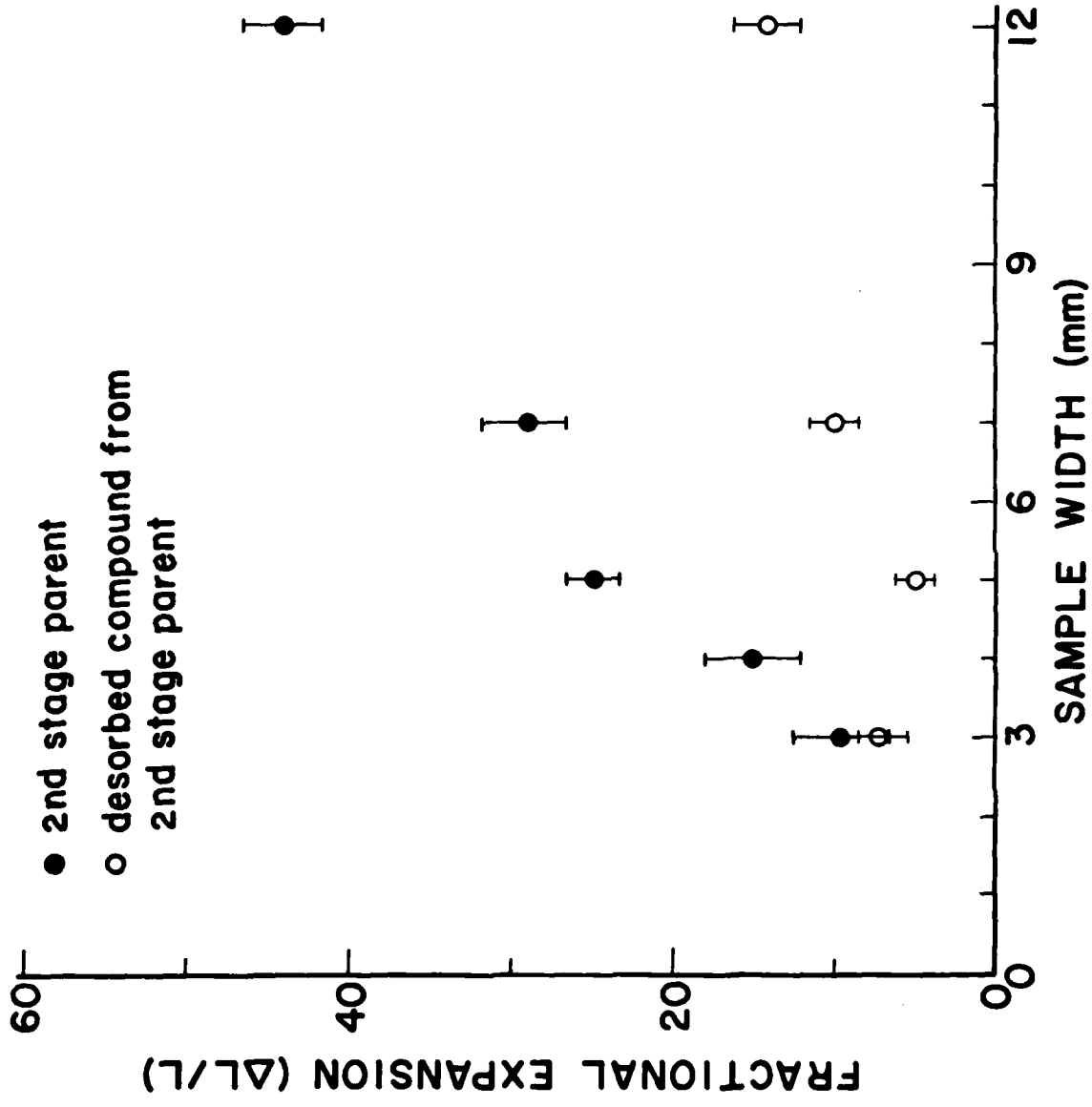
FRACTIONAL EXPANSION (ΔL/L)
60
40
20
0
0
3
6
9
12
SAMPLE WIDTH (mm)
● 2nd stage parent
o desorbed compound from 2nd stage parent

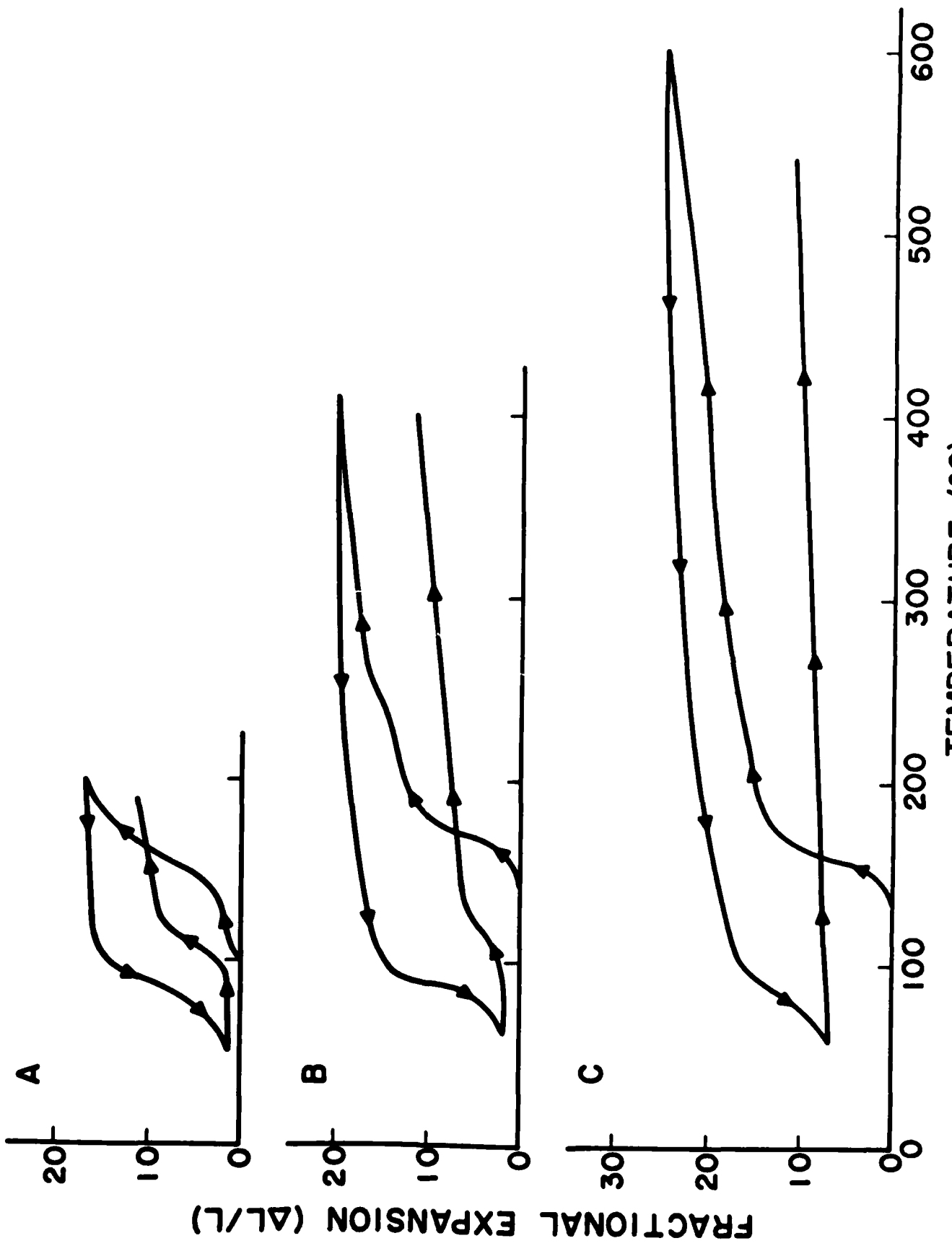
A
B
C
20
10
0
20
10
0
30
20
10
0
100
200
300
400
500
600
TEMPERATURE (°C)
FRACTIONAL EXPANSION (ΔL/L)

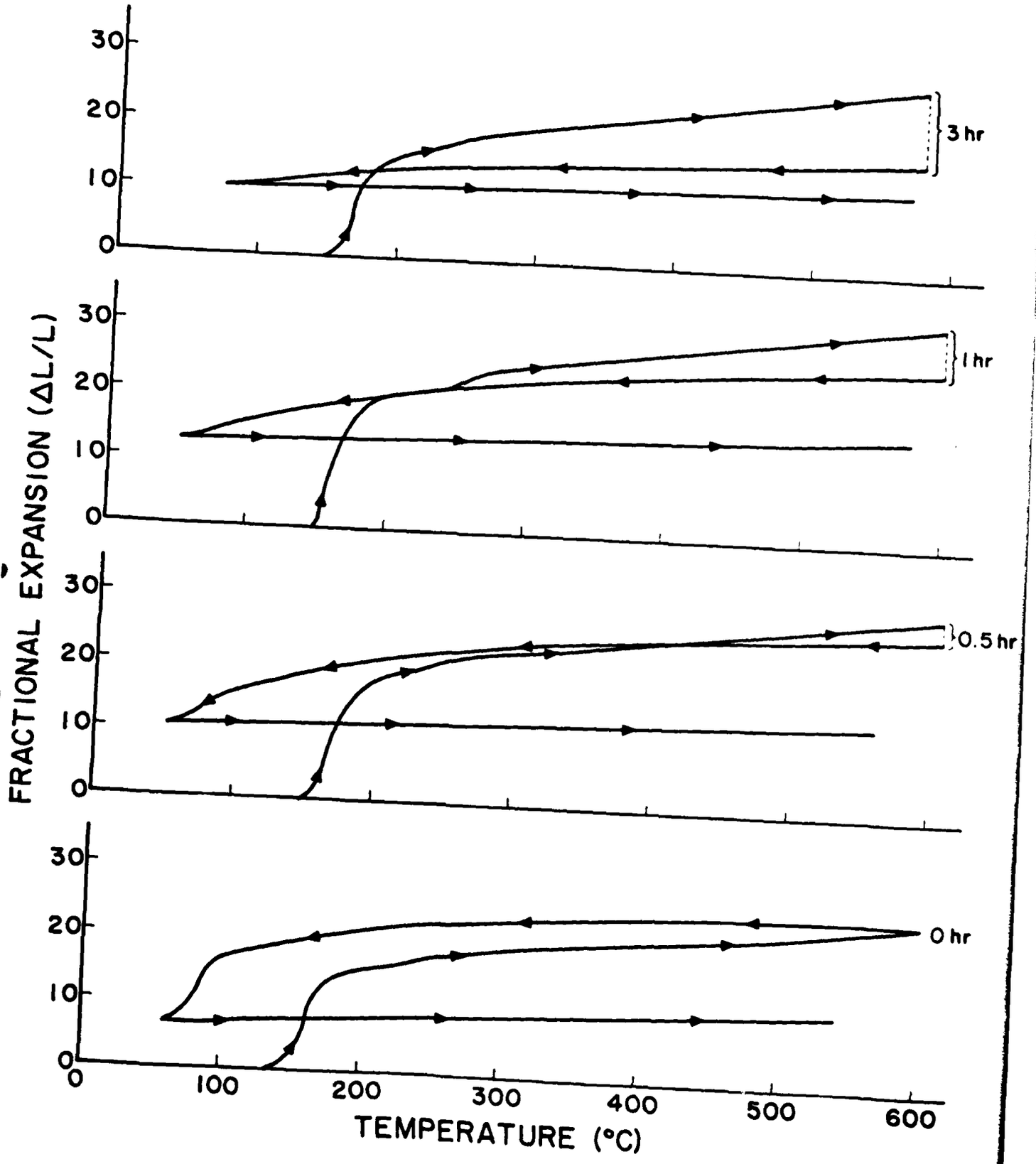
FRACTIONAL EXPANSION (ΔL/L)
30
20
10
0
3 hr
1 hr
0.5 hr
0 hr
0
100
200
300
400
500
600
TEMPERATURE (°C)

Fig.

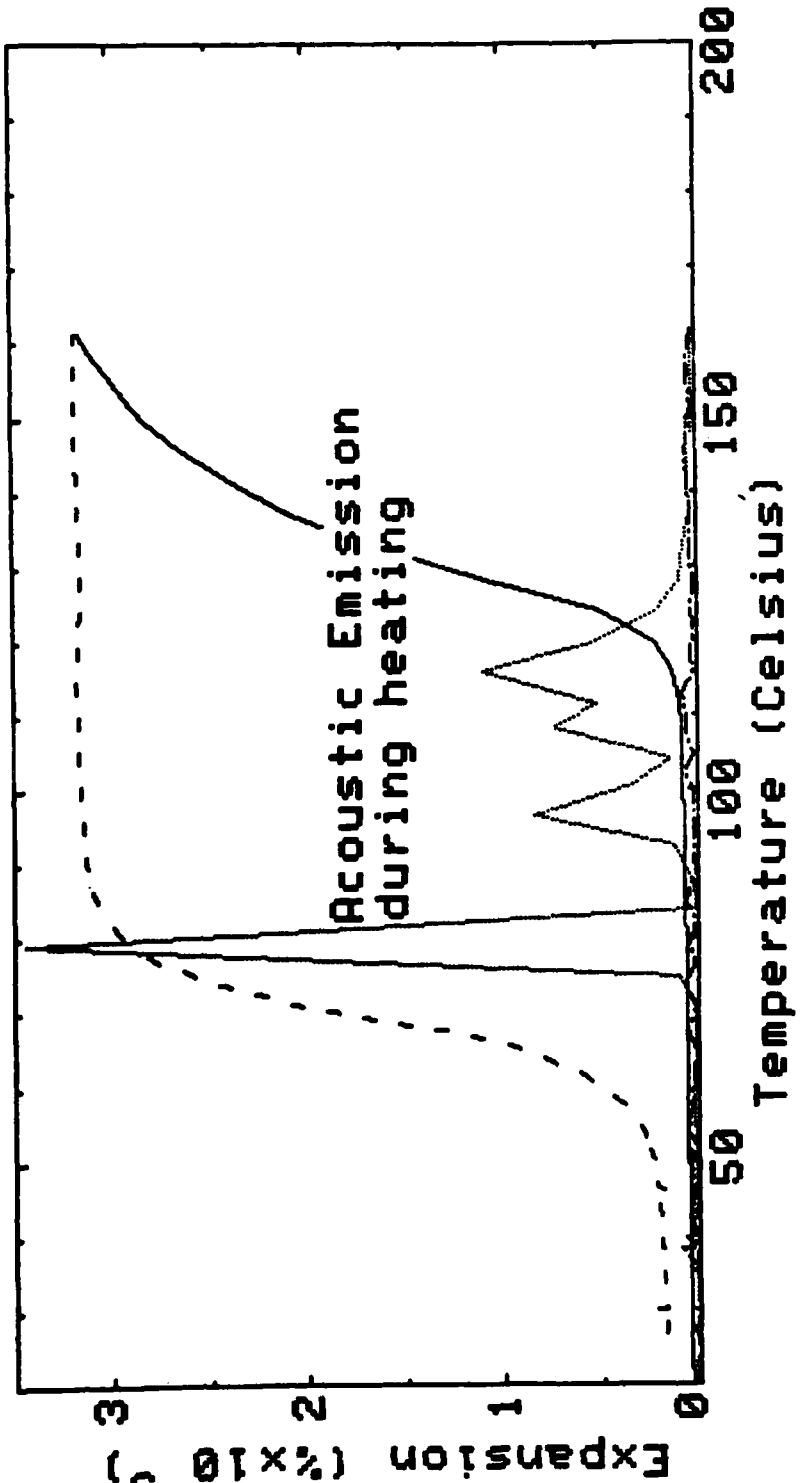
Acoustic Emission
during heating
Expansion (%x10^-3)
Temperature (Celsius)
0
1
2
3
50
100
150
200

Fig. 11

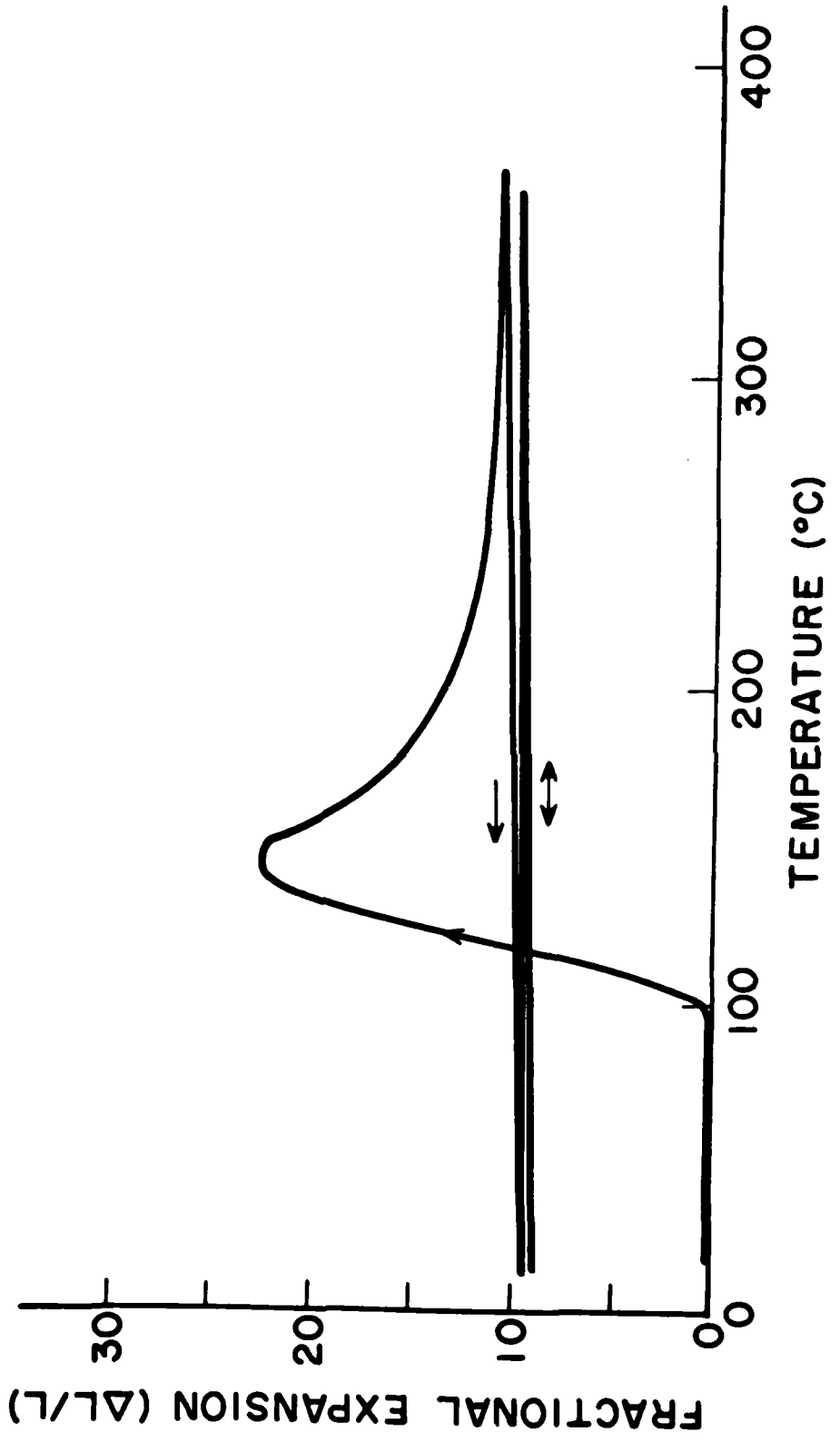
FRACTIONAL EXPANSION (ΔL/L)
0
10
20
30
100
200
300
400
TEMPERATURE (°C)

APPENDIX 7

Ext. Abstr. Program - Bienn. Conf. Carbon 16 (1983).

EXFOLIATION OF SINGLE CRYSTAL GRAPHITE-BROMINE*

S. H. Anderson and D.D.L. Chung
Department of Metallurgical Engineering and Materials Science
Carnegie-Mellon University, Pittsburgh, Pennsylvania 15213

Introduction

The exfoliation phenomenon is of technological importance as well as scientific interest. The exfoliation of graphite-ferric chloride has been used to manufacture Grafoil (1), a flexible gasket and packing material. The exfoliation of graphite-HNO_3-H_2SO_4 has been used for making a thermal insulator for molten metals (2). The exfoliation of graphite-$FeCl_3$-NH_3 has been used for making blankets for the extinction of metal fires (3). In addition, exfoliated graphite is being investigated by the U.S. Army for use as a battlefield obscurant (4). The surface area increase resulting from irreversible exfoliation is attractive for catalytic applications of graphite intercalation compounds (5). In addition, exfoliation is a phenomenon that affects the thermal stability of graphite intercalation compounds, so understanding of this phenomenon is necessary for the use of graphite intercalation compounds at elevated temperatures.

The large expansion characteristic of exfoliation had been investigated by a number of workers using dilatometry (6,7,8), gaseous pycnometry (9), optical microscopy (9), and differential thermal analysis (9). However, the fundamental question of how exfoliation affects the crystal structure of the intercalation compound has not been previously addressed. To address this question, we have used x-ray diffraction to probe the in-plane structure of single crystal graphite-bromine before and after exfoliation. We found that the single crystal nature was retained after exfoliation and collapse, without noticeable bending or twisting of the intercalate layers, but with slight bending of the graphite layers. This observation suggests that the mechanism of exfoliation is intimately tied to the intrinsic structure of intercalated graphite, in contrast to the widely accepted notion (7,9-12) that it involves the migration of the intercalate to defects where gas bubbles form. Additional support for this contention was obtained by dilatometry, which showed that single crystal graphite-bromine exfoliated as much as its highly oriented pyrolytic graphite (HOPG) counterpart, and that single crystal graphite-bromine exhibit less hysteresis than HOPG. Thus, the presence of defects hinders exfoliation.

Experimental Techniques

A single crystal graphite flake (~5 mm in diameter, from a New York mine) was intercalated to a saturated graphite-bromine compound by exposure to liquid bromine at room temperature for a day. Then it was allowed to desorb at 90°C in air for a day.

Exfoliation expansion was followed with a probe connected to a linear variable differential transducer (LVDT). The sample was heated by a furnace around the support extending an inch above the sample. The sample temperature was measured by a Pt-Pt 10% Rh thermocouple bead in contact with the sample. A heating and cooling rate of 20°C/min was used in the exfoliation cycles. The weight of the probe on the sample was 28 grams. The samples were purged with nitrogen gas in the presence of air during the measurements.

Acoustic emission during exfoliation was detected by using an ultrasonic transducer (Aerotech Gamma, 0.5 MHz wideband) equipped with a high temperature delay line. The transducer signal was amplified and the acoustic emission pulses were counted by using a frequency counter.

Single crystal diffraction was performed at room temperature by the Precession Method before intercalation and after exfoliation. MoKα radiation and a precession angle of 10° were used.

Results and Discussion

Figure 1(a) shows the fractional expansion versus temperature during the first two exfoliation-collapse cycles of the single crystal graphite-bromine sample. Figure 1(b) shows such a plot for an HOPG graphite-bromine sample (7 x 8 mm) which had been similarly prepared. Several differences can be noted between single crystal and HOPG exfoliation.

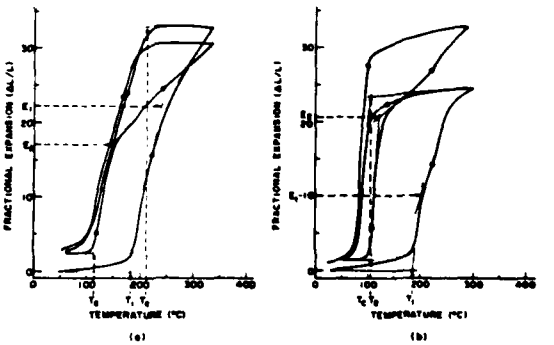

Fig. 1 Fractional expansion vs. temperature during the first two exfoliation-collapse cycles of graphite-bromine based on (a) single crystal graphite, and (b) HOPG.

1. The fractional expansion in first exfoliation was larger in single crystal graphite than HOPG. Consider, for example, the fractional expansion at 300°C during the first exfoliation-collapse cycle. Its value was 31 for the single crystal graphite and was 24 for the HOPG.

2. The collapse temperature T_c was 210±10°C for single crystal graphite-bromine, and was 100±10°C for HOPG graphite-bromine. As a result, the hysteresis was relatively small between the collapse and the next expansion for single crystal graphite.

3. The shoulders which were quite clear in the HOPG expansion characteristic were difficult to discern in the single crystal expansion characteristic.

The extent and reversibility of single-crystal exfoliation compared to HOPG exfoliation indicate that, as with intercalation, the presence of defects hinders exfoliation. In particular, the remnants of a turbostratic structure or claw defects (15) may hinder expansion by constraining a nearby crystallite which otherwise could either crack or buckle. This probably explains the lack of exfoliation in graphite fibers (16,17).

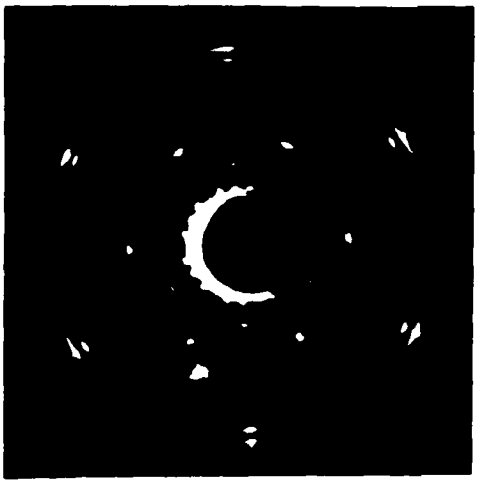

Fig. 2 hkO x-ray diffraction pattern of single crystal graphite-bromine at room temperature after exfoliation and collapse.

Figure 2 shows an hkO x-ray diffraction pattern of the single crystal graphite-bromine sample at room temperature after exfoliation and collapse. The hexagonal pattern of graphite spots indicates that the sample remained a fairly good single crystal. However, the graphitic spots were slightly broadened, showing that the graphite layers were slightly bent. Of most significance is the observation of the in-plane superlattice spots corresponding to the three-fold twinned in-plane intercalate structure (13). This observation indicates that exfoliation does not appreciably affect the in-plane orientation of the superlattice in the single crystal, so that the twinned domain structure (13) is preserved, even though the c-axis in exfoliated HOPG shows a considerable increase in the mosaic spread (14). Thus, exfoliation has little effect on a microscopic scale other than a small amount of local bending of the graphite planes.

For both single crystal and HOPG graphite-bromine, acoustic emission was detected during the first heating at 115±10°C, which is considerably below the exfoliation temperature T_j of 170±20°C. Perhaps coincidentally, the acoustic emission temperature was close to the second exfoliation temperature.

Conclusion

The in-plane superlattice and the twinned domain structure were found by single crystal x-ray diffraction to be preserved after exfoliation and collapse. The main deformation was a small amount of bending of the graphite planes. The fractional expansion due to exfoliation was found to be comparable for single crystals and HOPG, except that the fractional expansion in first exfoliation was larger for single crystals than HOPG. Moreover, the degree of hysteresis was less for single crystals than HOPG.

References

1. Union Carbide Trademark, U.S. Patent 3,404,061 (1968).
2. H. Mikami, Kokai (Japan.patent) 76 96, 793 (1976).
3. CECA S.A., Carbone-Lorraine S.A., Brit. Patent 1,588,876.
4. W. L. Garrett, J. Sharma, J. Pinto and H. Prask, Technical Report ARLCD-TR-81008, AD-E400 617; Order No. AD-A100727, May 1981, Avail. NTIS.
5. M. A. M. Boersma, in Adv. Mater. Catal., J. Burton and R. L. Garten, eds., Academic Press, 1977, pp. 67-99.
6. J. E. Brocklehurst, Nature, London, 194, 247 (1962).
7. W. H. Martin and J. E. Brocklehurst, Carbon 1, 133 (1964).
8. S. H. Anderson, H. H. Lee and D.D.L. Chung, Ext. Abstr. Program-Bienn. Conf. Carbon 15, 357 (1981).
9. C. Mazieres, G. Colin, J. Jegoudez and R. Setton, Carbon 13, 289 (1975).
10. K. Aoki, T. Hirai, and S. Yajima, J. Mat. Sci. 6, 140 (1971).
11. L. C. Olsen, S. E. Seeman and H. W. Scott, Carbon 8, 85 (1970).
12. M. B. Dowell, Ext. Abstr. Program-Bienn. Conf. Carbon 12, 35 (1975).
13. D. Ghosh and D.D.L. Chung, submitted for publication.
14. M. B. Dowell, Ext. Abstr. Program-Bienn. Conf. Carbon 12, 31 (1975).
15. A. R. Ubbelohde and F. A. Lewis, Graphite and Its Crystal Compounds, Oxford University Press, London, 1960.
16. M. Endo, T. Koyama and M. Inagaki, Synth. Met. 8, 177 (1981).
17. S. H. Anderson and D.D.L. Chung, to be published .

Acknowledgments

Thanks to R. Clarke for providing natural graphite flakes. The x-ray diffraction equipment support from the National Science Foundation (DMR-8005380 and DMR 76-81561 A01) is acknowledged.

*Research sponsored by the Air Force Office of Scientific Research, Air Force Systems Command, USAF, under Grant No. AFOSR-78-3536. The United States Government is authorized to reproduce and distribute reprints for Government purposes notwithstanding any copyright notation hereon.

APPENDIX 8

Carbon, submitted.

SUPERLATTICE ORDERING IN GRAPHITE-ICl SINGLE CRYSTALS AND FIBERS†

D. Ghosh,** R. Gangwar†† and D. D. L. Chung**
Carnegie-Mellon University
Pittsburgh, PA 15213

† Research sponsored by the Air Force Office of Scientific Research, Air Force Systems Command, USAF, under Grant No. AFOSR-78-3536. The United States Government is authorized to reproduce and distribute reprints for Governmental purposes notwithstanding any copyright notation hereon.

** Department of Metallurgical Engineering and Materials Science

†† Department of Physics

ABSTRACT

By using x-ray diffraction, a 3-fold or 6-fold twinned monoclinic $\sqrt{301}$ x 2 (-3.3^{o}, 0^{o}) superlattice (a=4.92 Å, b= 42.68 Å, c=7.0 Å, γ =93.3^{o}) was observed in stage-1 graphite-ICl single crystals intercalated in ICl vapor. This in-plane superlattice was also observed in stage-1 and stage-2 graphite-ICl, which were based on Thornel P-100 graphite fibers and prepared by the two-bulb method, in which liquid ICl was at 95^{o}C while graphite was at 100^{o}C for stage 1 and 130^{o}C for stage 2. This work provides the first observation of in-plane intercalate ordering in intercalated graphite fibers and the first x-ray diffraction evidence of ICl intercalation in graphite fibers. A different in-plane superlattice was observed in stage-1 graphite-ICl single crystals intercalated in ICl liquid.

INTRODUCTION

The in-plane superlattice in stage-1 graphite-ICl single crystals prepared by exposure to iodine monochloride (ICl) vapor at 20-30°C was reported to have a six-fold twinned monoclinic unit cell with pseudo-cell dimensions of a=4.92 Å, b=19.2 Å, and γ=93.5°, as derived from x-ray oscillation photographs.[1] In this work, we obtained the same diffraction pattern by the precession method, but a three-fold or six-fold twinned monoclinic unit cell with a= 4.92 Å, b= 42.68 Å and γ= 93.3° was found to fit the diffraction pattern better. Furthermore, this same in-plane unit cell was observed in ICl-intercalated fibers by the Transmission Laue method, and hence provided the first observation of in-plane intercalate ordering in intercalated graphite fibers.

Intercalated graphite fibers have recently received considerable attention because of their use in polymer-matrix composites for high electrical conductivity applications.[2] The intercalation of graphite fibers with HSO_3F, AsF_5 or SbF_5 gave an up to 50 times increase in the electrical conductivity.[3] X-ray diffraction showed the formation of stage 2 graphite-AsF_5 in high modulus ex-PAN graphite fibers (e.g. Union Carbide TP 4104B).[4,5] Formation of stage 1 graphite-K in fibers was shown by x-ray diffraction[5] and the appearance of the gold color[5,6]; the formation of mixed stages of graphite-K, graphite-Rb and graphite-Cs was also indicated by x-ray diffraction (Debye-Scherrer method).[7] Absorption of Br_2 and ICl in graphite fibers was indicated by weight uptake measurement,[8,9] but confirmation of intercalation by using x-ray diffraction had not been reported. Warner et al.[8] interpreted the absorption as not being intercalation, but rather plasticization, whereas Hooley and Deitz[9] interpreted the absorption

as intercalation, Desorption of brominated graphite fibers resulted in a stable material having an electrical conductivity higher than that of pristine graphite fibers.[5,10] Similar treatment with ICl gave an even higher value of the electrical conductivity.[5] In this work, we have obtained the first x-ray diffraction evidence of intercalation of ICl in graphite fibers.

Although the in-plane superlattice pattern of stage-1 graphite-ICl prepared in ICl vapor at room temperature (Type A) was the same as that of Ref. 1, the pattern of stage-1 graphite-ICl prepared in ICl liquid (Type B) was dramatically different and was observed for the first time in this work.

EXPERIMENTAL TECHNIQUES

The graphite single crystals used in this work were typically 0.5-1.0 mm in diameter and ~0.05 mm thick. Intercalation to stage 1 was performed at room temperature by exposure to ICl vapor (Type A) or ICl liquid (Type B). The samples were sealed in glass capillaries while they were in contact with either ICl vapor (Type A) or ICl liquid (Type B). Single crystal x-ray diffraction was performed at room temperature by using a precession camera, with Zr filtered MoKα radiation. All diffraction patterns were generated by 5^{o} screenless precession, except that Type B photographs were generated using layer screens.

The graphite fibers used in this work are listed in Table 1. Intercalation was carried out by exposure of the fibers to ICl vapor in equilibrium with ICl liquid at 95^{o}C; this temperature was chosen for the ICl liquid because ICl boils at 97.4^{o}C. The purity of ICl was 95+%, as supplied by Alfa Products. While the ICl liquid was held at 95^{o}C, the fibers (typically ~1.0 cm long) were held at a temperature ranging from 100^{o}C to 135^{o}C. The reaction vessel was made of Pyrex glass and was sealed without evacuation. The intercalation time investigated ranged from 8 hours to 24 hours.

X-ray diffraction was used to characterize the crystal structural effects of intercalation of the fibers. The Transmission Laue method was used, with MoKα radiation and a specimen-to-film distance of 6 cm. The accuracy of visual measurement of the diameter of an observed ring on the film was $\pm$ 0.5 mm, so that the maximum error in the measured d-spacing was $\pm$ 1.7%. The set-up allowed d-values ranging from 0.8 Å to ~ 6 Å to be measured. The intercalated fibers were removed from the reaction vessel, cut to a typical length of ~2 mm, and then sealed in a glass capillary of 1 mm I.D. and 0.01 mm wall thickness; this procedure took typically ~ 1 min. The fiber axes thus had a preferred orientation along the capillary axis. The exposure time was 6 hr for every sample.

Ref. 1 could not explain the observed diffraction pattern as well as the one reported here, which we found to be the smallest unit cell with the maximum symmetry, although it could be a pseudo-cell with the real cell being larger. In addition to their pseudo-cell, Turnbull and Eeles[1] mentioned about a real cell which is larger. However, in our diffraction pattern, we could not identify this larger unit cell.

The monoclinic in-plane unit cell of Type A is hence $\sqrt{301}$ x 2 (-3.3^{o},0^{o}). This convention is adapted for non-hexagonal cells. The graphite in-plane unit cell is 1 x 1 (30^{o}, 0^{o}). The angles are described by two in-plane orthogonal axes.

One important feature of the hkO diffraction pattern is that some spots in Fig. 1 (denoted by circled dots) constitute a pattern identical to that of pure graphite. In other words, only the superlattice reflections exhibit the "twinning" effect. Thus, the effect is produced by the intercalate layers. Similar twinning was also noted in graphite-bromine.[11]

Type B single crystals

Figure 3 shows the hkO and hOℓ diffraction patterns (precession photographs) of Type B, which was intercalated in liquid ICl and photographed in contact with the liquid. The complicated hkO pattern, characterized by sharp reflection spots, probably arises from two different orthorhombic systems. It is yet to be fully analyzed. The hOℓ diffraction pattern showed the diffraction spots along the c* direction and gave an intercalate-carbon-intercalate sandwich thickness of 7.17 Å; the axial repeat distance along this direction was either 7.17 Å or 14.34 Å. This photograph does not show any streak at h≠ 0 positions, while a similar photograph for Type A exhibits streaks parallel to c* at those positions (Fig. 4). This suggests that the Type B superlattice is more three-dimensionally ordered than that of Type A.

EXPERIMENTAL RESULTS

Type A single crystals

The hk0 diffraction pattern (precession photograph) of Type A (single crystal) represented in Fig. 1 appears to be the same as Fig. 2 and Fig. 4 of Ref. 1. This pseudo-hexagonal pattern in Fig. 1 is the result of diffraction spots from a three-fold (or six-fold) twinned monoclinic lattice, having three (or six) possible in-plane orientations, rotated with respect to one another by 120° (or 60°) about the c-direction of the graphite lattice (Fig. 1 in reciprocal space, Fig. 2 in real space).

Designating the unique axis of the monoclinic cell as c (which is parallel to the c-axis of graphite), one can easily express the reciprocal lattice vectors $\vec{a}_s^*$ and $\vec{b}_s^*$ in terms of the graphite reciprocal lattice vectors $\vec{a}_g^*$ and $\vec{b}_g^*$ (thereby ensuring the commensurability of the superlattice 's') by the following simple relations:

$$\vec{a}_s^* = (1/2)\vec{a}_g^* - (9/40)\vec{b}_g^* \qquad (1)$$

$$\vec{b}_s^* = (1/20)\vec{b}_g^* \qquad (2)$$

With $|\vec{a}_g^*| = |\vec{b}_g^*| = 0.4694\ \text{Å}^{-1}$, Eq. (1) and (2) yield the superlattice lattice parameters

$$|\vec{a}_s| = (\sqrt{301}/40)\,|\vec{a}_g^*| = 4.92\ \text{Å}$$

$$|\vec{b}_s| = (1/20)\,|\vec{b}_g^*| = 42.68\ \text{Å}$$

and $\gamma_s = 93.3^{\circ}$,

where γ_s is the angle in real space between the $\vec{a}_s$ and $\vec{b}_s$ axes. The c-axis length was determined from a h0ℓ photograph yielding c= 7.0 Å, which agrees with the published c-axis periodicity of stage-1 graphite-ICl compound.[1] This cell is approximately double the size of the monoclinic cell given in Ref. 1, which has a= 4.92 Å, b= 19.2 Å and $\gamma = 93.5^{\circ}$. The smaller cell in

Figure 5 shows the x-ray diffraction photographs of the three types of pristine graphite fibers listed in Table.1. The Thornel P-100 fibers gave the largest number of diffraction lines, as listed in Table 2. The Celion GY-70 fibers gave fewer lines, but they are as sharp as those of Thornel P-100. On the other hand, the Panex 30 fibers gave only a few relatively diffused lines. Hence, the crystalline perfection of the graphite fibers decreased in the order (1) Thornel P-100, (2) Celion GY-70, and (3) Panex 30 .

Figure 6 shows the x-ray diffraction photographs of (a) HOPG, (b) Thornel P-100, (c) Celion GY-70, and (d) Panex 30 after exposure to ICl. The HOPG sample was intercalated by exposure to ICl vapor at room temperature for 1 day, and resulted in a stage 1 compound (Fig. 6 (a)); the indexing of the diffraction lines is shown in Table 3. All three types of fibers were treated identically by holding the fibers at 130^{o}C and the ICl liquid at 95^{o}C for 8 hr. After the treatment, the Thornel P-100 fibers (Fig. 6(b)) showed superlattice diffraction lines, which were absent in Fig. 5 (a). Indexing of the pattern in Fig. 6 (b) showed that the intercalated Thornel P-100 fibers were predominantly stage 2. (The indexing of the pattern for stage 2 Thornel P-100 fibers is given later in this paper). The same treatment for Celion GY-70 and Panex 30 fibers did not yield any superlattice lines. It should be mentioned that <u>room temperature</u> exposure of any type of fibers to ICl did not yield any superlattice lines, although such treatment of HOPG resulted in stage 1. Thus, Fig. 6 shows that the ease of intercalation of the various graphite materials decreased in the order (1) HOPG, (2) Thornel P-100, (3) Celion GY-70, and (4) Panex 30. In fact, no diffraction evidence of ICl intercalation was obtained for Celion GY-70 nor Panex 30 fibers, although intercalation was clearly shown for Thornel P-100.

Figure 7 shows x-ray diffraction patterns of intercalated Thornel P-100 fibers after various lengths of desorption time (0 min, 10 min, 2 hr, 1 week). Intercalation was performed by holding the fibers at 130°C and the ICl liquid at 95°C for 24 hr. Desorption was allowed to occur in air at room temperature. Fig. 7 (a) shows the pattern obtained after a negligible length of desorption time (0 min); the indexing of this pattern is shown in Table 4. Note that the second stage (00ℓ) type lines were observed for ℓ= 2,3,5,6,8,9. The (001) line was not observed because its large d value caused it to be blocked by the beam stop. The absence of (00ℓ) lines for ℓ=4,7 is probably systematic due to the space group, which is presently not known since the positions of the intercalate molecules within a unit cell has not been determined. In addition to the (00ℓ) lines, (hk0), (h0ℓ) and (0kℓ) lines were observed. The in-plane superlattice was thus found to be the same as that of Type A single crystals. Desorption resulted in a gradual decrease of the intensities of the superlattice lines without shifting any line. This means that the initial stage (stage 2) was maintained during desorption. The presence of superlattice diffraction lines even after a week of desorption indicates that (1) desorption of intercalated fibers results in a material which is still intercalated, and (ii) desorption of intercalated fibers occurs over an appreciable long time.

By lowering the sample temperature to 100°C, with the ICl liquid maintained at 95°C, stage 1 graphite-ICl (mixed with small quantities of stages 2 and 3) was obtained in Thornel P-100 graphite fibers. Although we were able to obtain relatively pure stage 2, we have not been able to obtain pure stage 1. The in-plane superlattice of stage 1 was also found to be the same as that of Type A single crystals.

DISCUSSION

The large size of the in-plane unit cell makes it difficult to determine the positions of all the atoms in the unit cell. As guided by weight-gain results[2] and the in-plane atomic arrangement proposed by Turnbull and Eeles[1], one might assume that there are 9 ICl units in our in-plane unit cell, so that the stoichiometry of Type A is $C_{8.9}ICl$, which is close to the previously reported stage-1 stoichiometries of C_9ICl[1] and $C_{8.5}ICl$[12,13].

The ICl chains in the model of Turnbull and Eeles[1] are approximately 4.26 Å apart in the b-direction. Since our unit cell is 42.68 Å long in the b-direction, it may be possible for our unit cell to contain 10 chains, which corresponds to 10 ICl units in our unit cell and a stoichiometry of C_8ICl. As weight measurement does not give an accurate determination of the stoichiometry, an intensity analysis using four-circle diffractometer results is needed to determine the stoichiometry, which could be C_8ICl (10 ICl units per cell), $C_{8.9}ICl$ (9 ICl units per cell) or $C_{10}ICl$ (10 ICl units per cell).

The diffraction patterns from graphite-ICl, though seemingly indicative of more ordered structures than graphite-bromine, are complicated and difficult to interpret. This might stem from the fact that ICl has two possible forms, α and β, both with melting points near room temperature. It might be noted that the Type A unit cell resembles that of β-ICl, which is monoclinic but pseudo-orthorhombic, with the angle being 91° 21'.[14] Furthermore, β-ICl consists of nearly planar atomic layers, whereas α-ICl does not.[14]

The ICl intercalation method used in this work is based on the two-bulb method developed for potassium intercalation.[15] In contrast, previous work on intercalation of ICl in fibers involved exposure to ICl vapor at room temperature.[8,9] We have found that the two-bulb method used in this work

gave graphite-ICl of specific stages, whereas room temperature exposure to ICl did not lead to superlattice formation.

The ease of intercalation was found to increase with increasing crystal perfection of the graphite material, such that the crystal perfection decreases in the order (1) HOPG, (2) Thornel P-100, (3) Celior GY-70, and (4) Panex 30. In fact, Thornel P-100 was the only type of fibers which could be intercalated using our method, as indicated by the superlattice formation. Note that we consider superlattice formation to be conclusive evidence for intercalation. In this work, the first such evidence was obtained for the intercalation of ICl in graphite fibers.

Of significance is that we have observed for the first time in-plane intercalate ordering in intercalated graphite fibers. Moreover, we have found that the in-plane unit cell of stage 1 and stage 2 ICl-intercalated fibers is the same as that of stage 1 graphite-ICl single crystal graphite and that of stage 1 graphite-ICl HOPG. In addition to the in-plane superlattice, staging was observed.

The Transmission Laue method used in this work was found to be more suitable for fiber material compared to the Debye-Scherrer method and the diffractometer method. This is because the preferred orientation of the fibers results in incomplete Debye rings, which might be missed by the film in the Debye-Scherrer method. Moreover, the need of a small sample quantity, the availability of thin-walled capillaries for sealed samples, and the possibility of a long exposure time make the Transmission Laue method more attractive than the diffractometer method.

ACKNOWLEDGMENTS

The authors thank Union Carbide Corporation, Celanese Research Co. and Stackpole Corporation for providing the carbon fiber materials. Stimulating discussion with Mr. S. H. Anderson of Carnegie-Mellon University is gratefully acknowledged. The x-ray diffraction equipment grant from the Division of Materials Research of the National Science Foundation under Grant No. DMR-8005380 was essential for this work. Support from the Materials Research Laboratory Section, Division of Materials Research, National Science Foundation under Grant No. DMR 76-81561 A01 is also acknowledged.

REFERENCES

1. J. A. Turnbull and W. T. Eeles, Proceedings of Second Conference on Industrial Carbons and Graphite 1965, p. 173-9, Soc. Chem. Ind., London, 1966.

2. F. L. Vogel, Synth. Met. 1, 279 (1979/80).

3. I. L. Kalnin and H. A. Goldberg, Synth. Met. 3, 159 (1981).

4. I. L. Kalnin and H. A. Goldberg, Ext. Abstr. Program - Bienn. Conf. Carbon 15, 367 (1981).

5. D. D. Dominguez, R. N. Bolster and J. S. Murday, Ext. Abstr. Program-Bienn. Conf. Carbon 15, 365 (1981).

6. M. Sano, N. Sato, H. Inokuchi and S. Tamura, Physica 105B, 296 (1981).

7. P. Kwizera, M. S. Dresselhaus, D. R. Uhlmann, J. S. Perkins and C. R. Desper, Carbon 20, 387 (1982).

8. S. B. Warner, L. H. Peebles and D. R. Uhlmann, Int. Conf. Carbon Fibers, Their Place in Modern Technology, London (1974).

9. J. G. Hooley and V. P. Deitz, Carbon 16, 251 (1978).

10. M. Endo and T. Koyama, Synth. Met. 3, 177 (1981).

11. D. Ghosh and D. D. L. Chung, submitted for publication.

12. Y. Mizutari, Kyoto Daigaku Kenkyusho Iho 41, 61 (1972).

13. Y. Mizutari, Kyoto Daigaku Genshi Energi Kenkyusho Iho 44, 58 (1973).

14. G. B. Carpenter and Stephanie M. Richards, Acta Cryst. 15, 360 (1962).

15. A. Herold, Bull. Soc. Chim. France 187, 999 (1955).

Table 1 Specifications of Graphite Fibers Used

Table 1

Manufacturer	Union Carbide Corp.	Stackpole Fiber Co.	Celanese Corp.
Grade	Thornel P-100 Grade VS-0054	Panex 30	Celion GY-70
Precursor	Pitch	PAN	PAN
Tensile modulus (10^6 psi)	100	32	75
Tensile strength (10^6 psi)	0.325	0.375	0.27
Density (g/cm^3)	2.16	1.74	1.97
Electrical resistivity ($10^{-4}\Omega$-cm)	2.5		6.5

Table 2 X-ray diffraction lines obtained from pristine graphite fibers (Thornel P-100)

Table 2

Line No.	d_{obs} (Å)	d_{cal} (Å)	h	k	ℓ	Strength
1	3.38	3.35	0	0	2	S
2	2.11	2.13	1	0	0	M
3	1.69	1.68	0	0	4	S
4	1.23	1.23	1	1	0	Diffuse
5	1.17	1.15	1	1	2	Diffuse
6	1.13	1.12	0	0	6	M

Table 3 X-ray diffraction lines obtained from stage 1 graphite-ICl based on HOPG flakes.

Line No.	d_{obs} (Å)	d_{cal} (Å) (Stage 1)	hkℓ (Stage 1)			Strength
			h	k	ℓ	
1	5.32	5.33	0	8	0	W
2	4.86	4.89	1	0	0	VS
3	4.35	4.35	1	4	0	W
4	4.07	4.02	1	0	1	W
5	3.54	3.53	0	0	2	VS
6	3.38	3.42	0	3	2	W
7	3.19	3.16	0	6	2	W
8	3.09	--	--	--	--	VW
9	2.95	2.86	1	0	2	M
10 *	2.62	2.62	1	6	2	M
11	2.49	2.45	2	0	0	M
12	2.33	2.35	0	0	3	S
13	2.18	2.18	2	8	0	W
14	2.12	2.13	0	20	0	M
15 *	2.03	2.04	2	$\bar{1}$	1	W
16 *	1.93	1.94	2	5	2	VW
17 *	1.87	1.82	2	$\bar{1}$	2	W
18	1.78	1.76	0	0	4	W
19	1.65	1.63	3	0	0	M
20 *	1.56	1.58	2	$\bar{1}$	3	Diffuse
21	1.47	1.48	3	0	2	W
22 *	1.36	1.36	2	$\bar{1}$	4	Diffuse
23	1.32	1.34	3	0	3	W
24	1.18	1.18	0	0	6	S
25	1.14	1.14	1	0	6	M

* Tentative hkℓ assignment, since the streaks due to the two-dimensional character were not observed.

Table 4 X-ray diffractions lines obtained from graphite fibers intercalated with ICl by holding the fibers at 130°C

Table 4

Line No.	d_{obs} (Å)	d_{cal} (Å) (Stage 2)	hkℓ (Stage 2)			Strength
			h	k	ℓ	
1	5.30	5.20	0	0	2	W
2	4.80	4.89	1	0	0	W
3	4.25	4.26	0	10	0	W
4	3.89	3.92	0	10	1	W
5	3.43	3.46	0	0	3	VVS
6	2.86	2.83	1	0	3	W
7	2.13	2.13	0	20	0	S
8	2.07	2.07	0	0	5	M
9	1.84	1.82	0	20	3	Diffuse
10	1.73	1.73	0	0	6	W
11 *	1.70	1.70	10	$\bar{5}$	6	W
12	1.63	1.63	3	0	0	W
13	1.31	1.30	0	0	8	W
14 *	1.26	1.26	2	$\bar{1}$	8	VW
15	1.23	1.23	4	$\bar{2}$	0	S
16	1.16	1.16	0	0	9	W
17 *	1.12	1.11	2	$\bar{1}$	4	W
18	0.99	0.99	4	0	4	W

* Tentative hkℓ assignment, since the streaks due to the two-dimensional character were not observed.

FIGURE CAPTIONS

Fig. 1 The hkO x-ray diffraction pattern (schematic) of a Type A graphite-ICl single crystal.

Fig. 2 In-plane unit cell of Type A graphite-ICl

Fig. 3 The hkO and hOℓ x-ray diffraction patterns of a Type B graphite-ICl single crystal.

Fig. 4 The hOℓ x-ray diffraction pattern of a Type A graphite-ICl single crystal.

Fig. 5 X-ray diffraction patterns of pristine graphite fibers: (a) Thornel P-100, (b) Celion GY-70, (c) Panex 30.

Fig. 6 X-ray diffraction patterns of (a) HOPG, (b) Thornel P-100, (c) Celion GY-70, and (d) Panex 30 after exposure to ICl.

Fig. 7 X-ray diffraction patterns of intercalated Thornel P-100 fibers after various lengths of desorption time: (a) 0 min, (b) 10 min, (c) 2 hr, (d) 1 week. Every other line in (a) is labeled by its Line No., which is defined in Table 4.

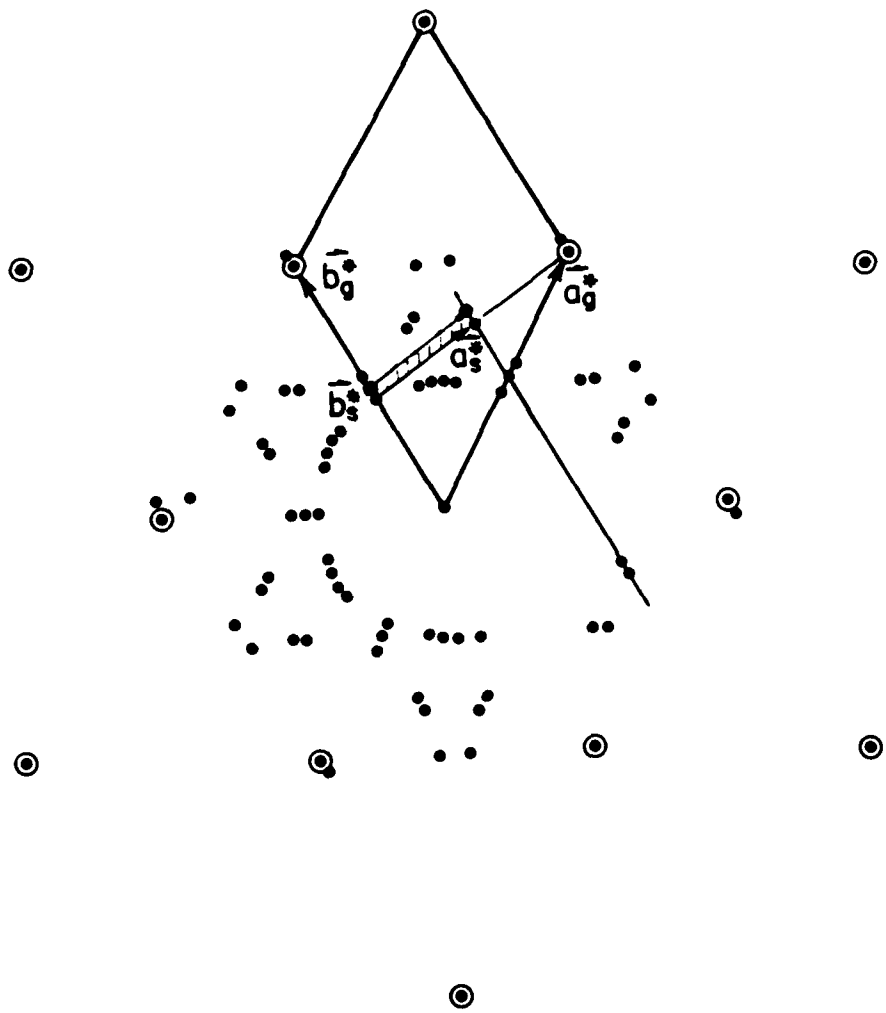

Fig. 1

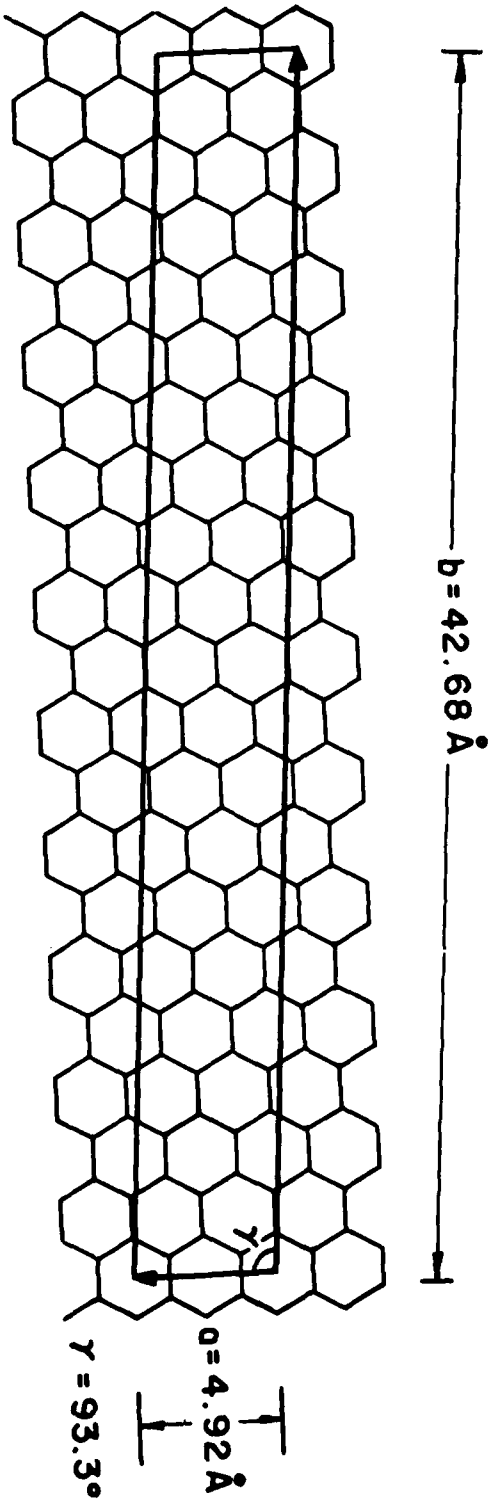

Fig. 2

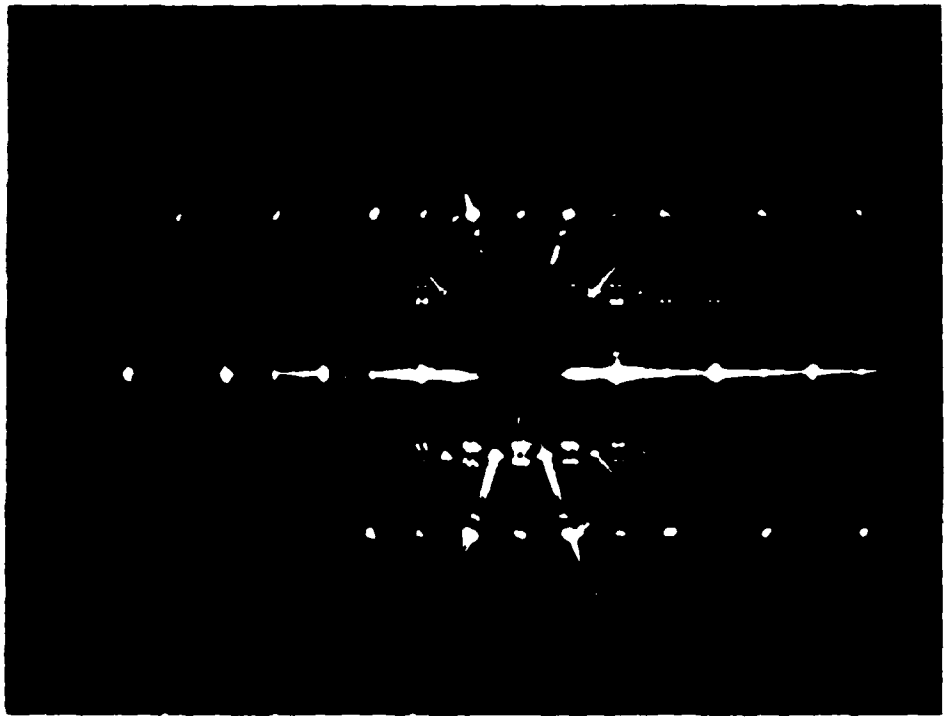

hOl

hkO

Fig. 3

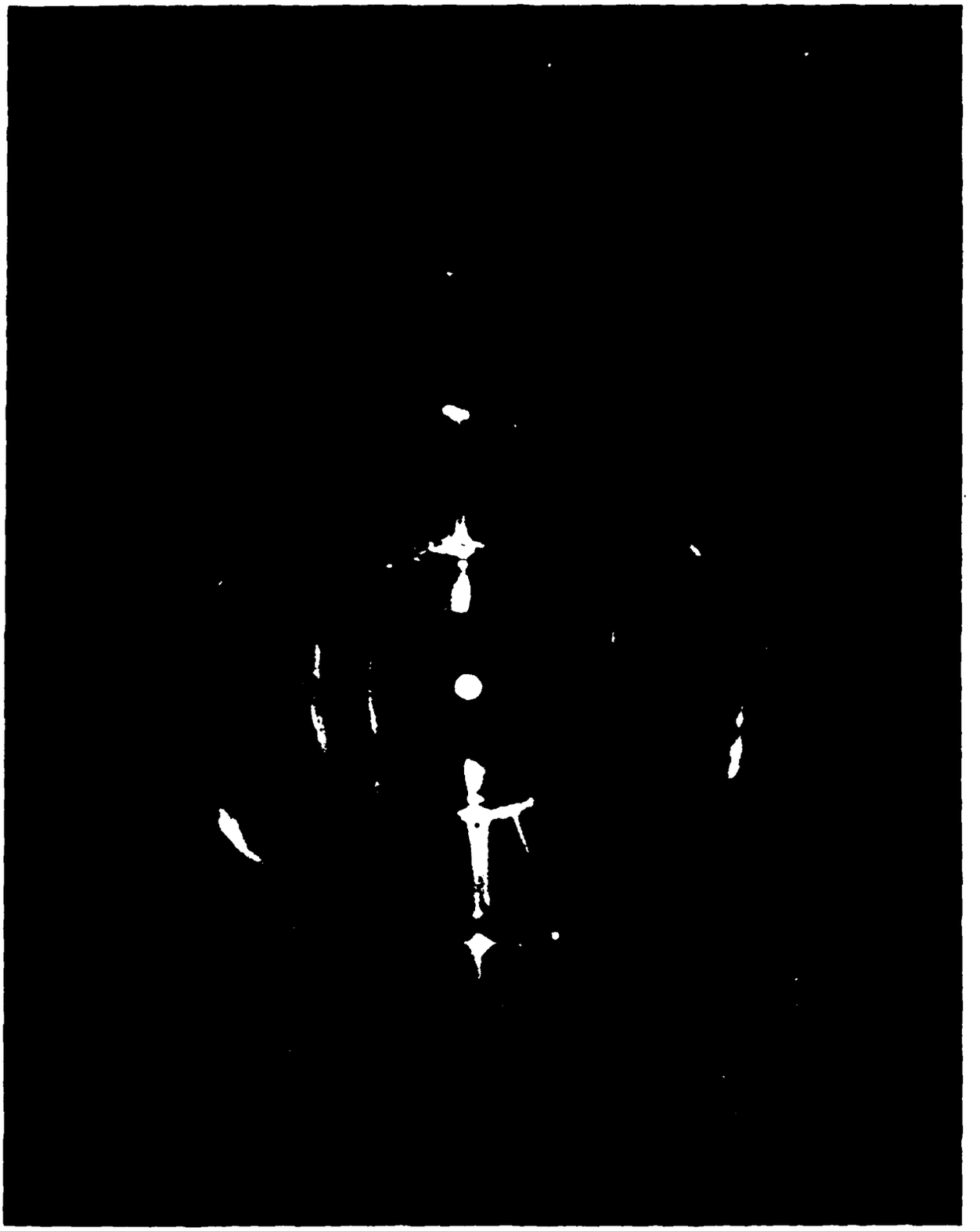

(a) Thornel P-100

(b) Celion GY-70

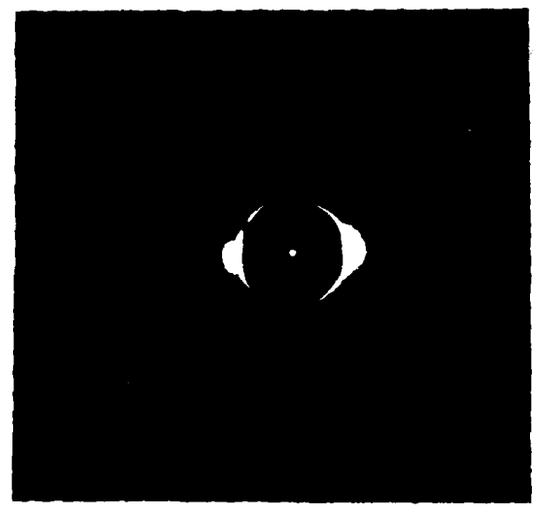

(c) Panex 30

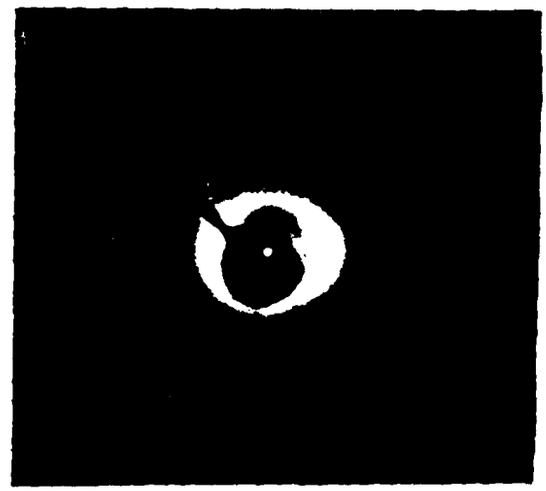

Fig. 5

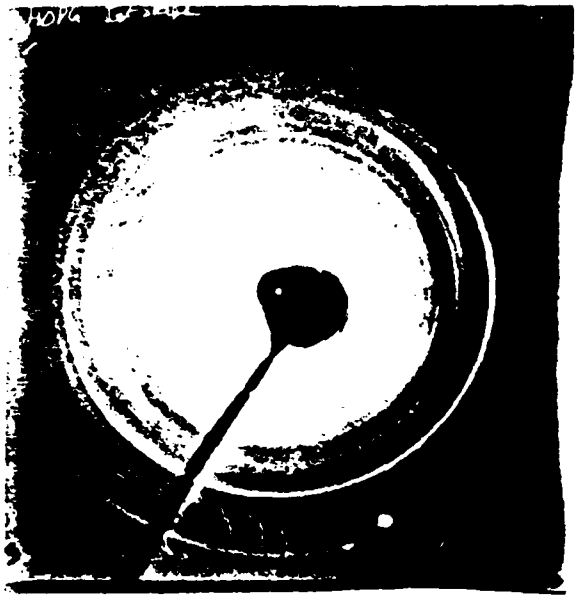

(a) HOPG

(b) Thornel P-100

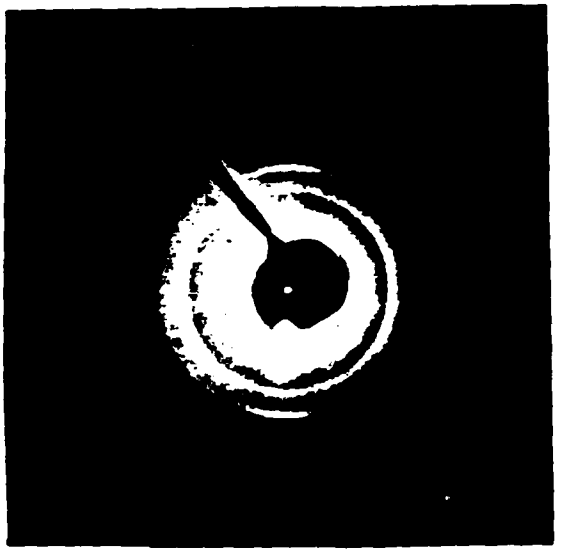

(c) Celion GY-70

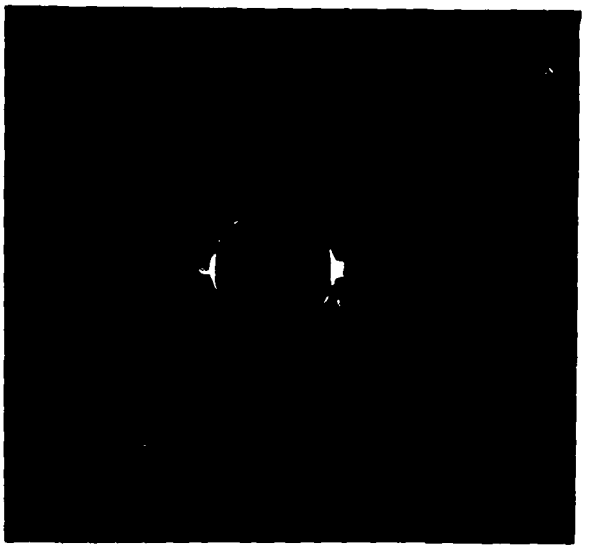

(d) Panex 30

Fig.

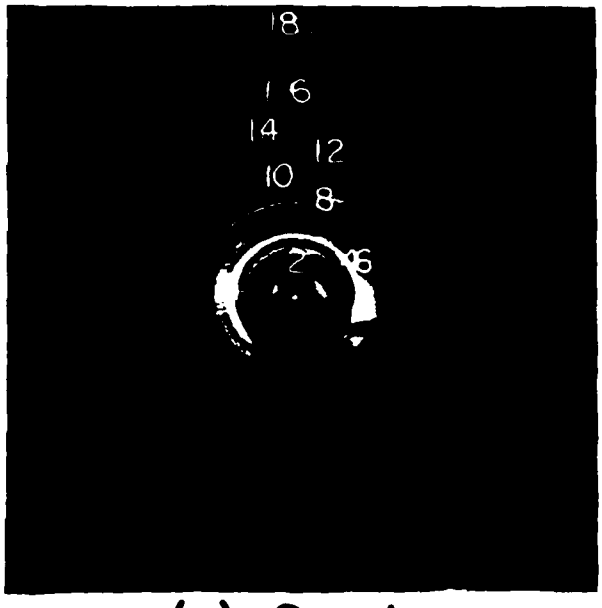

(a) 0 min

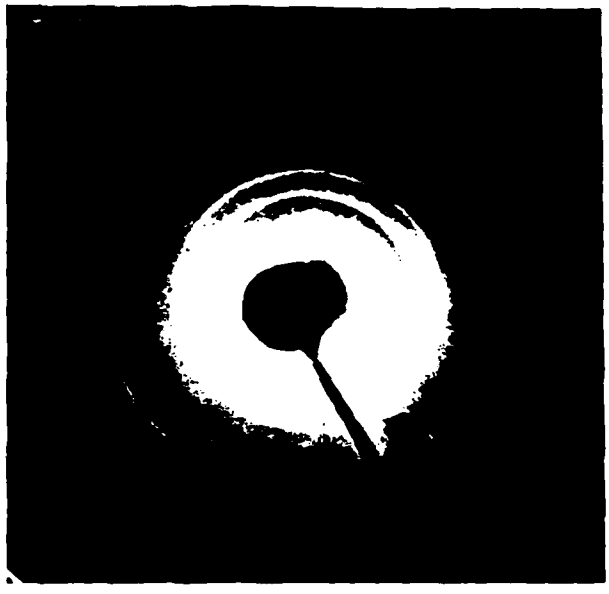

(b) 10 min

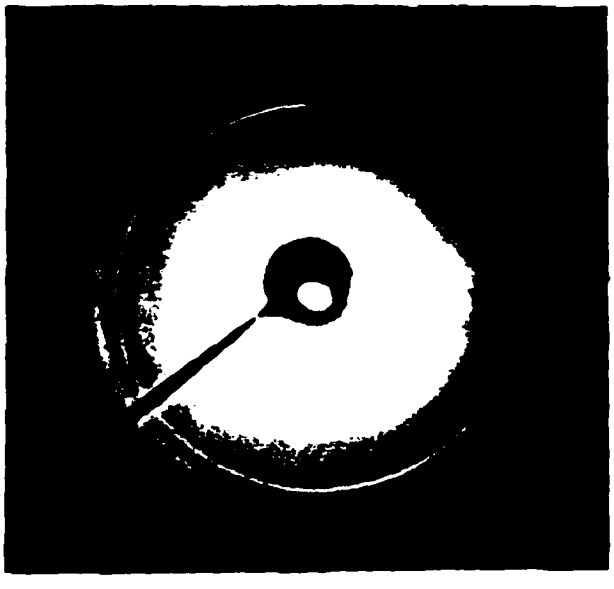

(c) 2 hr

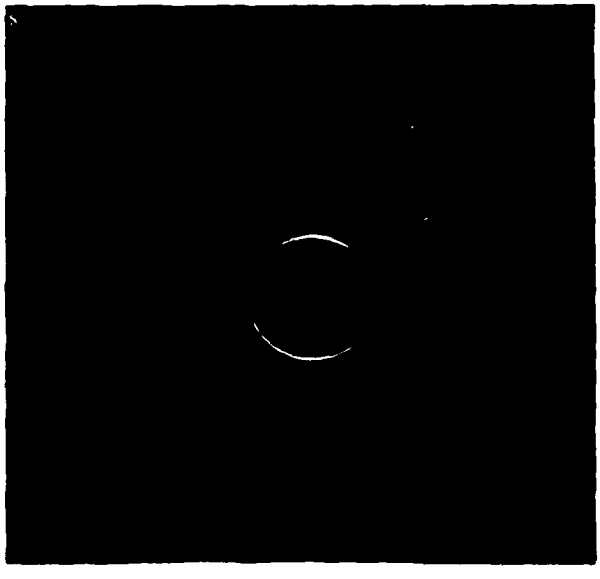

(d) 1 week

Fig. 7